ROYAUME DU MAROC
Université Mohammed V - RABAT -
جامعة محمد الخامس – الرباط –
Faculté des sciences
كلية العلوم
CENTRE D'ETUDES DOCTORALES - SCIENCES ET TECHNOLOGIES

N° d'ordre 3193

THESE

En vue de l'obtention du : ***DOCTORAT***

Structure de Recherche: *Équipe de Sciences de la Matière et du Rayonnement*
Discipline: *Physique*
Spécialité: *Physique et Instrumentation Nucléaire*

Présentée et soutenue le 01/04/2019 par:

Mounia LAASSIRI

Neutron Signals Nonnegative Tensor Blind Source Separation: Application to Neutron/Gamma Discrimination

JURY

Latifa ELOUADRHIRI	*Dr, Jefferson Laboratory, Newport News, Virginia, US*	*Président*
Kétévi Adiklè ASSAMAGAN	*Dr, Brookhaven National Laboratory, Upton, US*	*Rapporteur*
Mohamed CHABAB	*PES, FSSM, Université Cadi Ayyad, Marrakech*	*Rapporteur*
Yahya TAYALATI	*PES, FSR, Université Mohammed V, Rabat*	*Rapporteur*
Farida FASSI	*PH, FSR, Université Mohammed V, Rabat*	*Examinateur*
Rajaa CHERKAOUI EL MOURSLI	*PES, FSR, Université Mohammed V, Rabat*	*Directeur de Thèse*
El-Mehdi HAMZAOUI	*Chercheur, CNESTEN*	*Co-Directeur de Thèse*

Année Universitaire: 2018/2019

I would like to dedicate this work to my great mother, who has been my pillar and back bone in everything I do. She has given me a very high role to look up to; a woman that is so dedicated, passionate, ambitious, and courageous, not afraid to explore with endless challenges, I have learned so much from you (mama)... and I am very grateful to Allah for you, and everyone around me that has added so much to my life...

Acknowledgements

All works presented in this thesis have been carried out in the Laboratory of the Materials and Radiation Sciences Team (ESMaR), Physics Department, Faculty of Sciences, Mohammed V University - Rabat, under the supervision of the Prof. Rajaa CHERKAOUI EL MOURSLI and the co-supervision of the Dr. El-Mehdi HAMZAOUI.

First of all I would like to thank my supervisor, Prof. Rajaa CHERKAOUI EL MOURSLI for her endless mentoring, tutoring and support both in academic life and in life.

My co-supervisor at CNESTEN, Dr. El-Mehdi HAMZAOUI. I received an incredible amount of help. I had the opportunity to learn about every possible detail of fission chambers, pulses, simulations and signal processing. His careful reading, critique, and suggestions have greatly improved this dissertation.

I'm deeply grateful to Dr. Latifa ELOUADRHIRI from Jefferson Laboratory, Newport News, Virginia (US), for having accepted to be president of this thesis.

I would like to express my appreciation to my thesis reporter Dr. Kétévi Adiklè ASSAMAGAM from Brookhaven National Laboratory, Upton (US), who dedicated a great deal of his time for accurately reviewing this thesis.

I would like to thank Prof. Mohamed CHABAB from the Faculty of Sciences Semlalia in Marrakech, for reporting and reviewing this thesis.

I'm very thankful to the Prof. Yahya TAYALATI (Head of the Materials and Radiation Sciences Team (ESMaR)), Faculty of Sciences in Rabat, for his advice and encouragement and also for accepting to evaluate this thesis.

I'm deeply grateful to Prof. Farida FASSI from the Faculty of Sciences in Rabat, for her encouragement, kindness and also for welcoming to participate to the jury member to evaluate my thesis.

A special thank should go to Dr. John APOSTOLAKIS from CERN; which I met him at African School of Physics (ASP2016) and I had a lot of useful discussions with him about Geant4 toolkit.

I would like to thank Dr. Rob VEENHOF from CERN, author of Garfield and Dr. Dorothea PFEIFFER from CERN, author of Geant4/Garfield++ interface for priceless help on this toolkit.

I am indebted to Dr. Zsolt ELTER, author of pyFC, for our extensive discussions about fission chamber simulations and for his help on the fission chamber data simulated with this toolkit.

Finally the most important I have to thank are my family, my friends and ESMaR colleagues for their continuous support.

Résumé

L'un des aspects de la sûreté et de la sécurité des réacteurs nucléaires consiste à cerner la distribution du flux neutronique à l'intérieur du réacteur avec la meilleure précision possible. A cet effet, les détecteurs chambres à fission sont largement utilisées pour mesurer le champ neutronique et ainsi permettre le contrôle du flux neutronique au sein des réacteurs. Toutefois, avec les neutrons, les rayonnements gamma sont également émis par les noyaux et détectés par les chambres à fission. Par conséquent des processus physiques sont utilisés pour ressortir le spectre neutronique désiré.

Dans cette thèse, nous proposons une nouvelle approche pour résoudre le problème de la discrimination neutron/gamma à la sortie du préamplificateur d'une chambre à fission. Il s'agit de l'application des méthodes de séparation aveugle des sources basée sur la décomposition des signaux en élément de tenseurs pour extraire les composantes indépendantes constituant les signaux délivrés par une chambre à fission.

Pour des raisons de sûreté nucléaire, nous avons procédé à la simulation du flux de neutrons à l'intérieur du réacteur TRIGA Mark II du CNESTEN à l'aide des méthodes de Monte Carlo sous Geant4 lié à Garfield++. En effet, Geant4 nous a permis la modélisation de la chambre à fission tandis que Garfield++ nous a permis de simuler les paramètres de dérive à partir de l'ionisation du gaz de remplissage. Nous avons comparé ces modèles avec ceux obtenus en utilisant interface pyFC (python-based simulation of Fission Chambers).

Mots clés: Discrimination neutron/gamma, Chambre à fission, Geant4/Garfield++, Séparation aveugle des sources, Factorisation en tenseurs nonnégatifs.

Abstract

One aspect of the safety and security of nuclear reactors is to identify the distribution of neutron flux within the reactor with the highest possible accuracy. For this purpose, fission chamber detectors are widely used to measure the neutron field and thus allow control of the neutron flux within the reactors. However, with neutrons, gamma-rays are also emitted by nuclei and detected by fission chambers. As a result, physical processes are used to bring out the desired neutron spectrum.

In this thesis, we propose a new approach to solve the problem of neutron/gamma discrimination at the output of the preamplifier of a fission chamber. It is the application of blind source separation methods based on the decomposition of tensor element signals to extract the independent components constituting the signals delivered by a fission chamber.

For nuclear safety reasons, we simulated the neutron flux inside CNESTEN's TRIGA Mark II reactor using Garfield++ bound Geant4 Monte Carlo methods. Indeed, Geant4 allowed us to model the fission chamber whereas Garfield++ allowed us to simulate the drift parameters from the ionization of the filling gas. We compared these models with those obtained using pyFC (python-based simulation of Fission Chambers).

Keywords: Neutron/gamma discrimination, Fission chamber, Geant4/Garfield++ interface, Blind source separation, Nonnegative tensor factorization.

Résumé détaillé

Les travaux de cette thèse s'inscrivent dans un projet ambitieux entre l'Équipe Sciences de la Matière et du Rayonnement (ESMaR) et le Centre National de l'Énergie, des Sciences et des Techniques Nucléaires (CNESTEN), et ont pour objectif d'améliorer les techniques de mesure du flux neutronique dans la perspective d'une meilleure estimation de ce flux dans un champ de rayonnements mixtes, en particulier auprès du réacteur de recherche TRIGA Mark II du CNESTEN.

Les recherches menées dans ce travail ont consistées à chercher les meilleurs méthodes pour discerner les neutrons des rayonnements gamma au cours du processus de détection neutronique avec la meilleure précision possible. Le problème principal de la détection neutronique est le bruit de fond. Il existe généralement trois sources de bruit de fond dans la détection des neutrons: les particules de rayonnements alpha, bêta et gamma. Les particules alpha et bêta peuvent facilement être éliminées par divers matériaux de protection (plomb, plastique, thermo-charbon, etc.). Cependant, les rayonnements gamma traversent des barrières physiques et, lorsqu'ils sont mélangés à des neutrons dans l'environnement de détection, ils se comportent presque comme des neutrons et ne permettent pas de savoir si c'est des neutrons qui sont détectés ou des rayonnements gamma. Il existe plusieurs types de détecteurs de neutrons pour estimer ce flux dans un réacteur dans des conditions d'irradiation extrême. Le détecteur à chambre à fission est largement utilisé pour surveiller ce flux au sein des réacteurs. Par ailleurs, l'analyse des signaux électriques délivrés par la chambre à fission est utilisé comme base pour contrôler et calculer certaines paramètres critiques, tels que l'énergie nucléaire, la répartition énergétique des fragments de fission, la combustion du combustible et les dommages causés aux matériaux de structure.

De puissantes méthodes plus adaptées au traitement des signaux enregistrés sont nécessaires pour extraire le signal neutronique utile du mélange enregistré. Ceci permettra d'obtenir un spectre plus net du flux neutronique. Dans ce travail de recherche appliquée, nous nous proposons de réaliser une discrimination logicielle des neutrons et des rayonnements gamma détectés en utilisant une chambre à fission installée au sein du réacteur TRIGA Mark II du CNESTEN. Il s'agit d'enregistrer les signaux de sortie du préamplificateur et de les décomposer en plusieurs composantes indépendantes en utilisant des méthodes de séparation aveugle des sources (en anglais: Blind Sources Separation (BSS)). Ces méthodes consistent à estimer, instantanément et avec précision, les signaux originaux (sources) ainsi que de retrouver la manière avec laquelle elles étaient mélangées (matrice de mélange) et ce en se basant uniquement sur les signaux enregistrés (observations). Pour des raisons de sécurité, il est impossible d'accéder directement pour ce travail aux données réelles délivrées par la chambre de fission. Pour cette raison, une conception complète et la simulation d'un détecteur de chambre à fission WL-7657 installé à l'intérieur du réacteur TRIGA Mark II du CNESTEN a été réalisé via l'interface Geant4/Garfield++. Geant4 permet la construction de la chambre tandis que le modèle à Garfield++ permet de simuler les paramètres de dérive à partir de l'ionisation du gaz de remplissage, ce qui n'est pas possible autrement. Nous avons comparé ces modèles avec ceux obtenus en utilisant interface pyFC (python-based simulation of Fission Chambers).

Les observations enregistrées à la sortie du préamplificateur d'une chambre à fission sont ensuite agencées sous forme tensorielle pour permettre leur analyse par décomposition en tenseurs nonnégatifs (NTF). Cette décomposition NTF est la plus

récente parmi les algorithmes de séparation aveugle des sources appliqués dans le domaine de traitement numérique des signaux stochastiques.

Nous avons procédé au traitement des signaux issus de la simulation de la chambre à fission. Ainsi, plusieurs algorithmes de factorisation non-négative en éléments de tenseurs ont été testés. A partir des indices de performance de séparabilité, nous avons constaté que les algorithmes NTF1 et NTF2 permettent d'aboutir à une meilleure séparation aveugle des signaux neutroniques par rapport à ceux des rayonnements gamma, une fois l'algorithme NTF défini, nous allons évaluer le rapport signal sur interférence (SIR) à partir de la matrice de mélange. Les valeurs de ce paramètre nous permettront de détecter facilement le nombre de particules. En outre, grâce au calcul des fonctions de corrélation entre les signaux sources estimés et des signaux de neutron et gamma pur, nous pouvons associer chaque source estimée à un rayonnement donné et ce pour des fins de discrimination neutron/gamma.

La thèse divisée en trois parties, et composée de six chapitres. Le premier chapitre donne un aperçu de la physique nucléaire liée à la spectrométrie neutronique, la classification neutronique et ses interactions avec la matière, les sources de neutrons et les détecteurs de neutrons Ex-core et In-core. Le deuxième chapitre présente la description théorique du fonctionnement de la chambre à fission. Par conséquent, le troisième chapitre décrit le travail effectué à l'aide d'interfacer deux boîtes à outils de simulation, Geant4 et Garfield++, en partie pour la simulation de la chambre à fission WL-7657. Le quatrième chapitre présente l'état de l'art concernant les algorithmes de séparation aveugles des sources (SAS) et leurs diverses approches en tant que techniques alternatives qui peuvent améliorer l'utilisation du signal de sortie du FC pour l'estimation "idéale" des signaux neutroniques. Le cinquième chapitre décrit la performance des méthodes conventionnelles de discrimination des formes d'impulsions (analogiques et numériques) utilisées pour séparer différents types de particules. Enfin, le sixième chapitre concerne la mise en œuvre de méthodes de factorisation en tenseurs nonnégatifs dans le traitement des signaux nucléaires ainsi la vérification du code développé, via la comparaison des résultats à ceux obtenus par pyFC (python-based simulation of Fission Chambers).

Appended papers

This thesis is an introduction to and a summary of the work published in the following papers

PAPER I

M. Laassiri, E.-M. Hamzaoui, and R. Cherkaoui El Moursli. "Application of Nonnegative Tensor Factorization for neutron-gamma discrimination of Monte Carlo simulated fission chamber's output signals". Results Phys., vol. 7 (2017), p. 1422-1426.

PAPER II

M. Laassiri, E.-M. Hamzaoui, and R. Cherkaoui El Moursli. "Nonnegative Tensor Factorization Approach Applied to Fission Chamber's Output Signals Blind Source Separation". J. Phys. Conf. Ser., vol. 966 (2018), p. 012063.

PAPER III

M. Laassiri, E.-M. Hamzaoui, and R. Cherkaoui El Moursli. "Validation of the neutron and gamma fields in the Moroccan TRIGA Mark II reactor using Nonnegative Tensor Factorization approach: Comparison of performances of the Geant4/Garfield++ and pyFC interfaces". Acta Phys. Pol. B Proc. Suppl., vol. 11 (2018), p. 73.

Contents

List of Figures

List of Tables

List of Abbreviations

ADC	**A**nalog-to-**D**igital **C**onverters
ANN	**A**rtificial **N**eural **N**etworks
AMS	**A**eroball **M**easurement **S**ystem
CC	**C**harge **C**omparison method
CENM	**N**uclear **S**tudies **C**entre of **M**aâmora
CF	**C**urve **F**itting method
CIC	**C**ompensated boron-coated **I**onization **C**hamber
CNESTEN	**N**ational **C**enter for **N**uclear **E**nergy, **S**ciences and **T**echnology
DC	**D**irect **C**urrent
DSP	**D**igital **S**ignal **P**rocessors
FC	**F**ission **C**hamber
FF	**F**ission **F**ragment
FGA	**F**requency **G**radient **A**nalysis
FOM	**F**igure **O**f **M**erit
FPGA	**F**ield **P**rogrammable **G**ate **A**rrays
HOS	**H**igher **O**rder **S**tatistics
HTFC	**H**igh **T**emperature **F**ission **C**hamber
NGD	**N**eutron/**G**amma **D**iscrimination
NGMA	**N**eutron **G**amma **M**odel **A**nalysis
NMF	**N**onnegative **M**atrix **F**actorization
NS	**N**on**S**tationarity
NTF	**N**onnegative **T**ensor **F**actorization
PARAFAC	**P**arallel **F**actor **A**nalysis
PGA	**P**ulse **G**radient **A**nalysis
PI	**P**erformance **I**ndex of Separability
PMT	**P**hoto **M**ultiplier **T**ube
PSD	**P**ulse **S**hape **D**iscrimination
RT	**R**ise **T**ime method
SDCC	**S**implified **D**igital **C**harge **C**ollection
SFR	**S**odium cooled **F**ast **R**eactor
SIR	**S**ignal to **I**nterference **R**atio
SNR	**S**ignal to **N**oise **R**atio
SOS	**S**econd **O**rder **S**tatistics
SPND	**S**elf **P**owered **N**eutron **D**etoctors
STP	**S**pace-**T**ime-**F**requency
UIC	**U**ncompensated boron-coated **I**onization **C**hamber
WT	**W**avelet **T**ransform based method
ZC	**Z**ero **C**rossing method

Introduction - Problem Description

The topic of this thesis is to discern neutron from gamma-rays during neutron detection process with the best possible precision, is considered as an important aspect in safety and security studies of nuclear reactors since the earliest days of reactor technology. Neutron studies have been an active research topic at National Center for Nuclear Energy, Sciences and Technology (CNESTEN-Morocco) since the reactor was licensed. This thesis contains the work that the author has performed during the last four years, of which 1.5 years were spent at CNESTEN. Discrimination of neutron radiation in mixed fields of gamma-ray intensity by using Nonnegative Tensor Factorization is treated in this thesis through numerical simulation of fission chamber detector. The main concepts of this technique and the outline of this thesis are presented in this thesis.

- **Problem**

Extracting the distinguishing characteristics of neutron pulses from the background gamma-rays is considered as an important aspect in safety and security studies of nuclear reactors. There are several types of neutron detectors to estimate the neutron fluence rate inside a nuclear reactor under high irradiation conditions. One widely used detector type is fission chamber detector. In addition, it is used to give an estimation of the neutron spectrum inside the reactor. The analysis of the electrical signals delivered by the fission chamber is used as a basis for monitoring and calculating some of the most critical parameters, such as nuclear power, the energy distribution of the fission fragments, fuel burn-up and damage in structural materials.

The fission chamber consists of a pair of electrodes, one of which is coated with a fissile deposit, and the space between the two electrodes being filled with a gas, usually argon mixed with a small percentage of nitrogen. When a neutron interacts with the fissile deposit and produces fission, a couple of fission fragments appear, which due to their high emerging energy are released in almost opposite directions.

One of the fragments is absorbed in the anode while the second crosses the inter-electrode space, ionizing the filling gas on its path. Fission fragments are electrically charged particles, so they produce the ionization of the gas they are crossing, resulting in production of a high number of electron-ion pairs.

A DC voltage is applied to the electrodes producing an electric field, involving a migration of charges, the movement of those charges within the electric field produces a pulse signal that can be amplified and processed.

The DC voltage between the electrodes must be sufficient to collect all the charges, and low enough to avoid secondary ionization pairs. If both conditions are achieved, the fission chamber operates in the so-called saturation regime, for which the neutron induced current signal is proportional to the fission rate which, in turn, is proportional to the neutron flux. In addition, one can note that the gamma-ray particles that directly ionize the filling gas also generate a signal and introduce unwanted backgrounds in neutron spectra. For this reason, powerful extraction methods are needed to extract useful neutron signal from recorded mixture and thus to obtain clearer neutron flux spectrum. In particular, much research is being carried out these

years on the discrimination of neutron pulses from the gamma-rays in the detection environment. Most of these research use analog or digital pulse shape discrimination (PSD) methods. The research effort reported in this thesis is focused on the application of blind source separation (BSS) methods to discriminate real neutron from gamma-rays pulses.

- **Motivation**

The motivation of this work was to apply Nonnegative Tensor Factorization (NTF) algorithms to extract useful neutron signal from recorded mixture and thus to obtain clearer neutron flux spectrum. In this study, a full design and simulation of a WL-7657 fission chamber detector installed inside the TRIGA Mark II reactor of CNESTEN has been achieved using Geant4/Garfield++ interface. The code developed is capable to simulate accurately the most remarkable physical processes taking place in a fission chamber; from the transport parameters to the induced electrical signal and the verification of the code through comparison with the results of pyFC (python-based simulation of Fission Chambers).

- **Outline**

This thesis is divided into six chapters. First, Chapter 1 provides an overview of nuclear physics related to neutron spectrometry, neutron classification and its interaction with matter, neutron sources and Ex-core and In-core neutron detectors. Then, Chapter 2 describes the main characteristics of fission chambers, operation modes and electrical signals based on Paper I and Paper II. Chapter 3 presents the Geant4/Garfield++ interface and its application to simulate the fission chamber, which is based on Paper I. Then, Chapter 4 presents the state of the art about Blind Source Separation (BSS) algorithms and their various approaches as alternative techniques which may improve the use of FC's output signal for the "ideal" estimation of neutron signals. The Chapter 5 investigates the performance of the conventional pulse shape discrimination methods (analog and digital) used to separate different kinds of particles. It is shown that the digital methods offer significant advantages over the analog methods. Finally, Chapter 6 presents the implementation of Nonnegative Tensor Factorization methods in nuclear signal processing and a verification of our implementation through comparison with the results of pyFC (python-based simulation of Fission Chambers), based on Paper III.

Part I

Neutron signal generalities

Chapter 1

Neutron spectrometry

1.1 Introduction

Neutrons are neutral particles; their interactions with matter do not fall under Coulomb interactions as for charged particles. Neutrons interact with the nuclear particles predominantly via the nuclear force, which has an extremely short range. Being neutral particles, neutrons can pass close to the nucleus and penetrate matter until they undergo strong interactions with a nucleus and lose their energy (slowing down). This slowing down process is referred to as moderation and the material used for the purpose of thermalizing neutrons is called a moderator. The energy loss of neutrons is mainly due to scattering or absorption.

1.2 Neutron classification

The neutron is an indirectly ionizing particle. It is indirectly ionizing because it does not carry any electrical charge and hence it is not affected by the electric field of the atoms. They can be classified according to their speed. This speed is usually defined by υ and generally quoted in units of ms^{-1} [1]. At this speed, this corresponds to the non-relativistic domain, where the kinetic energy E_k, given by the formula:

$$E_k = \frac{1}{2}mv^2 \tag{1.1}$$

This energy is usually given in electron volts (eV).

The neutron energy can vary from a few electron-volts or a fraction electron-volts (eV), especially for so-called thermal neutrons (0.025 eV) to a few to a few tens of MeV for fast neutrons (1 - 10 MeV). Followed by the ranges of neutron energies define the different classes of neutrons:

Low or medium energy neutron:

- **Thermal Neutrons** have energy very low and equal to 3/2 kT (where k is the Boltzmann's constant and T is the temperature in Kelvin), i.e. 0.025 eV at 298 °k. This part of neutron's energy spectrum constitutes most important part of spectrum in thermal reactors.

- **Epithermal Neutrons** have energy between a few eV to 100 keV. Some of nuclear reactors designs operate with epithermal neutrons. This design (as compared with thermal reactors) allows to reach higher fuel breeding ratio.
- **Intermediate Neutrons** have energy between 100 keV to 1 MeV.

High energy neutron:

- **Fast Neutrons** have energy above 1 MeV and are usually named fission neutrons. These neutrons are produced by nuclear processes in particular nuclear fission. The fission neutrons have a mean energy (for ^{235}U fission) of 2 MeV. Inside a nuclear reactor the fast neutrons are slowed down to the thermal energies by the process of moderation.
- **Relativistic Neutrons** have energy higher than 90 MeV.

1.2.1 Interaction of neutrons with matter

For thermal to fast neutrons, neutrons may interact with nucleus via two possible types of interactions which are explained in the following:

- **Scattering** (elastic or inelastic) by a nucleus, with total cross section $\sigma_{Sca} = \sigma_{el} + \sigma_{inel}$. This process is only important at very fast neutron energies, one of whose products is a neutron (neutron conservation). The slowing down of fast neutrons is all the more effective when target nuclei have a mass close to that of the neutron.
- **Absorption** is the most important type of reactions that take place in thermal neutron energies. The neutron is completely absorbed by the target nucleus and produces electromagnetic particles and charged particles without causing fission (neutron disappearance).

$$\sigma_{total} = \sigma_{scattering} + \sigma_{absorption} \tag{1.2}$$

1.2.1.1 Elastic scattering (n, n)

Elastic scattering is the most frequent mode of interaction of neutrons with nuclei. In this interaction the target nucleus remains in the same state after scattering. This process can be written either as:

$$A(n,n)A \tag{1.3}$$

Or

$$^{1}_{0}n + ^{A}_{Z}X \rightarrow ^{1}_{0}n + ^{A}_{Z}X \tag{1.4}$$

Generally, an elastic scattering of neutrons by nuclei can occurs in two different modes: potential elastic and resonance elastic. In potential elastic, neutron scatters off of the nucleus without interacting with the particles inside, by means of the effect of short range nuclear forces of the nucleus. In resonance elastic, a neutron with the right amount of energy is absorbed by the nucleus, followed by the re-emission of another neutron to conserve the kinetic energy and the nucleus returns to its ground state [1]. Fig. 1.1 presents the elastic cross sections for ^{235}U, ^{238}U and ^{239}Pu computed from ENDF-B-VII-1.

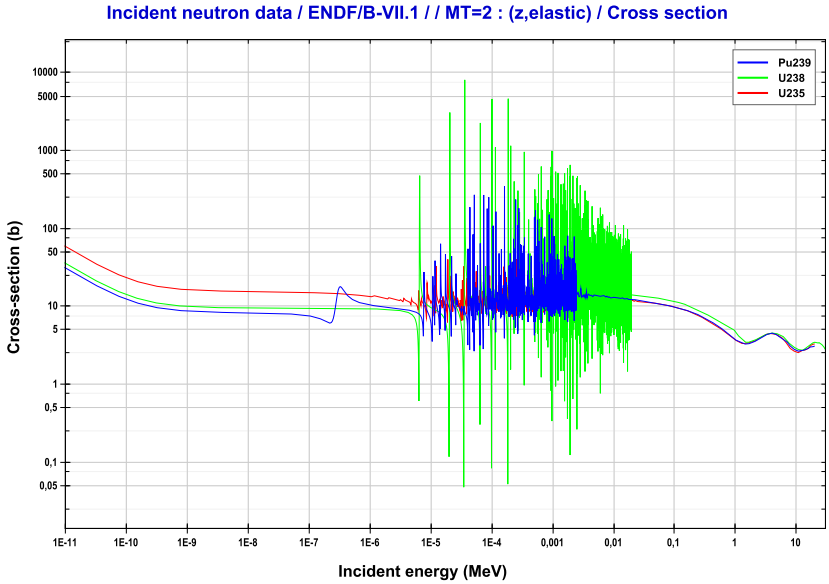

FIGURE 1.1: The elastic cross sections for ^{235}U, ^{238}U and ^{239}Pu computed from ENDF- B-VII-1 [2].

1.2.1.2 Inelastic scattering (n, n'γ)

Inelastic scattering occurs with the formation of an intermediate nucleus called the "compound nucleus". The incident neutron is absorbed by the target nucleus, forming a compound nucleus, which decays after about 10^{-17}s, by emitting a neutron of lower kinetic energy which leaves the residual nucleus in an excited state. The residual nucleus returns to the ground state by the emission of one or more gamma-rays. This process can be written as:

$$A(n, n'\gamma)A \tag{1.5}$$

Or

$${}^{1}_{0}n + {}^{A}_{Z}X \rightarrow {}^{A+1}_{Z}X^{*} \rightarrow {}^{1}_{0}n' + {}^{A}_{Z}X^{*} \tag{1.6}$$

Then

$${}^{A}_{Z}X^{*} \rightarrow {}^{A}_{Z}X + \gamma \tag{1.7}$$

In an inelastic scattering reaction, momentum and total energy are conserved, but kinetic energy is not. Indeed, a part of the kinetic energy of the incident neutron is transformed into excitation energy of the residual nucleus. These reactions are only possible for fast neutrons because the energy of slow neutrons is generally not sufficient to feed the excited states of the nucleus. Fig. 1.2 presents the inelastic cross sections for ^{235}U, ^{238}U and ^{239}Pu computed from ENDF-B-VII-1.

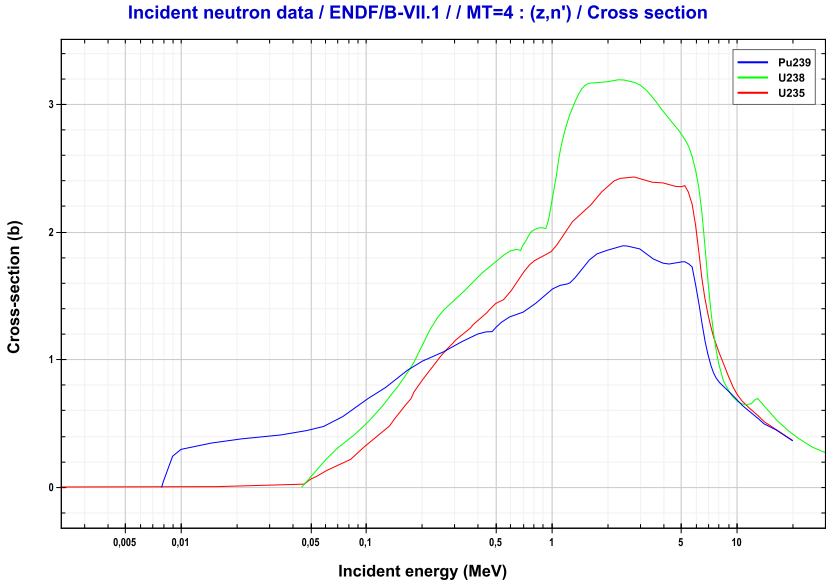

FIGURE 1.2: The inelastic cross sections for ^{235}U, ^{238}U and ^{239}Pu computed from ENDF- B-VII-1 [2].

1.2.1.3 Transmutation (n, Charged particle)

A nucleus may absorb a neutron forming a compound nucleus that will de-excited by emitting a charged particle (proton, alpha particle). A different nucleus is produced by this reaction called transmutation. Transmutation is the transformation of one element into another by a nuclear reaction [3]. Fig. 1.3 shows one of the most important neutron-induced transmutation reactions in the nuclear industry. ^{238}U (uranium), by capturing a neutron, is transformed into ^{239}U (uranium). The half-life of ^{239}U is approximately 23.5 minutes. ^{239}U decays (negative beta decay) to ^{239}Np (neptunium), whose half-life is 2.36 days. ^{239}Np decays (negative beta decay) to ^{239}Pu (plutonium), which takes 24 110 years to lose half of its mass by radioactive decay.

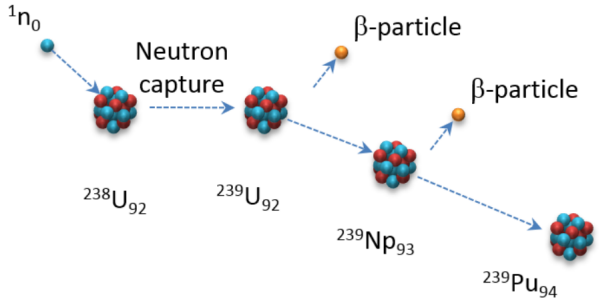

FIGURE 1.3: Schematic example of neutron-induced transmutation of ^{238}U into ^{239}Pu.

1.2.1.4 Radiative capture (n, γ)

In this case, the neutron is absorbed by the target nucleus to form a compound nucleus that will de-excite by emitting one or more gamma-rays in general of high energy (some MeV). This process can be written as:

$$ {}^{1}_{0}n + {}^{A}_{Z}X \rightarrow {}^{A+1}_{Z}X^{*} \rightarrow {}^{A+1}_{Z}X + \gamma \tag{1.8} $$

Fig. 1.4 presents the radiative capture cross sections for ^{235}U, ^{238}U and ^{239}Pu computed from ENDF-B-VII-1 and Fig. 1.5 shows the scheme of a generic radiative neutron capture.

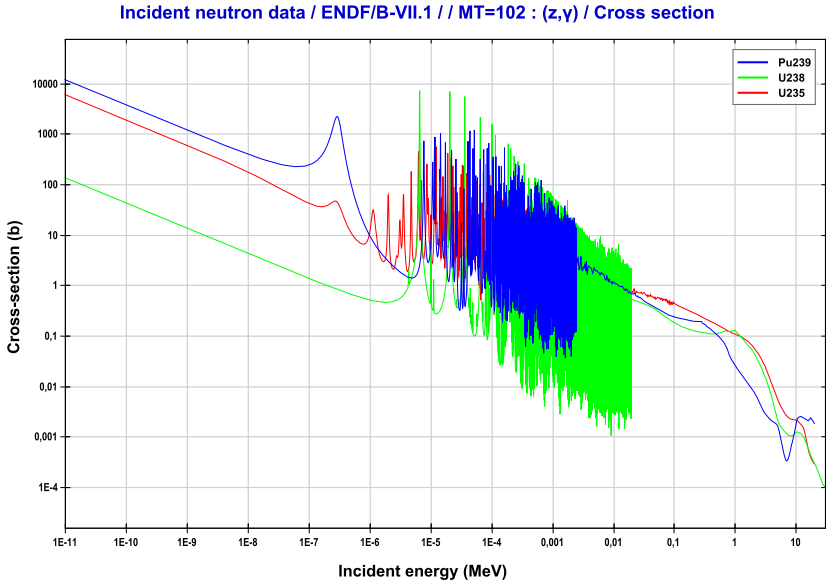

FIGURE 1.4: The radiative capture cross sections for ^{235}U, ^{238}U and ^{239}Pu computed from ENDF- B-VII-1 [2].

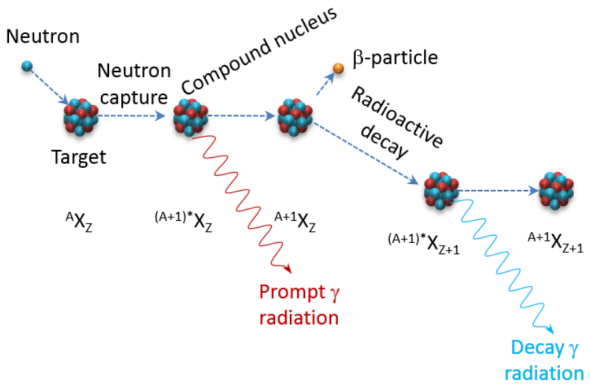

FIGURE 1.5: Scheme of the generic radiative neutron capture.

1.2.1.5 Spallation reaction

Spallation is a nuclear reaction that occurs when a high energy projectile (usually proton, neutron and alpha particle) interacts with a heavy nucleus; the nucleus that has absorbed the projectile is fragmented into several parts. It leads to the ejection of a number of particles many of which are light (mainly neutrons) [3]. Fig. 1.6 shows the spallation process in which the bombardment of a heavy metal atom by a proton causes the ejection of neutrons and protons.

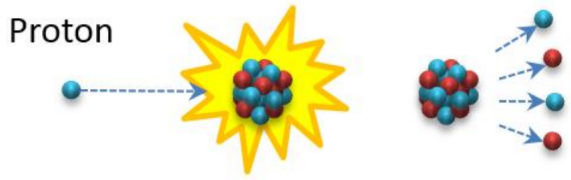

FIGURE 1.6: Spallation process induced by a proton upon a heavy metal atom.

1.2.1.6 Fission (n, f)

The nuclear fission reactions are of two types: spontaneous fission and induced fission. The first occurs spontaneously without the prior use of a projectile. They concern very heavy unstable nuclei (Z > 98), artificial for the most part, which have an excess of nucleons (neutrons and protons) such as ^{238}U and ^{252}Cf. In this case, the nucleus is unbalanced and splits into two lighter isotopes but still unstable, nuclei named fission products or fission fragments [4]. In addition to the fission products, the fission process often produces free neutrons and gamma-rays, with a large release of energy. This process can be written as:

$$ {}^{A}_{Z}X \rightarrow {}^{A1}_{Z1}FP1 + {}^{A2}_{Z2}FP2 + \bar{\upsilon} \quad neutrons \tag{1.9} $$

where $\bar{\upsilon}$ is defined as the number of neutrons emitted per fission.

The induced fission can be caused either by slow (thermal) neutrons or fast neutrons. This is called thermal or fast fission respectively. However the probability of achieving fission of slow neutrons is higher due to the bigger fission cross section of most of the fissile isotopes [4]. This is particularly true in the most popular fissile isotopes having an odd number of neutrons such as ^{233}U, ^{235}U, ^{239}Pu and ^{241}Pu. In this process a slow neutron is captured by a heavy nucleus, such as those mentioned before, taking it into an excited state [3]. The nucleus then splits into two fragments after a brief delay. This process can be written as:

$$ {}^{1}_{0}n + {}^{A}_{Z}X \rightarrow {}^{A1}_{Z1}\,FP1 + {}^{A2}_{Z2}\,FP2 + \bar{v} \quad neutrons + Energy \tag{1.10} $$

where $\bar{v}$ is defined as the number of neutrons emitted per fission, ranging from 0 to about 7. Typically, the number is 2 or 3.

In these reactions, the absorption of the neutron causes a resonant excitation of all nucleons, the nucleus deforms and splits into two nuclei (sometimes more) called fission fragments releasing between 2 and 3 neutrons on average (2.4355 ± 0.0023). Gamma-rays are also emitted, almost simultaneously and instantly with the fission-prompt particles (neutrons and gammas). Finally, some microseconds to a few tens of seconds after the fission reaction, some fission products emitted are invariably still unstable with too many neutrons and subsequently decay by β^- particle and gamma-ray emission followed by the emission of so-called delayed neutrons [4].

The fission process leads to a large catalogue of isotopes called fission products or fission fragments (FF). They are heavy charged particles with energies of several tens of MeV (∼90 MeV). These heavy charged particles are emitted in opposite directions and are strongly ionizing. Their interactions with the atomic nuclei cause ionizations and excitations that is used to detect the neutron through the collection of charges produced. The detectors that use the fission reaction to detect neutrons are called fission chambers and they are widely used to measure neutron flux in the experimental reactors and power reactors. Fig. 1.7 schematically shows this process.

The reaction commonly used in this type of detectors is the fission of ^{235}U.

$$ {}^{1}_{0}n + {}^{235}_{92}U \rightarrow \left({}^{236}_{92}U^{*}\right) \rightarrow FP1 + FP2 + 2 \quad to \quad 3 \quad neutrons + 194 \quad MeV \tag{1.11} $$

In the case of ^{235}U, nuclear fission creates a wide variety of fission fragments, such as

$$ {}^{1}_{0}\mathrm{n} + {}^{235}_{92}\mathrm{U} \longrightarrow {}^{236}_{92}\mathrm{U}^{*} \xrightarrow{85\,\%\ \text{nuclear fission}} \begin{cases} {}^{144}_{56}\mathrm{Ba} + {}^{89}_{36}\mathrm{Kr} + 3\,{}^{1}_{0}\mathrm{n} \\ {}^{144}_{55}\mathrm{Cs} + {}^{90}_{37}\mathrm{Rb} + 2\,{}^{1}_{0}\mathrm{n} \\ {}^{140}_{54}\mathrm{Xe} + {}^{94}_{38}\mathrm{Sr} + 2\,{}^{1}_{0}\mathrm{n} \\ {}^{146}_{57}\mathrm{La} + {}^{87}_{35}\mathrm{Br} + 3\,{}^{1}_{0}\mathrm{n} \\ {}^{160}_{62}\mathrm{Sm} + {}^{72}_{30}\mathrm{Zn} + 4\,{}^{1}_{0}\mathrm{n} \end{cases} \tag{1.12} $$

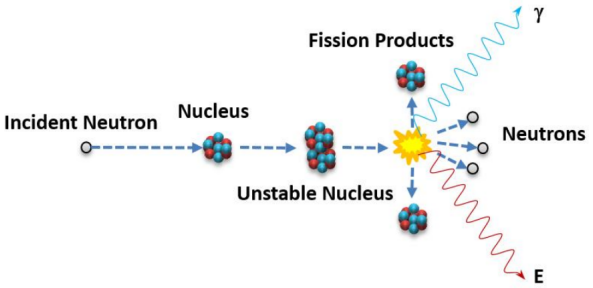

FIGURE 1.7: Schematic representation of a fission reaction of a fissionable isotope.

1.2.2 Cross section

Neutron interaction with matter can be either scattering or absorption reactions. The probability of occurrence of these reactions is primarily dependent on the energy of the neutrons and on the properties of the nucleus with which it is interacting. The standard unit for measuring the microscopic cross section (σ) is the barn, which is equal to 10^{-24} cm^2. The macroscopic cross section is also defined by the relation $\sum(cm^{-1}) = N\sigma$. Where N is the nuclei density. The sum of the cross sections for all possible types of neutron interactions is called total cross section $\sigma_t = \sum_i \sigma_i$.

$$\sigma_t = \sigma_s + \sigma_a + \sigma_\gamma + \sigma_f \tag{1.13}$$

Where $\sigma_s, \sigma_a, \sigma_\gamma$, and σ_f are the scattering cross section (elastic and inelastic), absorption cross section, radiative capture cross section and fission cross section, respectively. Fig. 1.8 presents the total cross sections for ^{235}U, ^{238}U and ^{239}Pu computed from ENDF-B-VII-1.

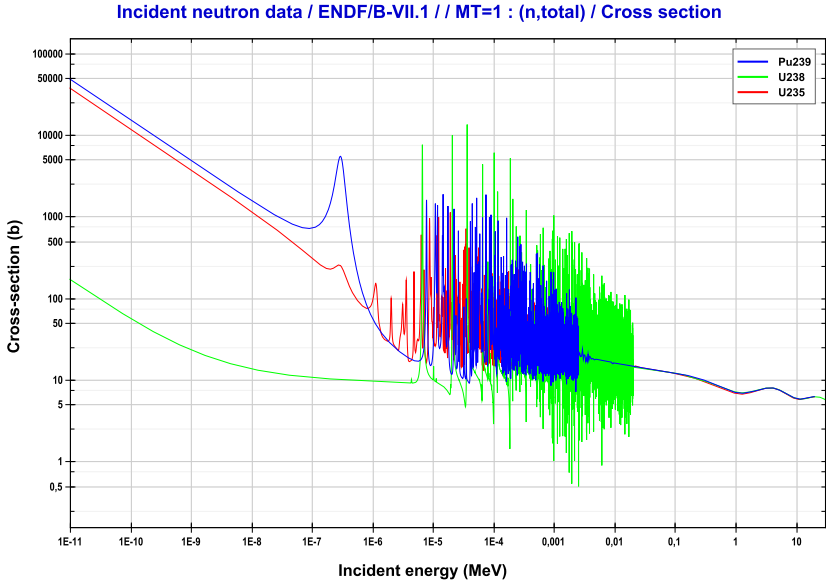

FIGURE 1.8: The total cross sections for ^{235}U, ^{238}U and ^{239}Pu computed from ENDF- B-VII-1 [2].

1.3 Neutron sources

Radioisotopes, as conventional neutron sources, do not exist in the same way that gamma-ray sources are available from many different nuclei populated by beta decay. The possible choices for radioisotope neutron sources are usually limited and fall into two main categories: spontaneous fission and nuclear reactions for which the incident particle is the product of a conventional decay process. The principle sources of neutrons in reactors are based on the fission reaction. However, in other applications of neutronics, other neutron sources can be implemented; and, even in a reactor, it is necessary to initiate the chain reaction by a source other than neutron induced fission.

There are several heavy nuclei that have an appreciable spontaneous fission decay probability. Each fission event produces several fast neutrons, thus a sample of such a radionuclide can be a convenient isotopic neutron source. Other products of fission process are the heavy fission products, prompt fission gamma-rays, and the beta and gamma activity of the fission products accumulated within the sample. When used as a neutron source, the isotope is usually encapsulated in a sufficiently thick container so that only neutrons and gamma-rays emerge from the source.

1.3.1 Spontaneous fission

Certain transuranic heavy nuclides (i.e. $^{252}_{98}$Cf or $^{248}_{96}$Cm) exhibit fission even in the ground state (without the addition of energy or a bombarding particle). This phenomena is known as the spontaneous fission and releasing neutrons as a result of this process.

$^{252}_{98}$Cf: $T_{1/2}$ = 2.645 years, decay by alpha emission (96.91 % probability) and spontaneous fission (3.09 % probability) releasing 3.7 ± 1.2 neutrons per fission event. ^{252}Cf emits $2.314{\cdot}10^{6}$ $neutrons$ $s^{-1}\mu g^{-1}$, its specific activity is 0.536 $mCi\mu g^{-1}$, is $1.98{\cdot}10^{7} Bq\mu g^{-1}$, i.e. a source de $1g$ of ^{252}Cf emits many neutrons as a power reactor [5].

$^{248}_{96}$Cm: $T_{1/2} = 3.4 \cdot 10^{5}$ years, specific activity is $1.57{\cdot}10^{5} Bqmg^{-1}$, decay by spontaneous fission (8.39 % probability) releasing 3.1 ± 1.2 neutrons per fission event. ^{248}Cm emits $\sim 4.1{\cdot}10^{5}$ $neutrons$ $s^{-1}mg^{-1}$; the lower neutron flux intensity of this source limits the application, although it has the advantage of a very long half-life providing invariability of sample intensity with time [6].

^{252}Cf is one of the most common spontaneous fission sources used in nuclear research [7]; it is an intense neutron emitter ($2.314{\cdot}10^{6}$ $neutrons$ $s^{-1}\mu g^{-1}$) that is usually doubly encapsulated in cylindrical capsules. Regarding the manufacture, the sources of ^{252}Cf contain very little active ingredient (usually a few micrograms). The spontaneous fission competes with alpha decay as the dominant decay mode (The alpha emission rate is about 32 times that for spontaneous fission), as shown in Fig. 1.9. In addition, one fission decay of ^{252}Cf emits about 3.8 neutrons and gamma-rays on average. Most of these gamma-rays (> 85 %) are relatively high-energy prompt gamma-rays that are emitted within the first nanosecond following the fission event.

Each fission produces two fission fragments, which, by the conservation of momentum, are emitted in opposite direction; only one fragment per fission can escape from the surface, while the second one is lost by absorption within the backing. The fission fragments are medium-weight positive ions with a mass distribution illustrated

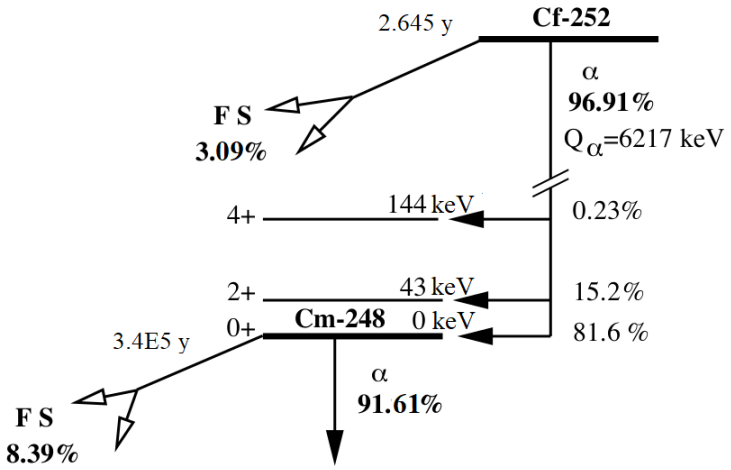

FIGURE 1.9: The mode of decay of ^{252}Cf and ^{248}Cm.

in Fig. 1.10 compared to that from ^{235}U fission. The fission is predominantly asymmetric so that the fragments tend to cluster into a light and heavy group, with average mass numbers of 108 and 143. The energy shared by the two fission fragments average of about 185 MeV.

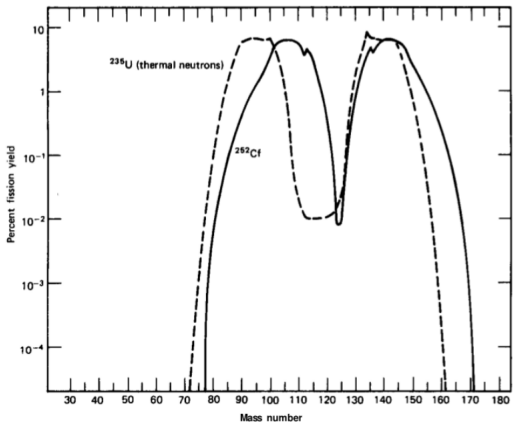

FIGURE 1.10: The mass distribution of ^{252}Cf spontaneous fission fragments compared to thermal neutron fission of ^{235}U.

The ^{252}Cf can also be used to produce a spectrum with a high thermal neutron component. One of the most used methods is to place a neutron moderator material around the source: its role is to "thermalize" the neutrons emitted by the source. In general, the moderator materials are characterized by three variables:

- The Average Logarithmic Energy Decrement ξ;
- The Macroscopic Slowing Down Power (MSDP);
- The Moderating Ratio (MR).

It is customary to place a ^{252}Cf source at the centre of a heavy-water (D_2O) sphere, because heavy-water absorbs much fewer neutrons than ordinary water. Indeed, heavy-water has a very high moderating ratio (of the order of 12000) and is therefore an excellent choice as a moderator material.

Part of our work was carried out on the modelling of the WL-7657 fission chamber detection system installed in the TRIGA Mark II reactor of the National Center for Nuclear Energy, Sciences and Technology (CNESTEN). We used the ^{252}Cf source as a neutron source. It is important to note that the ^{252}Cf source is also generating mixed neutron gamma-ray field, which can complicate neutron spectrum analysis, for that reason the neutron/gamma discrimination methods must be used in order to properly exploit neutron spectra.

1.3.2 Radioisotope (α, n) sources

Because the most energetic alpha particles are available from the direct alpha decay of a number of convenient radionuclides, it is possible to produce a neutron source by using a particle accelerator such as an alpha particle to bombard a suitable target material. Various different target materials can be used in (α, n) reactions for the alpha particle energies that are readily available in radioactive decay [7, 8]. The largest yield of neutron is obtained when beryllium is used in (α, n) reaction as a target, and neutron are produced by the following exothermic reaction:

$$^{4}_{2}He + ^{9}_{4}Be \rightarrow ^{12}_{6}C + n \quad Q - value = +5.71 \quad MeV \tag{1.14}$$

This reaction is commonly abbreviated as ^{9}Be(α, n)^{12}C, or just Be(α, n).

The yield of neutrons from an (α, n) reaction, when a beam of alpha particles interact with a target nucleus that is thick compared with their range, is shown in Fig. 1.11.

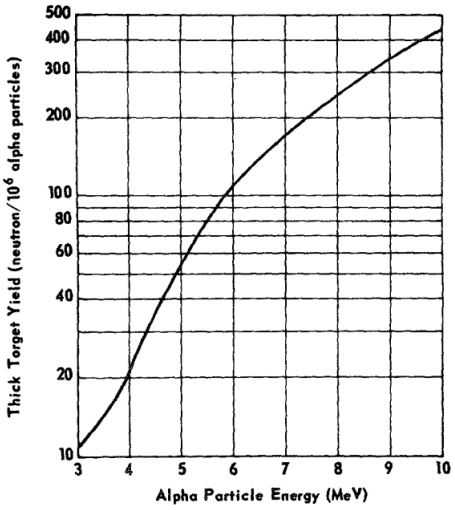

FIGURE 1.11: Thick target yield of neutrons for alpha particles on beryllium.

Most of the alpha particles are simply stopped in the target material and only 1 in about 10^4 reacts with the Be nucleus. From a practical point of view, all alpha emitters are actinides except from polonium in PoBe and radium in RaBe. Investigations have shown that a stable alloy can formed between the actinides and beryllium of the form MBe13 (M = actinide metal) [7]. Most of the existing sources described below (Table 1.1), are metallurgically manufactured in the form of this alloy, and each alpha particle has a possibility to interact with Be nuclei without any intermediate energy loss.

TABLE 1.1: Characteristics of Be(α, n) neutron sources

			Neutron yield			
Source	**Half-time**	E_α **(MeV)**	**Calculated** ($s^{-1}Bq^{-1}$)	**Experimental** ($s^{-1}Bq^{-1}$)	**Calculated** ($s^{-1}Ci^{-1}$)	**Gamma dose @ 1 m for 10^6 neutrons per second (mGy)**
^{239}Pu-Be	24000 y	5.14	$6.5 \cdot 10^{-5}$	$5.7 \cdot 10^{-5}$	$2.41 \cdot 10^{6}$	<0.01
^{210}Po-Be	138 d	5.30	$7.3 \cdot 10^{-5}$	$6.9 \cdot 10^{-5}$	$2.55 \cdot 10^{6}$	<0.001
^{238}Pu-Be	87.4 y	5.48	$7.6 \cdot 10^{-5}$	-	$2.92 \cdot 10^{6}$	<0.01
^{241}Am-Be	433 y	5.48	$8.2 \cdot 10^{-5}$	$7.0 \cdot 10^{-5}$	$3.03 \cdot 10^{6}$	0.01
^{244}Cm-Be	18 y	5.79	$1.0 \cdot 10^{-4}$	-	$3.70 \cdot 10^{6}$	<0.01
^{242}Cm-Be	162 d	6.10	$1.18 \cdot 10^{-4}$	$1.06 \cdot 10^{-5}$		<0.01
^{226}Ra-Be + daughters	1602 y	Multiple	$5.02 \cdot 10^{-4}$	-	$1.86 \cdot 10^{7}$	0.5
^{227}Ac-Be + daughters	21.6 y	Multiple	$7.02 \cdot 10^{-4}$	-	$2.59 \cdot 10^{7}$	0.7

The neutron energy spectra of all alpha/Be sources are pretty much similar, and any differences reflect only the small variations in the primary alpha energies. The neutron spectrum from the ^{239}Pu-Be source is shown in Fig. 1.12.

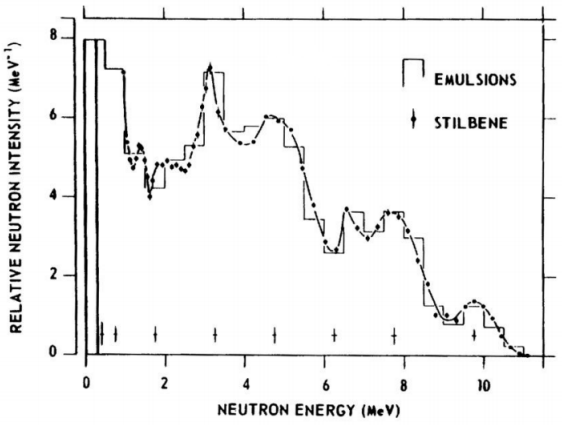

FIGURE 1.12: Measured energy spectra for neutrons from a ^{239}Pu-Be source containing 80g of the isotope.

1.3.3 Photoneutron (γ, n) sources

In contrast to the (α, n) reaction, which emits a spectrum of neutron energies, the (γ, n) reaction can also be used to produce monoenergetic neutrons (for monoenergetic gamma-rays) when combined with a suitable target material. The resulting photoneutron sources are based on supplying sufficient excitation energy to a target nucleus by absorption of a gamma-ray to emit a free neutron [7, 8]. Only two target nuclei are practical: ^{9}Be and ^{2}H. The photo-disintegration reactions in beryllium and deuterium can be written as:

$$^{9}_{4}Be + \gamma \rightarrow ^{8}_{4}Be + ^{1}_{0}n \quad Q - value = -1.6666 \quad MeV \tag{1.15}$$

$$^{2}_{1}H + \gamma \rightarrow ^{1}_{1} H + ^{1}_{0} n \quad Q - value = -2.226 \quad MeV \tag{1.16}$$

Because the incident gamma-rays are monoenergetic, the neutron spectrum will also be monoenergetic based on the conservation of energy and momentum. That means these reactions are endothermic in nature and the energy of neutrons is given by [9]:

$$E_n = \frac{A-1}{A}[E_\gamma - Q - \frac{E_\gamma^2}{1862(A-1)}] + \delta \tag{1.17}$$

Where E_n is the energy of the neutrons in MeV, A is the mass number of the target material, E_γ is the energy of the gamma-rays in MeV, and Q is the threshold energy in MeV for the (γ, n) reaction in the nucleus of mass A, δ is a small spread in energy and is a function of the angle θ between the direction of the impinging gamma-ray and the direction in which the neutron is emitted, it is given by:

$$\delta \simeq E_\gamma [\frac{2(A-1)(E_\gamma - Q)}{931 * A^3}]^{1/2} \quad cos(\theta) \tag{1.18}$$

1.3.4 Neutron production by other means

Sources produced by using radioactivity induced reaction are theoretically sufficient to start the chain reaction process in a reactor. An intense source is introduced in order to follow the divergence by neutron flux measurement until a significant power is reached, then the source can be removed or left in place, since the chain reaction of induced fissions becomes preponderant.

Auxiliary neutron sources usually are made by mixing an alpha or gamma emitter with beryllium. The reactions which produce the neutron are the (α, n) or the (γ, n) reactions with ^{9}Be. The binding energy of the last neutron in ^{9}Be is sufficiently low to enable it to be ejected relatively easily [10].

Some applications require more intense sources, it is the Deuterium–Tritium (D-T) reaction that is most often used; the usual technique is to accelerate deuterons (obtained by deuterium ionization) in which tritium is absorbed. Neutrons are generated through the following exothermic reaction:

$$D + T \rightarrow ^{4}_{2}He + ^{1}_{0} n + 17.59 \quad MeV \tag{1.19}$$

Neutrons can also be produced by the spallation process, in which a light projectile (proton, neutron, or light nucleus) that has been accelerated to high energies hit a heavy target material, causing the emission of a large numbers of neutrons. Spallation has two stages: intra-nuclear cascade and de-excitation [11–13]:

- First fast stage ($\sim 10^{-22}$s) is called Intra-Nuclear Cascade; the incoming nucleon makes a few, mainly incoherent scattering with nucleons of the target nucleus, depositing in this way some fraction of its energy. The incoming nucleon sees

the substructure of the nucleus, i.e. a bundle of nucleons, due to the reduced wavelength. This fast stage of nucleon-nucleon scattering interaction leads to the ejection of some of the nucleons and to the excitation of the residual nucleus which will cool itself afterwards (in the second stage).

- Second slow stage ($\sim 10^{-16}$s); the de-excitation of the residual nucleus can proceed in two main ways: evaporation and fission. The evaporation is the dedicated de-excitation channel and the excited nucleus emits nucleons (mainly neutrons) or light and heavy ions (D, T, He, Li, Be, B, ..., γ). The second important de-excitation mode is fission. In the fission process the nucleus is ultimately splits into two fragments of different masses. Generally the fate of the nucleus is its fragmentation.

Globally, the incident proton induces the production of a large amount of neutrons with wide energy spectra. These neutrons can be used for transmutation of relevant nuclei.

1.4 Detection of neutron

The reactor instrumentation has two objectives: the first is to allow the optimal exploitation of reactor (including the safety and security of the reactor core) and the second is to allow, after an event of an accident or equipment failure, to have residual information about the state of the core. For these last two objectives, it is important to discern neutron flux distribution inside and outside the reactor with the best possible precision. The two main types of detectors which are intended to measure the neutron flux are ex-core and in-core neutron detectors. In-core neutron detectors are those that are located inside the core and are used to provide information of the flux shape within the core. Ex-core neutron detectors are located outside the core and thus respond to properties of the neutron flux integrated over the entire core [7].

Neutron flux measurement use converters because the neutron is an indirectly ionizing particle. The converter materials and associated reactions, commonly used in neutron detectors, are:

- Helium 3 (^{3}He), ^{3}He(n, ^{1}H)^{3}H reaction, with a quantity of energy released Q = 0.764 MeV:

$$^3_2He + ^1_0n \rightarrow ^1_1H + ^3_1H \tag{1.20}$$

- Boron 10 (^{10}Be), ^{10}Be(n, α)^{7}Li reaction, with Q = 2.792 MeV:

$$^{10}_5B + ^1_0n \rightarrow \begin{cases} ^4_2\text{He} + ^7_3\text{Li} \;\; (2.792\,\text{MeV}) \quad 6\% \quad (ground \quad state) \\ ^4_2\text{He} + ^7_3\text{Li}^* \;\; (2.310\,\text{MeV}) \quad 94\% \quad (excited \quad state) \end{cases} \tag{1.21}$$

$$^7_3Li^* \rightarrow ^7_3Li + \gamma \quad (0.48 \quad MeV)$$

- Uranium 235 (^{235}U), ^{235}U(n, f) reaction, with Q ≈ 200 MeV:

$$^{235}_{92}U + ^{1}_{0}n \rightarrow FP1 + FP2 + 2.5 \quad ^{1}_{0}n \tag{1.22}$$

- Lithium 6 (^{6}Li), ^{6}Li(n, α)^{3}H reaction, with Q ≈ 4.78 MeV:

$$^{6}_{3}Li + ^{1}_{0}n \rightarrow ^{4}_{2}\alpha + ^{3}_{1}H \tag{1.23}$$

The energy released by these reactions is carried away as kinetic energy of the reaction products whose charged particles (nuclei of ^{1}H, ^{3}H, ^{4}He, ^{7}Li, α and fission products) that ionize the gas, thus leading to the formation of the electrical detection signal. Fig. 1.13 presents the total cross sections for ^{3}He, ^{10}B, ^{6}Li and ^{235}U computed from ENDF-B-VII-1.

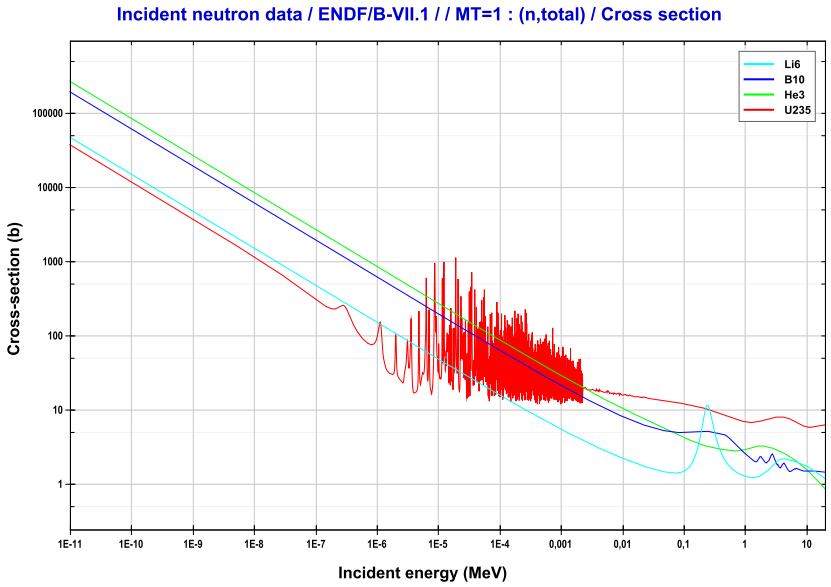

FIGURE 1.13: The total cross sections for ^{3}He, ^{10}B, ^{6}Li and ^{235}U computed from ENDF-B-VII-1 [2].

1.4.1 Ex-core neutron detectors

In research reactors, the neutron flux has to be monitored from a low level to full power level. The detected flux is about 10 to 12 orders of magnitude and is typically divided into three subranges, source range, also known as "start-up" (below 10^4 nv, equivalent to 10^{-3} percent of nominal power), intermediate range (from 10^3 to 10^9 nv, or 10^{-4} to 10^2 percent of nominal power), and power range (from 10^7 to $2{\cdot}10^9$ nv, or 1 to 200 percent of nominal power) [10] as shown in Table 1.2. In the source range interval, due to the low rate of events occurring within the detector, pulse mode is traditionally used, whereas the current mode is adopted in the intermediate and power range intervals.

TABLE 1.2: Typical ranges covered by Ex-core neutron detectors [10]

Power (%)	10^{-7}	10^{-6}	10^{-5}	10^{-4}	10^{-3}	10^{-2}	10^{-1}	10^{0}	10^{1}	10^{2}	10^{3}
Thermal neutron Flux $(n/cm^2/s)$	10^{0}	10^{1}	10^{2}	10^{3}	10^{4}	10^{5}	10^{6}	10^{7}	10^{8}	10^{9}	10^{10}
Decade	1	1	1	1	1	1	1	1	1	1	
Start-up		→									
Intermediate				→							
Power								→			

1.4.1.1 Boron (^{10}B) coated proportional counters

The boron-10 coated proportional counters are a type of gas-filled neutron detectors used in a pulse mode and designed to measure the neutron flux in the source range. These detectors are an ideal solution for neutron detection in mixed radiation field. With the correct choice of electronics and discriminator settings these detectors are operable in a gamma flux of 10 R/h with an approximate 10 % loss in neutron sensitivity [14]. These detectors are also widely used to spent nuclear fuel measurements in safeguards.

1.4.1.2 Boron (^{10}B) coated ionization chambers

Ionization chambers are normally used in ex-core reactor to measure neutron flux distribution and provide on-line evaluation of the reactor power for both control and safety [15]. Since neutrons are indirectly ionizing particles, neutron sensitivity is obtained by introducing some sensitive material with which neutrons interact to produce ionizing particles. For example, the electrodes may be coated with a suitable material such as boron (^{10}B). The isotope ^{10}B has a high thermal neutron cross section for the ^{10}Be(n, α)^{7}Li reaction. One of the product particles is ejected into the gas volume and produces ionization of very high density along its path and consequently generates a high number of electrons and positive ions. The collected charges are responsible for the creation of an electric field producing a signal that can be amplified and processed. The gas is usually a neutral gas such as argon or nitrogen. In the particular case of fission chambers, a certain amount of nitrogen (N_2) is added to the gas mixture in order to increase the electronic mobility and thus improve the chambers performance.

These detectors are used in both pulse mode (as counters) and current mode (as chambers). As counters, they are used in the source range, and as chambers they can be used either as intermediate or as power range detectors. Usually when used in the intermediate range they are compensated ionization chambers, and when used in the power range they are uncompensated ionization chambers [10].

- **Compensated boron-coated ionization chamber (CIC)**

These detectors respond to both neutron and gamma radiations. Most of the gamma radiation is proportional to the reactor power. However, radiation due to long-lived fission products, radioactive neutron capture that leads to the formation of long-lived activation products is not indicative of the prompt neutron flux. This delayed component

of the signal generated by gamma-rays does not represent reactor power. Thus, to derive signals proportional to the neutron flux and eliminate gamma contribution, gamma compensation is employed.

The CIC consists of three concentric cylindrical electrodes which define two chambers in a single case (Fig. 1.14). The first chamber is located between the external positive polarization electrode and the central electrode which collects the total current. The surfaces of the electrodes are coated with an enriched ^{10}B. It is, therefore, sensitive to neutrons and gamma-rays. The second chamber is located between the internal negative polarization electrode and the signal electrode. The surfaces are not coated with boron and the chamber is, therefore, only sensitive to gamma-rays. The currents of these two chambers are subtracted one from the other due to their opposite polarization and the resulting current is, therefore, only proportional to the neutron flux. The typical values of neutron sensitivity of a CIC are between 10^{-14} A/nv to 10^{-13} A/nv. The CIC is designed to eliminate the gamma contribution [10].

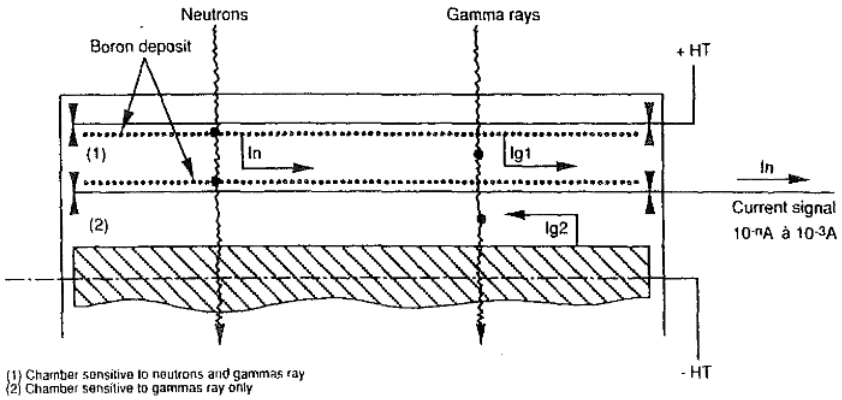

FIGURE 1.14: Compensated ionization chamber diagram.

- **Uncompensated boron-coated ionization chamber (UIC)**

The UIC uses amorphous boron as a fissile material which is deposited on the surfaces of two concentric cylindrical electrodes in order to monitor the power level of the reactor [10]. The outer electrode is polarised at a positive voltage of the order of +600 V and the central electrode collects the electrons produced in the gas without multiplication resulting in a DC current. The current depends on the quantity of fissile material (^{10}B) on the electrodes and, therefore, on the size of the chamber. The UIC detectors are sensitive to both neutrons and gamma-rays. The typical values of neutron sensitivity of a UIC are between $2{\cdot}10^{-14}$ A/nv for small detectors and $3{\cdot}10^{-13}$ A/nv for large detectors. It is important that the chamber voltage is located in the saturation regime, the higher the neutron flux the higher is the voltage where the chamber reaches its saturation regime (Fig. 1.15). The chamber also has sensitivity to gamma-rays; typical values of gamma sensitivity are between 10^{-9} A/Gy/h for small detectors and 10^{-8} A/Gy/h for large detectors.

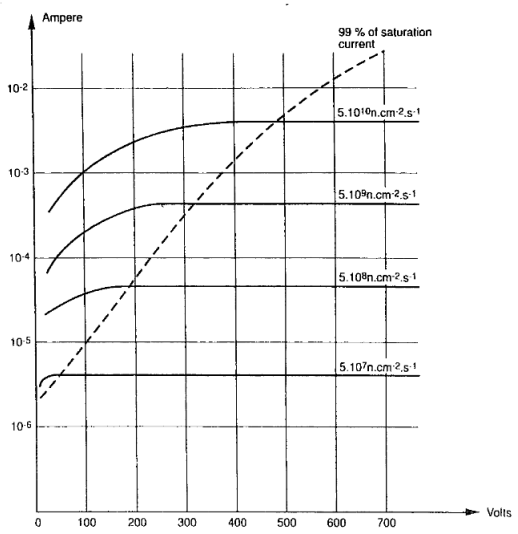

FIGURE 1.15: Saturation curve array.

1.4.1.3 Scintillators

Scintillation detectors make use of the property that certain materials, when struck by a nuclear particle or radiation, emit a flash of light (i.e. scintillation) which is created in the visible or ultraviolet field (it is a short – lasting luminescent effect – fluorescence). When a scintillator is coupled to an amplifying device such as a photomultiplier tube (PMT), the PMT absorbs the light produced by the scintillator and re-emits it in the form of electrons via the photoelectric effect. The subsequent multiplication of these electrons (photoelectrons) results in an electrical pulse which can then be analyzed and the type of the particle which struck the scintillator identified. A typical scintillation detector consists of a scintillator and an electronic light sensor, i.e. PMT and can be divided into [7]:

- **Organic scintillators:**

  Pure organic crystals;

  Liquid organic solutions;

  Plastic scintillators;

  Thin film scintillators;

  Loaded organic scintillators.

- **Inorganic scintillators:**

  Alkali Halide scintillators;

  Unactivated fast inorganics;

  Cerium activated fast ionorganics;

  Glass scintillators;

  Scintillators gases.

1.4.1.4 Fission chambers

Fission chambers (FCs) are nuclear detectors that are widely used to locally characterize the in-core and ex-core neutron flux [7]. This type of detector is an ionization chamber containing a thin layer of fissile material (Uranium, Plutonium, and Neptunium) in order to detect neutrons. The most common design are the cylindrical chambers which consist of one or more electrode pairs and at least one electrode is coated with a fissile layer (from a few μg to a few hundreds of μg) depending on the application. The choice of the fissile deposit depends on the neutron energy range of interest. The inter-electrode space between each anode (the inner electrode) and cathode (the outer electrode) goes from tens of microns to a few millimetres and filled with pressurized gas (i.e. Argon-Nitrogen) at close to atmospheric pressure. The body of the chamber is sealed and an insulating material insures the electrical separation between the cathode and the anode. The fission chambers principles and operations are detailed in Chapter 2.

1.4.2 In-core neutron detectors

The In-core instrumentation system allows reactor operators to provide information on neutron flux distribution and fuel assembly outlet temperatures into the selected core locations. The neutron flux information given by the system is used to check the calibration and response of ex-core flux detectors, monitor fuel burn-up and fuel inventories, or control the reactor components (i.e. rod drives and detector cables). The operating conditions for the in-core instrumentation are very severe since the temperature up to 300 °C and the external operating pressure up to 150 bars are required. The neutron flux is in the order of 10^{14} $n \cdot cm^{-2} \cdot s^{-1}$ [16], gamma flux up to 10^8 R/h. Two types of in-core instrumentation are possible, one fixed based on Self Powered Neutron Detectors (SPND) and one mobile based on Aeroballs or fission chambers [16].

The Three detectors applied to determine the neutron flux are the following:

- **Self-powered neutron detectors (SPNDs):** Fixed in-core detectors;
- **Aeroballs:** Mobile in-core detectors;
- **Fission chambers:** Mobile in-core detectors.

1.4.2.1 Self-powered neutron detectors

Self-powered neutron detectors (SPNDs) are widely used to monitor in-core thermal neutron flux for control, safety, and mapping applications because they have a number of interesting properties (i.e. small size, ruggedness and simplicity) [17, 18]. These devices are used to produce a positive charge on an inner electrode (emitter) by emitting electrons when exposed to radiation. The net flow of electrons from emitter produces a direct current (DC) signal, which is proportional to the incident neutron flux. The electrons flow up the wire attached to the electrode replacing escaping beta particles (beta decay). The term "self-powered" is derived from the fact that no external bias voltage is applied to the detector.

The typical SPND is a coaxial cable that consists of three main regions: The neutron absorber/beta emitter region (the emitter), the insulator, and the collector/shield (the collector). A schematic diagram for SPND is shown in Fig. 1.16. The processes leading to a current pulse after a neutron enters the detector are the following:

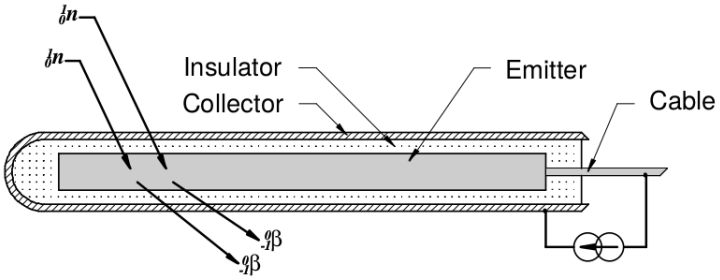

FIGURE 1.16: Schematic diagram of SPND.

- **The emitter:** The materials for the neutron absorbing, beta emitting region are subject to a few constraints, the first of which is that, the emitter is the heart of device which is made from a material chosen for its relatively high cross section for thermal neutron capture leading to beta-active radioisotope. A second consideration is the half-life, which should be reasonable to quickly reach the saturation so allowing to follow the time dependent variation of the neutron flux in real-time. The emitter can be made with several pure materials including Rhodium (Rh), Vanadium (V) and Cobalt (Co). These materials should be used because they possess relatively high melting temperatures, relatively high cross sections to thermal neutrons and are compatible with the SPND manufacturing process. Table 1.3 gives some characteristics for typical SPNDs emitters used in power reactors. These detectors can be divided into two categories: the ones with fast respond instantaneously to change in the reactor flux of which Co is the best, and the others with delayed response, specially Rh and V (as shown in Fig. 1.17) .

- **Insulator:** Many materials can be used to insulate the emitter region from the collector region, which must be chosen to withstand the extreme temperature and radiation environment typically found in a reactor core. Magnesium oxide (MgO) and/or aluminium oxide (Al_2O_3) are most commonly used.

- **Collector:** The collector materials are typically made of high purity stainless steel or Inconel. These materials must be compatible with the harsh environment in which the detector has to be located.

The major disadvantage of the SPND is that the emitter material of the detector decays with a characteristic half-life. In the case of Rh and V, which are two of the most SPNDs suitable emitters operated on the basis of a (n, β) reaction and are especially used for flux mapping, the half-lives are 42 seconds and 3.76 minutes, respectively. This means that the detector cannot respond immediately to a change in neutron flux, but takes as long as 3.76 minutes to reach 63 % of steady-state value. This disadvantage is overcome by using Co emitters which operate on the basis of a (n, γ-e) prompt reactions and are especially used for reactor control and safety; the Co emit their electrons within 10^{-14} seconds after neutron capture. SPNDs with cobalt emitters are called prompt neutron detectors.

TABLE 1.3: Characteristics of representative emitter materials

Emitter	^{59}**Co**	^{195}**Pt**	**Ag**	^{103}**Rh**	^{51}**V**	**Remarks**
Thermal neutron absorption cross section (barns)	37	24	113($^{109}_{47}$Ag) 45($^{107}_{47}$Ag)	145	4.9	
Sensitivity ($\times 10^{-22}$ **A/nv/cm)**	1.4 to 4.1	1.4 to 2.5	2.5	1.4 to 4.1	1.4 to 4.1	Dependent on emitter diameter (0.5 to 2 mm)
Current (nA) (emitter length 20 cm, $\phi = 10^{13}$ $n \cdot cm^{-2} \cdot s^{-1}$ **)**	$\sim$ 3.4 to 2.5	$\sim$ 10 to 18	$\sim$ 280	$\sim$ 230 to 540	$\sim$ 15 to 96	
Response time (s)	>0.05	>0.05	30	66	330	
Burn-up rate/month (%) at 10^{14} $n \cdot cm^{-2} \cdot s^{-1}$	1.0	0.3	1.6	3.9	0.12	
Thermal neutron signal (μA) **at** 10^{14} $n \cdot cm^{-2} \cdot s^{-1}$	0.54	-	-	0.87	0.51	-

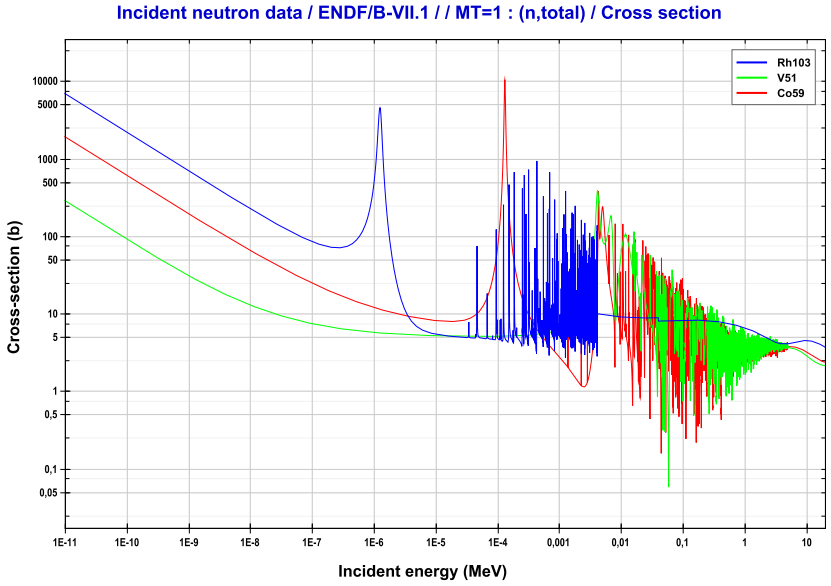

FIGURE 1.17: The total cross sections for ^{59}Co, ^{51}V and ^{103}Rh computed from ENDF-B-VII-1 [2].

1.4.2.2 Aeroballs

The Aeroball Measurement System (AMS) [19] is an indirect flux mapping system based on the movable activation of steel balls alloyed with 1.5 % vanadium content, which acts as neutron sensitive material. The diameter of the steel balls is 0.17 cm. These balls are in a double tube with an outside diameter of 0.3 cm in which they form stacks. The length of these balls corresponds to the core height. The balls are normally located outside the core. To take a measurement, all the balls can be pneumatically pushed back with nitrogen gas at the same time into the core where each extends over the entire active core height, where they are activated by the neutron flux for about 3 minutes. This short irradiation time makes flux mapping like a snapshot and enables accurate measurement even under semi-transient conditions (xenon-redistribution). During irradiation, a process computer records all data needed for subsequent processing. On completion of irradiation, the nitrogen gas is applied from the other

direction, driving the balls out of the core into a detector array which is located outside the biological shield. The gamma radiation emitted by the balls is then read by detector arrays arranged in a measuring table (Fig. 1.19). The recorded counts are the primary data, which are further processed by a computer to yield the 3D power density distribution and other parameters representative of core conditions (i.e. nuclear and thermal hydraulic conditions). Whilst the ball stack is being irradiated, the plant process computer make a calibration based on thermal power, which is determined by means of a heat balance and the resulting thermal power is then used to convert the relative values of power densities obtained from the activation rates into absolute values (W/cm). The AMS measurement can in principle be repeated every 10 minutes. The Fig. 1.18 shows a schematic diagram of the AMS.

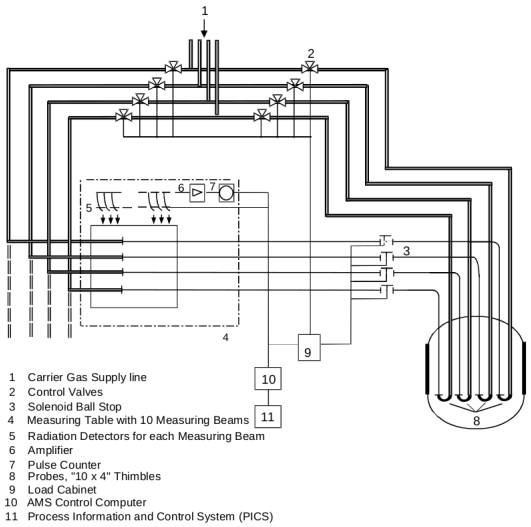

FIGURE 1.18: The Aeroball Measurement System (AMS).

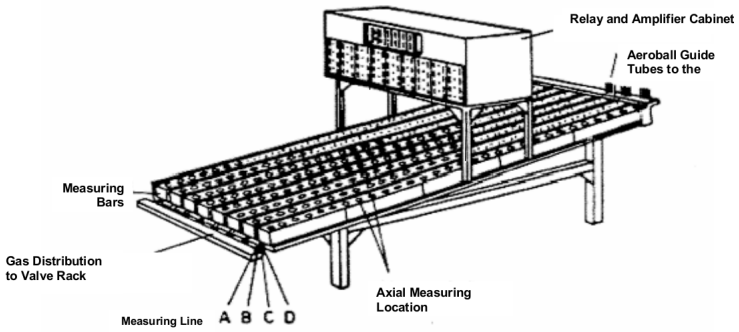

FIGURE 1.19: AMS Measurement Table.

1.4.2.3 Fission chambers

Miniaturized fission chambers (FC) can be tailored for in-core neutron measurements of quantities such as fission rates or reactor power. Walls of the chamber are usually lined with enriched uranium to making it sensitive to neutrons. These small chambers are typically made of stainless steel electrodes, and the operating voltage varies from about 50 to 300 V. Argon is a most common choice for the chamber fill gas and is used at a pressure of several atmospheres [7]. When a neutron crosses the detector, it is likely

to induce fission reaction inside the fissile deposit and high energy fission products (the probability is proportional to the fission process). The resulting reaction generates two charged particles (Fission Fragments) produced by fission. One of these is absorbed in the anode; while the second crosses the inter-electrode space, ionizing the filling gas on its path and consequently generates a large number of charge pairs (Ar^+, e^-) [20]. When a voltage of a few hundred volts is applied, an electric field is generated between the two electrodes, producing a migration of charges.

1.5 Conclusion

This chapter provides an overview of nuclear physics related to neutron spectrometry. It includes a description of the ways in which a neutron can interact with matter, which are important to nuclear material measurements, the possible choices for radioisotope neutron sources which are usually limited into two main categories: spontaneous fission and nuclear reactions for which the incident particle is the product of a conventional decay process. In addition, we describe the operation principles of several ex-core and in-core neutron detectors are used to provide full reactor neutron flux measurements. The following Chapter will be devoted to the presentation of one widely used detector, that is the fission chamber on which this thesis work is based.

Chapter 2

Basic principles of fission chamber operation

2.1 Introduction

For efficient exploitation of research reactors, it is important to discern neutron flux distribution inside the reactors with the best possible precision. For this reason, fission chambers are used to detect and measure the neutron fluence rates over the exposure time (neutron flux monitoring). Depending on the application, neutron detectors may experience a wide range of constraints, of three orders of magnitudes (neutron flux, gamma-ray flux, temperature). The development of special fission chambers based on fissile deposit started since 1957s, and has continued ever since. This chapter involves different design features of the chamber, from geometry to different fissile isotopes as well as different filling gas and operational modes.

2.2 Fission chambers

The fission chambers (FCs) are nuclear detectors that are widely used to detect and measure the in-core and ex-core neutron flux [7]. These types of neutron detectors are simple generic ionization chambers with a small amount of fissile deposit in order to detect neutron flux. Several detector geometries are available, however, the cylindrical geometry has been the most popular. Fission chambers are composed of two concentric electrodes called anode and cathode. The fissile deposit layer (from a few μg to a few hundreds of μg) lies on either of the electrodes. Most of fission chambers use ^{235}U or enriched ^{235}U as a fissile deposit, since ^{235}U is very convenient for operations in environments with thermal neutrons; however other isotopes such as depleted U, Pu, Np and Th can be used according to the neutron spectrum which is intended to be processed. The inter-electrode space goes from tens of microns to a few millimetres and filled with pressurized gas at a few bars, often argon, sometimes with a small percentage ($\sim 4\%$) of nitrogen or other polyatomic gases. These chambers are sealed devices and are typically made using insulator material to maintain the voltage between the electrodes. A schematic design of a cylindrical fission chamber is shown in Fig. 2.1. The processes leading to a current pulse after a neutron enters the chamber are the following:

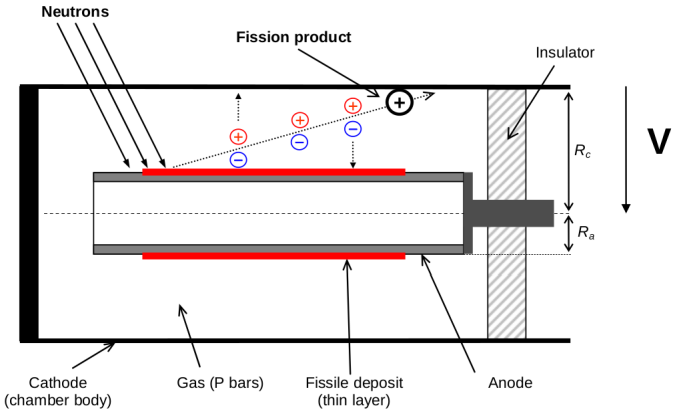

FIGURE 2.1: A schematic design of a cylindrical fission chamber.

- When a neutron crosses the detector, it is likely to induce fission reaction inside the fissile deposit and high energy fission products (the probability is proportional to the fission process). The resulting reaction generates two charged particles (Fission Fragments) produced by fission reaction, emerge with energies of several tens of MeV (90 MeV each in average for ^{235}U) and with almost opposite directions;
- One of these is absorbed in the anode; while the second crosses the inter-electrode space, ionizing the filling gas on its path and consequently generates a high number of electron-ion pairs;
- When a DC voltage of a few hundred volts being applied between the electrodes, therforce the electrons and positive ions drift across the filling gas in opposite direction towards the anode and cathode respectively;
- The collected charges are responsible for the creation of an electric field producing a pulse signal that can be amplified and processed.

The DC voltage applied between the electrodes must be high enough to collect all the electron–ion pairs, and low enough to prevent the production of secondary ionization pairs (a phenomenon occurring in proportional counters) [21]. If both conditions are fulfilled, the fission chamber operates in the so-called saturation plateau in which the neutron-induced current signal produced by the chamber is directly proportional to the fission rate produced by neutrons and independent to the DC voltage applied. In addition, one can note that the gamma-rays that directly ionize the filling gas also generate a signal.

Overview of neutron and gamma-ray interactions occurring in a fission chamber

An outline of the interactions yielding neutron and gamma-ray pulses occurring in a fission chamber are given in Fig. 2.2. For the sake of clarity, the following discussion refers to the numbers featured on the figure.

The incoming γ-ray flux (1) can generally be divided into two groups: prompt and delayed flux. The former is produced by nuclear interactions within the core (mainly due to fission and radiative captures), for which the γ-ray flux is proportional to the neutron flux (into the selected core location). After a reactor stop, the delayed flux

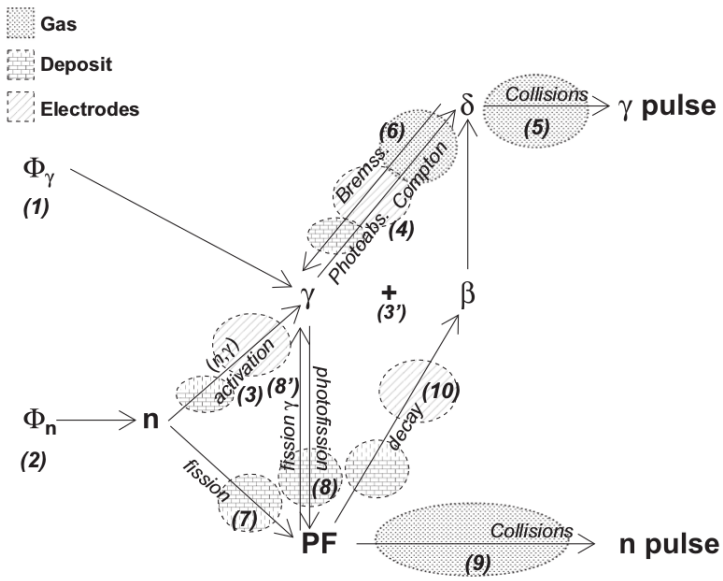

FIGURE 2.2: Outline of the neutron and γ-ray interactions occurring in a fission chamber. The numbers in parenthesis refer to the discussion in the text [22].

drops practically to zero due to the multi-exponential decay curve. Another source of γ-rays inside the chamber is the incoming neutron flux (2): the structures of the chamber (electrodes, insulator, fissile deposit) may perform a radiative capture (n, γ) (3). This activation eventually produces a decay product, usually an electron β^- (3').

The γ-rays can interact with all the materials in the chamber (4), including the fissile deposit, the electrodes and the filling gas, by Compton scattering or photoelectric effect. The balance between these two physical processes depends on the atomic number of the target material. For the energy range between 0.1 MeV to 2 MeV, typical of nuclear reactors, and usual materials, they are about the same order of magnitude. The reaction rate is also proportional to the atomic density of the target material and its volume in the case of an isotropic flux. Therefore, there will be much more interactions in the electrodes of a chamber than in the filling gas. Pair production process is considered but not taken into account, since it is efficient only for γ-rays energies well above 1.02 MeV.

The interactions of γ-rays with matter yield the production of a δ-ray, the energy of which is less than the one of the photon, but of the same order of magnitude. The highly chaotic path of the δ-ray and its relatively long range leave the possibility for a δ-ray to be created in an electrode and reach the filling gas (and possibly then an electrode and the gas again).

The δ-rays lose their energy essentially via a collisional process (5). The energy loss per unit of length may be described by the Bethe formula [7]. A detailed modelling of this process is presented in Ref. [23]. The energy loss is proportional to the atomic number and density of the target material. If occurring within the filling gas, this energy loss creates electron–ion pairs along the path of the δ-ray (5), producing an electric pulse (labelled as γ pulse). This process must not be confused with the avalanche regime, in which the secondary electrons are accelerated in very high energy to induce further ionizations. The δ-rays may also lose their energy through bremsstrahlung (6): this effect accounts for only few percent of collisions, and produces other γ-rays.

The neutron flux also interacts with the fissile deposit and produces a couple of fission products (fission fragments) released in almost opposite directions (7). It is also possible to produce fission products via the photofission process (8), which has been found to be negligible in current mode, but can be a significant part of the γ-ray induced signal in fluctuation mode [24].

The fission product that crosses the filling gas produces electron–ion pairs by collisions (9) and therefore an electric pulse (labelled as the neutron pulse). The fission product is much more energetic than the δ-rays (10 – 100 MeV), thus yields much more electron–ion pairs. Both fission products are eventually trapped in the electrodes or the fissile deposit, and decay usually via a β^- process (10). The fissile deposit itself may also contain β^- emitters (before or after activation), such as ^{241}Pu or ^{243}Pu, and also α emitters like ^{238}Pu.

The fission process also release up to 20 prompt γ-rays (8'). The resulting gas ionization is simultaneous with the one caused by the fission product, so that it is not possible to distinguish between these two radiations. As a result, the radiation of those fission-induced γ-rays is considered to be a part of the neutron-induced signal. Anyway, their impact is negligible: they carry only about 8 MeV, and they lose in proportion less energy within the gas than the fission products.

2.2.1 Fission layers

The rate of fission reaction is given by:

$$\tau_f(t) = N_i(t) \int \sigma_{f,i}(E)\Phi(E)dE \tag{2.1}$$

Where $N_i(t)$ is the number of the isotope i present in the fissile deposit at time t (evolving with time), $\sigma_{f,i}(E)$ is the microscopic fission cross section of the isotope i and Φ(E) is the neutron spectra seen by the coating of the detector [25].

The choice of the fissile deposit is determined depending on the application and the neutron environment. The most common fissile deposits used for neutron flux monitoring are natural or enriched uranium. Note that ^{242}Pu has also been suggested as a fissile deposit for monitoring the fast component of a high neutron flux [21]. Fig. 2.3 shows the microscopic fission cross sections for ^{235}U and ^{242}Pu. One can see that ^{235}U is the preferred fissile deposit when the chamber is going to be used in a thermal neutron spectrum environment: The cross sections below 1 eV are several orders of magnitude higher than above 1 MeV, so that the neutrons below 1 eV, that represent less than 1 % of the total flux at each of our two locations, can contribute significantly to the signal. However, when the chamber is intended to work in a fast neutron spectrum environment, ^{235}U can be replaced by ^{242}Pu, which is characterized by having threshold energy above 1 MeV. Nevertheless, the fission cross section of ^{242}Pu also has a significant thermal neutron spectrum environment. The joint estimation of both thermal and fast components is possible with the combination the two types of fission chambers, in order to distinguish the contributions of the thermal and fast neutrons [26].

Eq. (2.1) shows, that the fission rate evolves with time due to the depletion (burn-up) of the fissile deposit. This evolution highly depends on the neutron fluence and

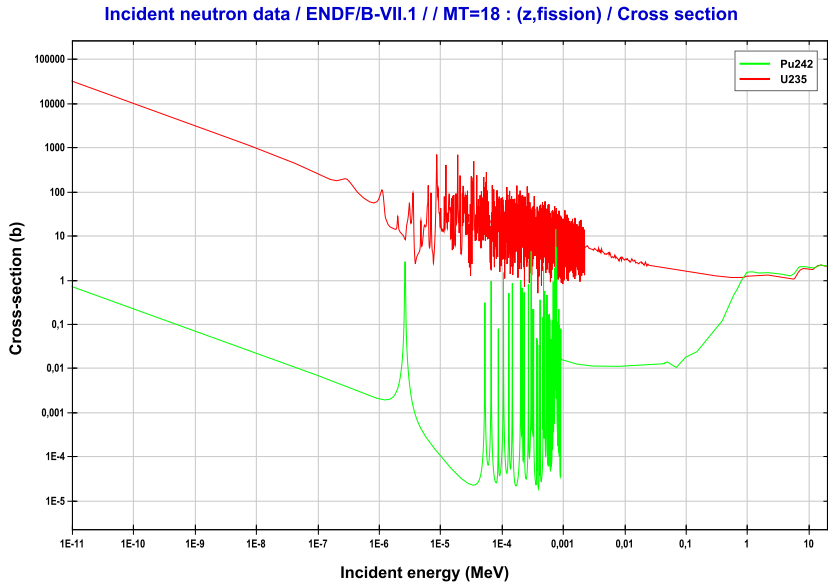

FIGURE 2.3: Microscopic fission cross sections for ^{235}U and ^{242}Pu computed from the JEFF 3.2 [2].

spectrum which has a large timescale (from hours or decades in different reactors). However, for the applications considered in this thesis (from a few ms to a few hours), the change of the fission rate due to depletion is found to be negligible compared to the investigated count rate changes (movements of control rods). Two possible methods are considered to correct the problem of the time evolution of signal: fission chambers containing regenerable fissile deposit to compensate for fissile material burn-up [25, 27] and acquisition systems coupled with depletion codes [25].

2.2.2 Filling gas

The ideal filling gas for the fission chambers is a mono-atomic noble gas, since there is no interaction between the material of the electrodes and the filling gas and since the gamma-rays should not break up molecular bounds. The most often chosen filling gas for fission chambers is an argon-based gas pressurized at a few bars. The addition of a few percents of polyatomic gas such as nitrogen has a dramatic effect on the electron drift velocity due to the excitation of the vibrational modes of the nitrogen molecule, the so-called quenching effect [28] and therefore allows to decrease the charge collection time and hence the width of the individual current pulses [29]. Fig. 2.4 shows the drift velocity of a gas mixture as a function of the reduced electric field (which is the ratio E/N, where E is the electric field and N is the concentration of neutral particles). One can see that the electron drift velocity can be increased by a factor of four by introducing 1 % of nitrogen into the mixture.

2.3 Operation modes

As mentioned in the previous chapter, FCs are designed to operate in three possible modes: Pulse, Campbell (also known as "fluctuation mode" or "mean square voltage

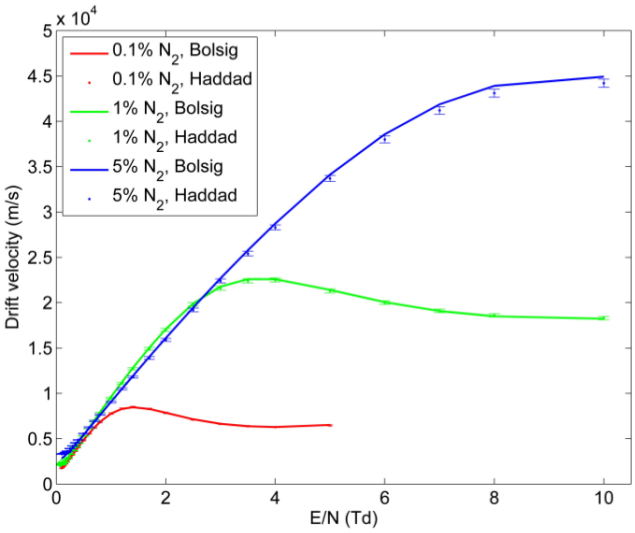

FIGURE 2.4: Electron drift velocity in Ar-N_2 mixtures (experimental results of Haddad [30] and BOLSIG [31] results with Biagi-v8.9 libraries [32].

mode") and Current. These three modes constitute a wide dynamic range depending on the neutron flux level and on the externally coupled electronic devices.

2.3.1 Pulse mode

Pulse mode is used for low fission rates (i.e. low neutron fluxes or low detector sensitivity). The sensitivity range of FCs is between 0.01 cps/nv to 4 cps/nv. The maximum count rate such a chamber can perform depends on various parameters such as size of the chamber, inter-electrode distance, filling gas pressure and composition and nature of fissile deposit. In the pulse mode the pulses do not pile-up, so the fission rate, which is proportional to the flux, is retrieved. For a very sensitive chamber (typically 1 cps/nv) with charge collection time less than 80 ns, the counting rate may reach $1E^6$ cps. A low sensitive chamber (0.01 cps/nv) may measure neutrons up to $1E^8$ cps. FCs operating in this mode are therefore well-suited for operation in a high gamma flux (up to $1E^4$ Gy/h) [10] and the suppression of the signals resulting from gamma-rays contribution is possible via pulse height discrimination (by triggering threshold as the corresponding pulses from gamma-rays are much smaller than those coming from neutrons). Fig. 2.5 shows a schematic diagram of a fission chamber working in pulse mode.

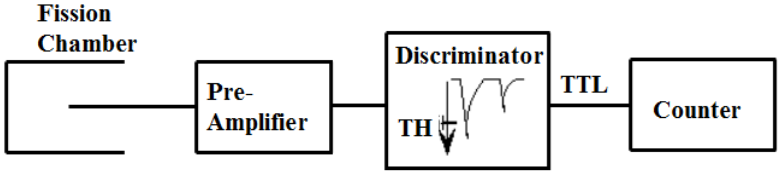

FIGURE 2.5: Schematic diagram of a fission chamber working in pulse mode.

2.3.2 Campbell mode

The Campbell mode (also referred as "fluctuation mode" or "mean square voltage mode") is used for low to medium fission rates (i.e. low to medium neutron fluxes or low to medium detector sensitivity). It is based on the second part of Campbell's theorem [33] that states that the average value of the current from a source of random current pulses (< I >) is directly proportional to the average pulse rate (< N >) and the charge produced per event is itself related to the pulse height [i(t)] (the first part of Campbell's theorem Eq. (2.2)). It also states that the variance of this current (< I ^{2} > - < I > ^{2}) is proportional to the average pulse rate and to the square of the charge produced per event which is turn related to the square pulse height (the second part of Campbell's theorem Eq. (2.3)).

$$< I >=< N > \int_0^\infty i(t)\,\mathrm{d}t \tag{2.2}$$

$$< I^2 > - < I >^2=< N > \int_0^\infty [i(t)]^2\,\mathrm{d}t \tag{2.3}$$

At high fluence rates no individual pulses can be detected due to the overlapping of the pulses (the pile-up phenomenon) [7, 10]. One pulse has no time to disappear before the new pulse appears and superposes itself on the preceding one. The result is a fluctuating chamber current. The electronics provided to process the pulses is not able to distinguish two successive pulses and counting loss is observed. It is, however possible to increase the operational range of the detector by using this pile-up phenomenon. The signal fluctuation is a measurement of the neutron fluence rate; this measurement is increasingly accurate the greater the energy deposit is caused by a neutron event.

Campbell mode operation can be employed to reduce the gamma-ray sensitivity because it takes advantage of the different amplitudes of the pulses produced by different types of radiation, such as neutrons and gamma-rays. The resulting signal is proportional to the square of the charge that is created by each incident particle of radiation, thus enhancing the difference between types of radiation. In fission chambers, which are the only kind of detectors able to create neutron proportional using fluctuations, the number of charge pairs created by a single fission product is of the order of 1E^5, which is much higher than the charge generated per gamma-ray. So by measuring the variance of the detector current within a suitable bandwidth the contribution of the abundant low-amplitude gamma-induced pulses will in principle be quite effectively suppressed [24]. Fig. 2.6 shows a schematic diagram of a fission chamber working in Campbell mode.

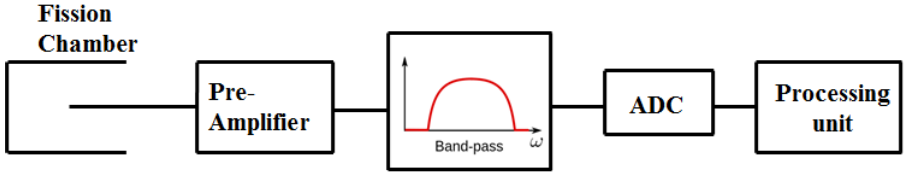

FIGURE 2.6: Schematic diagram of a fission chamber working in Campbell mode.

2.3.3 Current mode

The current mode is used for high fission rates (i.e. high fluxes or high detector sensitivity). It is based on the first part of Campbell's theorem [33]. The saturation characteristics of an FC operating in current mode are very similar to those of a UIC. Then, the sensitivity to neutrons is comparable to that of a UIC and depends on the quantity of fissile element deposited at the electrode; typical values are between $1E^{-14}$ A/nv and $1E^{-12}$ A/nv. The usual maximum current produced by an FC is in the order of 1 mA. Therefore, a very sensitive fission chamber with $6E^{-13}$ A/nv can measure a maximum fluence of about $2E^{9}$ nv. A typical value of its gamma-ray sensitivity as $1E^{-9}$ A/Gy/h [10]. It is noticed that gamma-ray contribution can be important (typically between 1 and 10 % of the signal) and can not easily be suppressed or discriminated against. An estimate is possible by jointly irradiating a chamber without fissile deposit [24]. Fig. 2.7 shows a schematic diagram of a fission chamber working in current mode.

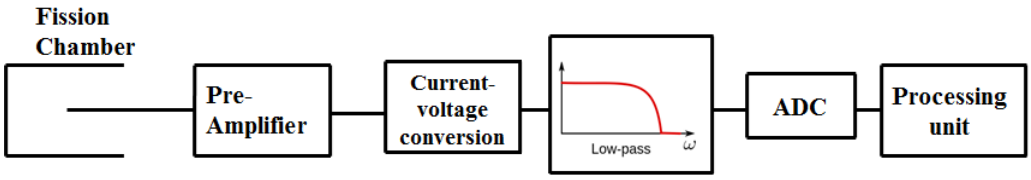

FIGURE 2.7: Schematic diagram of a fission chamber working in current mode.

2.4 Why fission chambers in CNESTEN?

The TRIGA Mark-II research reactor of Morocco is part of the National Center of Nuclear Energy, Sciences and Techniques (CNESTEN). It is only the one nuclear research reactor in Morocco that achieved initial criticality on May 2, 2007 of 2 MW natural-convection-cooled reactor. This reactor is moderated and cooled by light water, equipped with a graphite reflector, contains in-core and ex-core irradiation facilities including a thermal column and four beam ports, three radial and one tangential. It is designed to be used in various fields such as manpower training, radioisotope production, neutron activation analysis and in the various fields of the nuclear research. The work in this thesis corresponds to the safety and security aspects of TRIGA Mark II reactor. Hence, it is important to discern neutron flux distribution inside it with the best possible precision. For this reason, WL-7657 FC is used to detect and measure the neutron fluence rates over the exposure time (neutron flux monitoring). WL-7657 FC is profusely explained in Chapter 3.

2.5 Conclusion

Fission chamber is the ideal candidate for neutron flux monitoring in TRIGA Mark II reactor. They can provide online, in-core, ex-core, and real-time measurements covering the dynamic range of neutron flux including pulse, Campbell, and current modes over decades of reactor operation cycles. This work focused on the signal processing of fission

chamber. This type of neutron detector is an ionization chamber, containing fissile deposit in order to detect neutron flux. The chamber itself is filled with pressurized gas at a few bars, often argon, sometimes with a small percentage ($\sim 4\%$) of nitrogen or other polyatomic gases. Each detected neutron causes a detector response (i.e. electrical pulse), characteristic to the chamber. In addition, one can note that the gamma-rays that directly ionize the filling gas also generate a signal. For this reason the obtained time-series from the chamber will be processed by using Blind Source Separation (BSS) methods to extract independent components which will be characterized in order to reach the neutron/gamma discrimination goal.

Part II

Material and Method

Chapter 3

Simulation tools

3.1 Introduction

This chapter describes the work done to interface two simulation toolkits, Geant4 and Garfield++, in part for the simulation of the WL-7657 FC. This interface was done in order to add measurements such as ionization and drift parameters in the filling gas detector simulations. This was applied to charged particles traversing a WL-7657 FC to have a better understanding of how a signal is created inside the chamber.

Geant4 [34] is a C++ object-oriented toolkit which is used to simulate the interactions and passage of particles through matter. Geant4 implements a set of processes for simulating the interactions of neutrons with matter. These include Scattering and Absorption interactions. Geant4 can be used to simulate the fission reaction (the fission process) inside the chamber; however it is not able to simulate the resulting drift parameters created by ionizations of the filling gas inside the chamber. Geant4 is limited to the study of the particle energy loss and, by default does not have an integration with other packages specialized in gas characterization. For this reason an interface must be developed and integrated with the existent Geant4 to allow a simulation of the avalanche amplification and the induced signal.

Garfield++ [35] is a C++ object-oriented toolkit which is designed specifically for the simulation of particle detectors that use a gas mixture or a semiconductor material as sensitive medium. This makes it a useful program to interface to Geant4 to further the applications and simulation of physics processes inside a wide range of gas detectors.

This chapter describes how the interface has been created between these two simulation toolkits and its application to the WL-7657 FC. The extend of the physics of Geant4 is shown when it is used with the interface to Garfield++. Finally, the measurements of the induced signal on the own chamber is calculated and shown. The information is sent back to Geant4 and the interface is complete.

3.2 Background to computer simulation software

3.2.1 Geant4 simulations

The Geant4 (GEometry ANd Tracking) toolkit is designed and developed by an international collaboration of scientists and software engineers for the Monte Carlo simulation of particle interactions with matter in high-energy physics [34]. It is object-oriented architecture using C++ programming language, and it was developed to replace Geant3 (Fortran-77 version) [36]. It finds application in fields such as high-energy and nuclear physics, accelerator design, space engineering, medical applications and radiation protection and security. A schematic of the structure of Geant4 applications is shown in Fig. 3.1. In any Geant4 simulation the user must to implement three mandatory classes: detector construction, physics list and primary generator. These classes are to be registered to the G4RunManager, which controls the overall behavior of the program.

- The detector construction is derived from **G4VUserDetectorConstruction**. It is used to define the material and geometrical setup of the detector. Several other properties, such as detector sensitivities and visualization attributes, are also defined in this class.
- In the physics list all particles, physics processes and cut-off parameters that should be used in the simulation are specified. The virtual base class is **G4VUserPhysicsList**.
- The primary generation is used to specify the initial condition of a simulation. This includes the type of the initial particle and its initial properties like kinetic energy and momentum direction. The primary generator is derived from **G4VUserPrimaryGeneratorAction**.

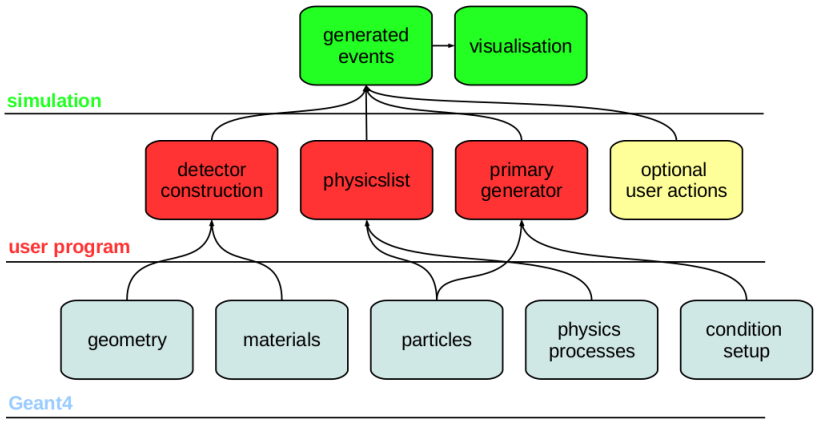

FIGURE 3.1: Schematic of a Geant4 simulation.

Additionally to these three mandatory classes, it is possible to add optional user classes allow the user to modify the default behaviour of Geant4, such as defining a histogram, analyzing the results, setting priority control to a track, storing particle trajectories, and terminating a track. The five optional user class bases are:

- **G4UserRunAction** for actions at the beginning and end of every run;
- **G4UserEventAction** for actions at the beginning and end of every event;
- **G4UserStackingAction** for customising access to the track stacks;
- **G4UserTrackingAction** for actions at the creation and completion of every track;
- **G4UserSteppingAction** for customising behaviour at every step.

A great advantage of the Geant4 toolkit is that it is designed for modern experiments and has a variety of controls, including the interface to other toolkits. It contains several components such as the event generator, detector simulation, physical interactions, and storage of data which can be tailored to the user's preferences.

For the creation and analysis of the FC, Geant4 is used to:

- create the geometry and material of the FC and physical world volume, defining the boundary of the process,
- initiate the neutron source, its energy, momentum direction, and charge, to launch at the FC,
- create the different gases inside the FC,
- include all the physical processes such as ionization and fission reaction inside the FC,
- to determine when a hit on the FC has occurred; thereby determining its position, particle identification, and momentum.

Using the information provided by Geant4 version 10.02 patch 02 (geant4.10.02.p02), an interface with the Garfield++ version 2015.1 simulation tools allows for a better modelling of the physical process inside the WL-7657 FC.

3.2.2 Garfield++ simulations

Garfield++ is a C++ object-oriented toolkit that was developed at CERN in 1984 by R. Veenhof to replace Garfield (Fortran version) [35]. It is generally used for the simulation of both gas and semiconductor detectors. It is able to create field maps, simulate the drift lines of electrons and ions, the electron avalanche creation and amplification and finally the simulation of induced signals resulting from the passage of charged particle through the chamber and readout of the signal. Garfield++ built on the ROOT framework [37] which allows the user to easily view the drift lines of electrons and ions, and also to do basic filtration of data by adding user-made functions to the final code.

Garfield++ allows the user to not only track some primary particles but also secondary particles, due to its implementation of various software such as Magboltz [38] written by S. Biagi, which calculates properties of gaseous mixtures used in the reaction volume and Heed [39] written by I. B. Smirnov, that simulate primary ionization process

in the medium. Moreover, the program can simulate the behaviour of the particles under the influence of either electric or magnetic fields.

The treatment of transport parameters in gas mixtures is done by the Magboltz software which is part of the Garfield++ toolkit. All necessary parameters such as energy, drift velocity and diffusion are calculated here, by using the same set of input data (i.e. the cross section for electron scattering by gas atoms/molecules). In case of ion transport properties, the toolkit cannot calculate ion mobility in gases and therefore the mobility file must be also imported manually from $GARFIELD_HOME/Data.

As previously mentioned, Garfield++ toolkit includes Heed software which simulate the initial ionization by the high energy particles traveling through a medium. The core of Heed is a photoabsorption ionization (PAI) model. This is based on the relation between energy deposited by the fast moving charged particle and the photoabsorption cross section of this medium and it also provides atomic relaxation processes and dissipation of high-energy electrons.

An overview of the class structure is given in Fig. 3.2. Two main categories can be distinguished: classes providing a "static" description of the detector (material properties, geometry, fields), and classes dealing with the transport which deal with tracing particles through the device. The two class types are linked by the class Sensor.

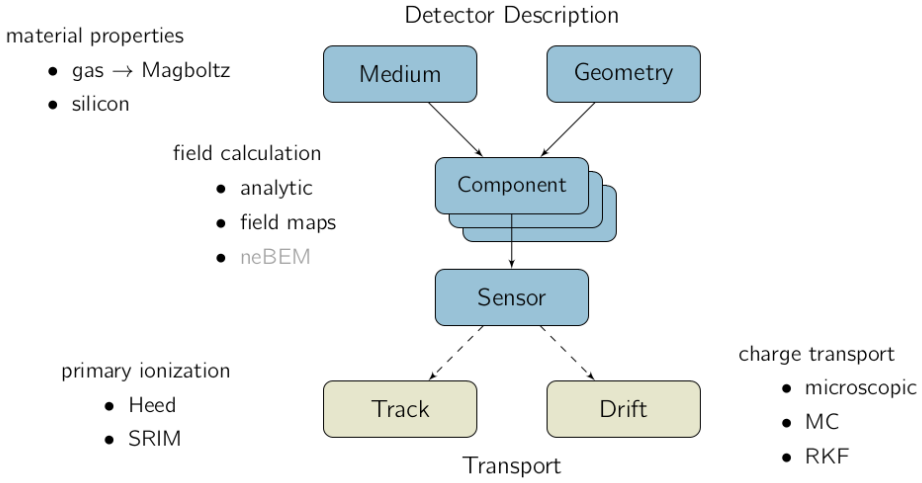

FIGURE 3.2: Overview of the main classes in Garfield++ and their interrelations.

3.2.3 Geant4/Garfield++ interface

3.2.3.1 Why interfacing Geant4/Garfield++?

The main parts of a gas detector simulation program are:

- Primary high energy particle ionization;
- Forming of ionization clusters in gas (using the interface with the HEED software);

- Electron and Ion drift properties in electric and magnetic fields (using the interface with the Magboltz software);
- Amplification/Creation of additional ionization via avalanche;
- Calculation of induced signal.

Geant4 is able to simulate only the first process, depending on the simulation, the deposited energy and the position where the primary ionization occurs can already be sufficient. For the last four processes, the user must to provide either his own code, or can use an existing software package like Garfield++. Garfield++ is used because of its predictive power of optimizing drift properties of electrons and ions, through the gas volume and calculating induced signal. it is possible to exchange data between Geant4 and Garfield++ via data files, but interfacing these two toolkits is the most efficient way.

3.2.3.2 How interfacing Geant4/Garfield++?

This paragraph describes a way to create an interface between Geant4 and Garfield++ toolkits. The interface uses the Geant4 physics parameterization or "fast simulation" facilities. The normal use case of the interface is the following: The user would like to simulate primary ionization, charge particle transport and/or avalanches in gas volume and finally the induced signals resulting and readout of the signal with Garfield++, but within a Geant4 simulation. Depending on the simulation, the point at which Garfield++ "takes over" from Geant4 varies. The major options concerning gas detectors are shown in the Fig. 3.3 and explained below [40].

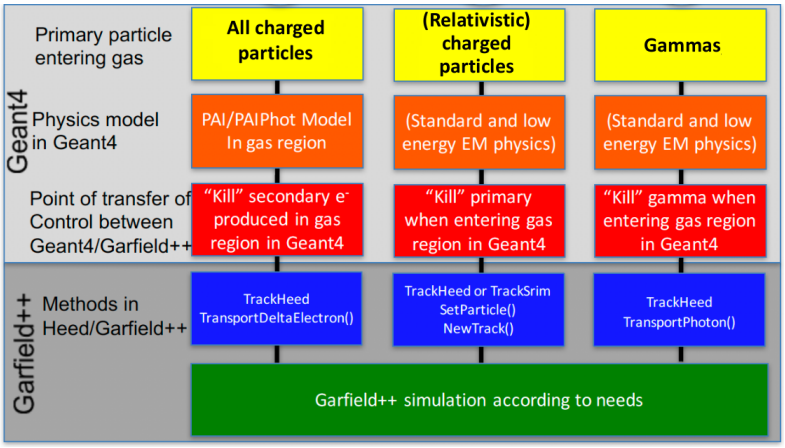

FIGURE 3.3: Schematic of a Geant4/Garfield++ interface.

Geant4/Heed PAI model interface for all charged particles This case applies to all charged particles independent of their kinetic energy. The PAI/PAIPhot models are actived in Geant4 to create only the primary ionization electrons in the gas volume, at which point Heed takes over. Heed is used to propagate all ionization electrons with a kinetic energy of a few keV and lower as δ-electrons. These δ-electrons have a certain probability to further ionize the gas volume, until all electrons reach thermal energies.

Heed PAI model for relativistic charged particles To simulate the interaction of relativistic charged particles, the PAI model of Heed can be chosen. Heed takes over

the control from Geant4 as soon as the primary particle enters the gas volume. In contrast to the PAI model in Geant4, however, Heed tracks the primary particle without Coulomb scattering. The stopping power of the primary is continuous and based on its initial energy, which works fine for Heed's intended purpose, the tracking of relativistic charged particles in thin absorbers. However, for slower particles in thicker absorbers, it leads to unrealistically straight tracks and an incorrect energy loss.

For ions, Garfield++ also contains an SRIM [41] interface.

Heed for gammas The gamma particle is stopped in Geant4 as soon as it enters the gas volume. Heed then used to transport the gamma particles.

3.2.3.3 Implementation of the interface

The physics parametrization feature in Geant4 offers the easiest way to interface Geant4 and Garfield++ [40]. The general idea of parameterisation is to create a region, in which the user provides her own implementation of the physics and the detector response. This region, defined by the G4Region class, is created during the detector construction, and consists of one or more G4LogicalVolumes, often corresponding to sub detector volumes. The complete syntax is shown in the class **DetectorConstruction**. To implement the parameterized physics model, the user has to create a new UserG4FastSimulationModel derived from G4VFastSimulationModel, and attach it to the region. It is possible to attach more than one UserG4FastSimulationModel to the same region.

In the physics list of the program, a G4FastSimulationManagerProcess has to be created. The G4FastSimulationManagerProcess is the physics process of the parametrization. It serves as interface between the Geant4 tracking and the user parametrization. At tracking time, the G4FastSimulationManagerProcess collaborates with the G4VFastSimulationManager of the current volume, and allows the user model to be triggered. In the AddParameterisation() method of the user physics list, the G4FastSimulationManagerProcess must be added as a discrete process to the process list of the particles for which the model shall apply.

The G4VFastSimulationModel has three pure virtual methods, which must be overridden in the UserG4FastSimulationModel :

- The first method, IsApplicable(), must return true when the parametrization model should be applied to the particle under consideration. If this is not the case, the default Geant4 physics will be applied.
- The second method, ModelTrigger(), is called in every step along the track and should return true if the user-defined conditions of the track are fulfilled.
- Finally, the implementation of the parameterized model occurs in the DoIt() method.

3.3 WL-7657 FC Simulation

3.3.1 WL-7657 FC Set-up and Run Action in Geant4 using Physical Applications from Garfield++

The simulation was performed using the Geant4 version 10.02 patch 02 (geant4.10.02.p02) [34] and Garfield++ (version 2015.1) [35] interfaces. Geant4 was carried out to simulate the fission reaction (the fission process) inside the chamber. We have included all necessary libraries in order to take all physical aspects of FC into account. The energy deposited in the FC by different particles is tracked by Geant4 until it reaches the boundary of the world volume. Geant4 stores the energy and position for all the steps of particles being able to ionize the gas. Then, from the factor corresponding to the energy required to produce one electron-ion pair, we can determine the number of electron-ion pairs produced and their positions under a uniform electric field. We remember that the drift field is relatively uniform except in the region near the chamber. The output data are afterwards imported in Garfield++ which allows to measure the electron-ion drift lines and the induced signal generated by the drifting of both electrons and ions (pulses that are generally separated and can be obtained by cumulating electron and ion pulses).

3.3.1.1 Detector construction

The FC used in our research work is the WL-7657 fission counter chamber [42]. It is the one used inside the Moroccan TRIGA Mark II reactor. It is designed to detect thermal neutrons in the range of 1.4 to $7{\cdot}10^5$ n/cm^2/s when operated as a counter and from $5{\cdot}10^5$ to $5{\cdot}10^{10}$ n/cm^2/s when operated as a chamber. On the wide range of measurements, the WL-7657 can be operated in three different modes. The WL-7657 is of guard-ling construction, a feature which decreases electrical leakage across the internal insulators, and it may be operated in any position at temperature below 575 °F [42].

The first object which is created in our simulation is the world volume (the root volume of the hierarchy). This is the area in Geant4 at which our physical process will occur. It defines the physical boundary at which all of the physics aspects will be recorded. The creation of the objects, in this case the WL-7657 FC detector, is done in part with the aid of two central concepts. The first is the creation of the logical volume, which includes the material properties, and physical characteristics. The second is the creation of the physical volume, which creates the physical attributes of the logical volume. The world volume is filled with air.

The considered WL-7657 contains approximately 1.68 g of more than 90 % ^{235}U and is filled with a (Ar: 96; N_2: 4) gas mixture maintained at 574.817 °K and 1 atm. The outer radius of the cathode is 38.1 mm and the inner radius of the anode is 21.0 mm. The sensitive length of he chamber is 177.8 mm. A ring of field wires divide the Ar/N_2 volume into an insensitive region at $r < 21$ mm and a sensitive region at $21 < r < 38.1$ mm. Ionization produced at $21 < r < 38.1$ mm is swept by an electric field, of average value $\sim$ 750 V/cm. Our simulations of the WL-7657 are made with an averaged over 10 runs of $1.8{\cdot}10^4$ events based on its mechanical and physical features given by the Table 3.1 below and are all created in Geant4 and can be visualized from Geant4 control as in Fig. 3.4.

TABLE 3.1: WL-7657 Fission chamber mechanical and physical characteristics

Mechanical	
O.D. nominal	3.00 Inches
Length nominal	13.62 Inches
Sensitive Length nominal	7.00 Inches
Net Weight	2.50 Pounds
Shipping Weight	10.00 Pounds
Materials	
Other case	Aluminum
Electrodes	Aluminum
Insulation	AL_2O_3
Fissile deposit (mass)	90 % enriched ^{235}U in U_3O_8 (1.68 g)
Filling gas (pressure)	Argon 96 % Nitrogen 4 % (76 cm of Hg)
Typical operation as a chamber (at approx. 25 °C)	
Operating voltage	300-1000 Volts
Thermal neutron flux:	
Lower limit	$7.0 \cdot 10^{5}$ nv
Upper limit	$1.0 \cdot 10^{10}$ nv
Thermal neutron sensitivity	$1.4 \cdot 10^{-13}$ A/nv
Gamma sensitivity	$4.0 \cdot 10^{-11}$ A/R/Hr
Alpha background current	$2.0 \cdot 10^{-8}$ A

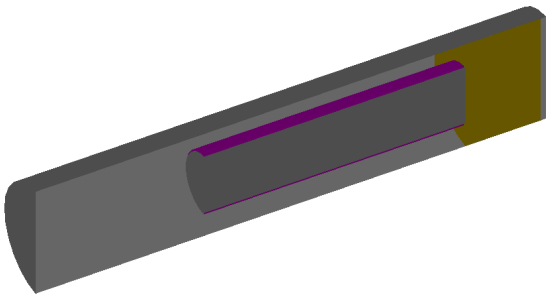

FIGURE 3.4: Three-dimensional cut-away view of WL-7657 FC constructed in Geant4 and visualized by OPENGL.

In order to simulate the overall behaviour of a WL-7657 FC detector, it is necessary to create an interface with Garfield++. Since all the hit parameters will be passed during the simulation, the gas must be created beforehand for ionization purposes. It is created by Magboltz, seeding the gas and HEED model for ionizations which will be described in detail later.

3.3.1.2 Gas in detector

The gas in the simulated WL-7657 FC is constructed in Geant4 which is not able to analyze the electron-ion drifting inside the chamber. Therefore, to achieve this analysis, Garfield++ is used to create the gas inside the chamber. Thus we use Magboltz (9.01) [32], a code which is fully integrated within Garfield++ and allow to creates a gas mixture of (Ar: 96; N_2: 4) at atmospheric pressure.

This process must be done separately in a gas file. This gas file is created ahead of time by the interface with Magboltz which contains all the parameters of the gas given the structure and size of the chamber. Using this information, it produces all of the

properties of the fields numerically and stores them to a file. This procedure takes quite some time and is needed to be completed ahead of the simulation.

3.3.1.3 Run Action

The Run Action is started by creating the WL-7657 FC from all the set parameters. Geant4 sets and describes the detector and the surrounding world volume by its list of properties and physical processes. Once the detector has been constructed, Geant4 then begins by shooting the neutron at the chamber.

The neutron traverses the Geant4 world volume until it reaches the WL-7657 FC, which is defined as the sensitive detector. This sensitive detector is the region in which Geant4 records hits using information from steps along particle track. When a particle hits the sensitive detector, it is stored in memory. As the hit is being processed by Geant4, the physics of Garfield++ is used. This is done by calling the class which uses the physics of Garfield++. Once the call to this class has been completed, with each step in the sensitive detector, the neutron continues to traverse the world volume after the sensitive detector until it reaches the boundary of the world volume. This boundary stops the run action and collects all the information from the event.

3.3.2 WL-7657 FC studies

This analysis uses the transport properties of the gas inside the chamber and calculates the particles transport due to ionizations from the (Ar: 96; N_2: 4) gas. The drifting charged particles are tracked and collected in the signal process.

3.3.2.1 Electron-ion pair production

One very important parameter for gas detectors is the average energy required to form an electron-ion pair in a gas. This energy is referred as W value. The W value depends on the gas composition and density, as well as on the type of the particle. It has been found that for noble gases, W values are lies within 25-45 eV per charge pair for most of the gases and types of radiation (see Table 3.2).

The charges created by the incident radiation are called primary charges to distinguish them from the ones that are indirectly created inside the gas volume. The production mechanism of those additional charges is similar to that of primary charges, except that they are produced by ionization caused by primary charges and not by incident radiation [1].

The W value represents all ionizations that occur inside the active volume of the detector. When a particle deposits $\triangle$E energy inside the gas volume, the W value can be used to determine the total number N of electron-ion pair produced by:

$$N = \frac{\triangle E}{W} \tag{3.1}$$

TABLE 3.2: Ionization potentials I_e, W values, stopping powers (dE/dx), primary ionization yield n_p, and total ionization yield n_t of different gases at standard atmospheric conditions for minimum ionizing particles (i_p stands for the number of electron-ion)

Gas	Z	Density ($\times 10^{-4} g/cm^3$)	I_e (eV)	W (eV/pair)	dE/dX (KeV/cm)	n_p (i_p/cm)	n_t (i_p/cm)
H_2	2	0.8	15.4	37	0.34	5.2	9.2
He	2	1.6	24.6	41	0.32	5.9	7.8
N_2	14	11.7	15.5	35	1.96	10	56
O_2	16	13.3	1.2	31	2.26	22	73
N_e	10	8.4	21.6	36	1.41	12	39
Ar	18	17.8	15.8	26	2.44	29	94
Kr	36	34.9	14.0	24	4.60	22	192
Xe	54	54.9	12.1	22	6.76	44	307
CO_2	22	18.6	13.7	33	3.01	34	91
CH_4	10	6.7	10.8	28	1.48	46	53

If the incident particle deposits all of its energy inside the gas volume, $\triangle$E would be the energy E of the particle. However in case of partial energy loss, the stopping power dE/dx is used to estimate the energy loss $\triangle$E by the ionizing particle, and the above Eq. (3.1) can be written as:

$$N = \frac{1}{W}\frac{dE}{dx} \triangle x \tag{3.2}$$

Where $\triangle$x is the path covered by the particle. Eq. (3.2) can also be rearranged to calculate the number of electron-ion pair per unit of length on the particle track.

$$N = \frac{1}{W}\frac{dE}{dx} \tag{3.3}$$

Gas detectors are sometimes filled with mixtures of gases instead of a single gas, due to the properties those mixtures introduce, regarding drift of charge carriers. In case of a gas mixture, when one pretends to determine the number total and primary charge pairs, a composition law of the Eq. (3.2) can be used, referring to the values in Table 3.2:

$$n_t = \sum_i x_i \frac{(dE/dx)_i}{W_i} \tag{3.4}$$

And

$$n_p = \sum_i x_i n_{p,i} \tag{3.5}$$

Here the i refers to the i^{th} gas in the mixture and x_i is the fraction of the volume gas i [1].

For the current simulation, the electron-ion pairs are implemented through the *MeanNumberOfIonsAlongStep()* method of the G4ElectronIonPair class for each step of

the primary and secondary particles. This class is used to sample ionization clusters in gaseous or silicon detectors. The Fig. 3.5 shows the energy deposited of the charged particles in the gas of each target with a ^{252}Cf source.

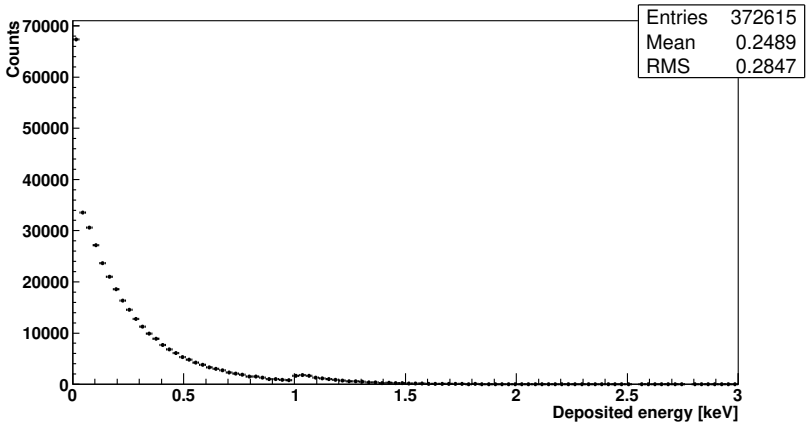

FIGURE 3.5: Energy deposited in gas vs. count.

The number of created pairs is shown on Fig. 3.6. The drift region is endowed with a specific production cut, or range cut-off, that is defined as a threshold (or distance) at which no secondary particle will be generated. Such a cut-in-range is converted into an energy threshold for the current gas mixture by Geant4. The obtained threshold in kinetic energy cannot be below a fixed lower limit. For the current simulation the range cut-off is 1 μm and the low energy limit is set to 26.53 eV, which is the weighted average of the ionization potential of Ar and N_2.

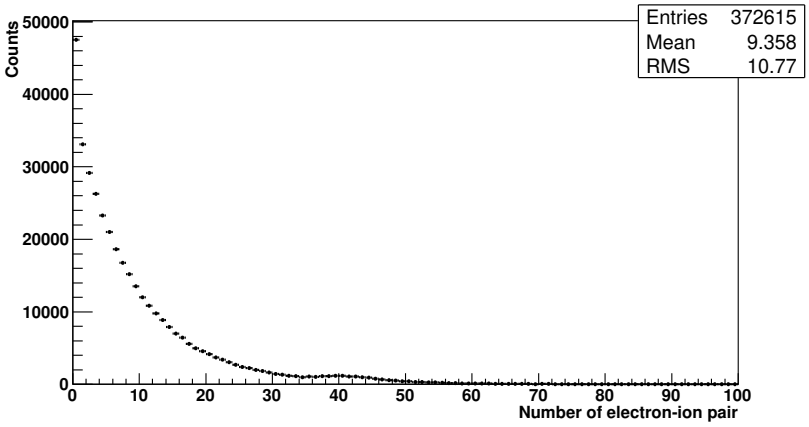

FIGURE 3.6: Number of created pairs vs. count.

3.3.2.2 Electric signal collection

The gas in the simulated FC is constructed in Geant4 which does not allow for the analysis of the electron-ion drifting in the FC. Therefore, to achieve this analysis, Garfield++ includes an interface to Magboltz (9.01) [32]. Furthermore, Garfield++ also includes interface to Heed, a PAI model implementation [39] similar to that in Geant4, can be used to create the initial ionization electron-ion pairs. An electric signal is consequently created inside the FC by Garfield++. The Fig. 3.7 shows the

electric signal generated by a FC. The amplitude of this signal is calculated from parameters of the chamber, such as the number of created pairs generated by one fission product in gas. The signal delivered by a FC is directly proportional to the neutron flux and can be used for the fast identification and selection of particles.

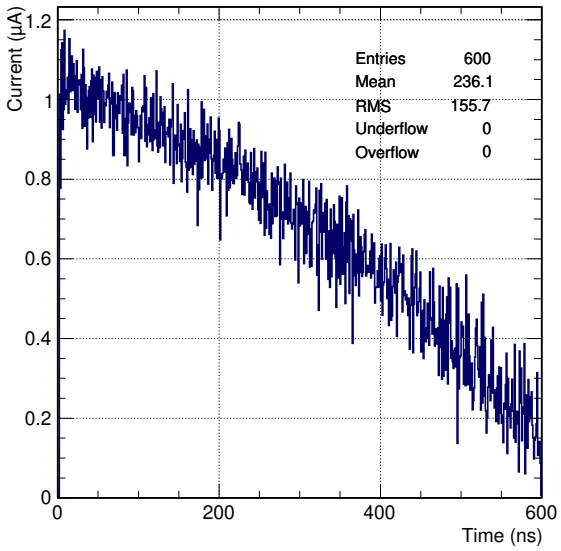

FIGURE 3.7: Electric signal inside the WL-7657 FC as a function of the time.

3.3.2.3 Mean spectra and Charge distribution

The mean pulse of WL-7657 FC, shown Fig. 3.8 has a nearly triangular shape, resulting from an average of 5 pulses. According to [43], the FC with the coated anode has a short rising part due to the heavy ion speed. The charge distribution shown in Fig. 3.9, has the distribution of the charge which is quite similar to CF8 [43]. The spectrum has two peaks which are comparable with the two peaks of the fission yield. Since the heavy ion originally have a two-peak kinetic energy distribution, the ones in the low energy peak are the ones which are stopped in the gas, so they will create less charge, therefore the charge distribution has also two peaks.

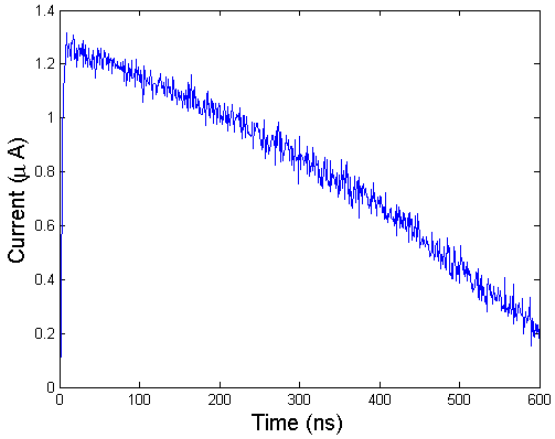

FIGURE 3.8: Mean pulses of WL-7657 FC.

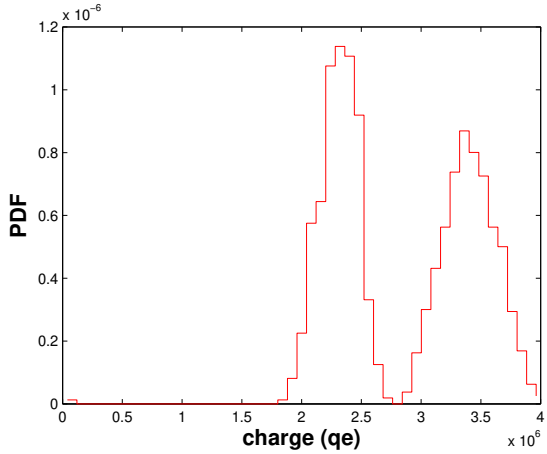

FIGURE 3.9: Charge distribution of WL-7657 FC.

3.4 Conclusion

The WL-7657 FC was simulated by using an interface between Geant4 and Garfield++ toolkits. This interface was done in order to add measurements such as ionization and drift lines of electrons and ions in gas simulation which allows generating an inducted signal produced under the influence of a neutron flux. The obtained time-series will be processed in Chapter 6 by using a new digital signal processing called Blind Source Separation (BSS) methods based on the decomposition of tensor element signals to extract independent components which will be characterized in order to reach the discrimination goal.

Chapter 4

Blind source separation methods

4.1 Introduction

In this chapter, we present the state of the art about Blind Source Separation (BSS) algorithms and their various approaches as alternative techniques which may improve the use of FC's output signals for the "ideal" estimation of neutron pulses and separated from gamma-rays in mixed fields during neutron detection process.

4.2 Blind source separation methods

4.2.1 Generalized blind signal processing problem

Several researches are being carried out these years with digital processing techniques of nuclear signals. We cite here as an example Elbadri et al. works in which they have applied linear and nonlinear adaptive filters to improve the signal to noise ratio (SNR) at the output of an HPGe detector which are used in environment monitoring gamma-ray spectrometry [44]. Trigano et al. used statistical methods to correct the pile-up phenomenon [45]. In addition, Amiri et al. used several quick algorithms to discriminate neutron and gamma radiations captured in a mixed environment [46].

The application of new digital signal processing methods based on Blind Source Separation (BSS), on nuclear data was first introduced by Mekaoui et al. [47–49] for detection and identification of gamma radiation emitters and for the pile-up problem correction at the output of HPGe preamplifier used in gamma spectrometry chains. This has encouraged us to apply this technique for neutron/gamma discrimination inside the Moroccan TRIGA Mark II reactor.

Moreover, BSS techniques now raise great interest and play an important role in a large number of applications in many areas. Their first application solved the "cocktail party" problem [50]. However, there has been no particular application to process and analyze the output signals of FC. Hence, the originality of our research consists in the application of tensor-based blind source separation methods to extract independent components from signals recorded at the WL-7657 FC preamplifier's output. The objective is to achieve software neutron/gamma discrimination.

The BSS principle can be schematized as shown in Fig. 4.1. Thus, BSS methods are used to solve the problem of recovering mutually independent unobserved signals (original sources) from a set of measured observations (mixture sources). The blindness refers to the fact that neither the sources nor the mixing is known.

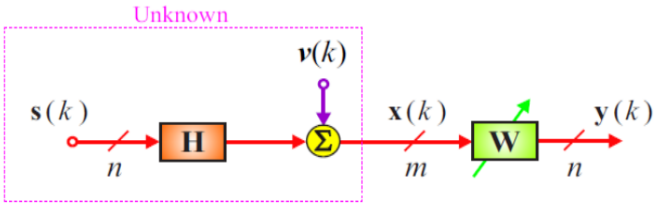

FIGURE 4.1: Block diagram illustrating the basic BSS problem.

4.2.2 Mathematical formalism of BSS

Assume m measureements $x_i(k)(i = 1, 2, ..., m)$ are recorded from a sensors such as antennas, microphones, cameras, and detectors, while coming from the mixture of the unknown sources $s_j(k)(j = 1, 2, ..., n)$ via the unknown m-by-n mixing matrix H (as shown in Fig. 4.1). This system can be formulated according to A. Cichocki et al. in vector form as:

$$x_i(t) = \sum_{j=1}^{n} h_{ij} s_j(k) + \upsilon_i(k) \quad (i = 1, 2, ..., m) \tag{4.1}$$

Or in the matrix notation

$$x(k) = Hs(k) + \upsilon(k) \tag{4.2}$$

Where

- $x(k) = [x_1(k), x_2(k), ..., x_m(k)]^T$ is a vector of observed signals;
- $s(k) = [s_1(k), s_2(k), ..., s_n(k)]^T$ is a vector of sources;
- $\upsilon(k) = [\upsilon_1(k), \upsilon_2(k), ..., \upsilon_m(k)]^T$ is a vector of additive noise;
- H is an unknown full rank $m \times n$ mixing matrix.

The power of BSS approaches resides in their ability to generate the matrix W, called "demixing matrix", approximate better H^{-1} matrix and the components of the vector $\hat{s}(k)$ based only on the recorded observation vector $x(k)$

$$y(k) = Wx(k) = \hat{s}(k) \tag{4.3}$$

The estimated sources are given by the vector $\hat{s}(k)$ and their corresponding projections to the different sensors are given by the estimated matrix of the mixture:

$$\hat{H} = W^{-1} \tag{4.4}$$

A variety of methods/algorithms for BSS have been developed for last decade [50]. Although many different source separation algorithms are available, their principles can be summarized by four distinctive approaches as shown in Fig. 4.2 and described below:

- The most popular approach to BSS exploits the marginal non-Gaussianity or sparseness. When original sources are assumed to be statistically independent and identically distributed (i.i.d.) with no temporal structure, the higher-order statistics (HOS) are essential (implicitly or explicitly) to solve the BSS problem. In such a case, the method is unable to separate more than one Gaussian or near-Gaussian source.
- If the sources are spatially uncorrelated (less restrictive condition than the statistical independence) but temporally correlated (i.e., each source has non-vanishing temporal correlations), then second-order statistics (SOS) is sufficient to estimate the mixing matrix and sources. Note that these SOS methods do not allow the separation of sources with identical power spectra shapes or independent and identically distributed (i.i.d) sources.
- The third approach exploits nonstationarity (NS) and SOS. Mainly, we are interested in the second-order nonstationarity (i.e. that sources have time-varying variances). The nonstationarity was first taken into account by Matsuoka et al. [51] and it was shown that a simple decorrelation technique is sufficient to perform the BSS task. In contrast to other approaches, the methods based on nonstationarity allow the separation of Gaussian sources with identical power spectra shapes. However, it is unable to separate the sources with identical nonstationarity properties.
- The fourth approach exploits the various diversities of signals, typically, time, frequency, (spectral or "time coherence") and/or time-frequency diversities, or more generally, joint space-time-frequency (STF) diversity.

More sophisticated or advanced approaches use combinations or integration of all the above mentioned approaches: HOS, SOS, NS and STF diversity, in order to separate or extract sources with various statistical properties and to reduce the influence of noise and undesirable interferences. In our research, we are interested in using the fourth approache to analyze FC's output signals.

The aim of our work consists in the application of NTF algorithms to extract independent components from signals recorded at the FC preamplifier's output. The objective is to achieve software neutron/gamma discrimination.

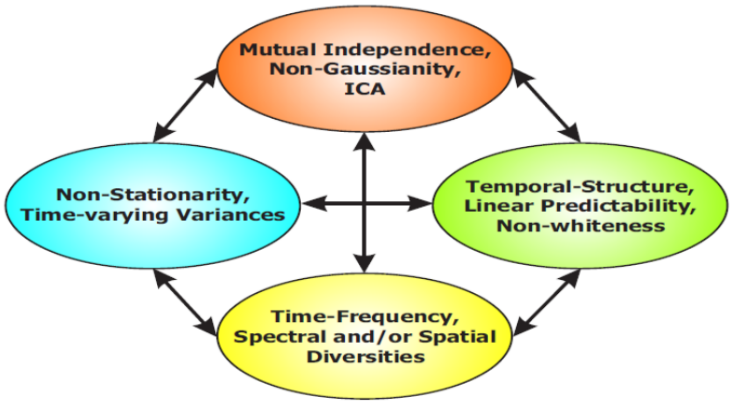

FIGURE 4.2: Basic approaches for BSS [50].

4.3 Nonnegative Tensor Factorization (NTF)

Tensors are mathematical objects for representing multi-way arrays or multi-dimensional arrays. Tensors include vectors and matrices as first-order and 2^{nd} order special cases, respectively, and more generally, tensors of N^{th} order can represent an outer product of N vector spaces and are used in various applications, ranging from neuroscience and psychometrics to chemometrics. Nonnegative Tensor Factorization (NTF) algorithm has been developed by A. Cichocki et al. [50], to allow simultaneous decomposition of non-negative value tensor of components defined by the user into sparse and reasonably interpretable factors. The guaranteed non-negativity of the factors is a distinctive property used as the matrix factorization methods does not always totally reflect these properties and does not convergence to a global solution [52]. Matrices can also be seen as 2^{nd} order tensors. For some applications, it is necessary to involve third or higher order tensors. For this purpose, Nonnegative Matrix Factorization (NMF) can be generalized to Nonnegative Tensor Factorization (NTF) [52].

The NTF model can be considered as a nonnegative Parallel Factor Analysis (PARAFAC) model, where the observed signals are jointly modelled by a 3D tensor (Fig. 4.3). Throughout this work, tensors are limited to three dimensions, and the model extracts two common factors: a basis mixing matrix A and unknown component factors represented by a matrix X, which can be represented in slice factorization form:

$$Y_k = AD_kX + E_k, \quad (\text{k} = 1,2, \ldots , \text{K}) \tag{4.5}$$

Where:

- $Y_k = \underline{Y}_{:,:,k} \in \mathbf{R}^{I \times T}$ represents a frontal slices of 3D tensor $\underline{Y} \in \mathbf{R}^{I \times T \times K}$, K is a number of frontal slices. In our application, Y is formed by recorded FC preamplifier's output signals;
- $A = [a_{ir}] \in \mathbf{R}_+^{I \times R}$ represents the mixing matrix;
- $D_k \in \mathbf{R}_+^{R \times R}$ represents a diagonal matrix that holds the k^{th} row of the matrix $D \in \mathbf{R}_+^{K \times R}$, in its main diagonal;

- $X \in \mathbf{R}_{+}^{R \times T}$ is unknown matrix of independent components to be estimated;
- $E_k = \underline{E}_{:,:,k} \in \mathbf{R}^{I \times T}$ is an additive noise for a k^{th} frontal slice of the tensor.

The NTF model can also be represented by a mathematical tensor-vector such as:

$$\underline{Y} = \sum_{r} a_r \otimes x_r^T \otimes d_r + \underline{E}, \quad (\text{r} = 1, 2, \ldots, \text{R}) \tag{4.6}$$

Where x_r are rows of the matrix X, and a_r and d_r are columns of the matrices A and D, respectively; and $\otimes$ denotes the outer products of vectors.

Or as a form of the scalar:

$$x_{itk} = \sum_{r} a_{ir} x_{rt} d_{kr} + e_{irt}, \quad (\text{i} = 1,2, \ldots, \text{I};\ \text{t} = 1,2, \ldots, \text{T};\ \text{k} = 1,2, \ldots, \text{K}) \tag{4.7}$$

Where x_{itk}, a_{ir}, x_{rt}, d_{kr} and e_{irt} are elements of corresponding tensors or matrices.

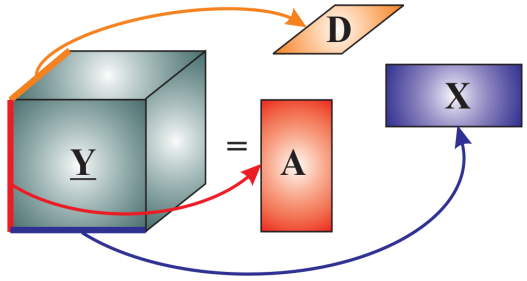

FIGURE 4.3: Decomposition of 3D tensor into three nonnegative matrices using the standard NTF model [53].

4.3.1 Algorithm choice

In order to define the best NTF method able to analyze our simulated WL-7657 FC preamplifier's output signals, we performed various tests. Thus, we used the NTF toolbox which regroups several algorithms. We apply all NTF algorithms to 5 by 5 data matrix formed by signals issued from the preamplifier of Monte Carlo simulated FC. The best NTF algorithm is selected on the basis of its Performance Index of Separability (PI), which is given by the following equation:

$$PI = \frac{1}{n(n-1)} \sum_{i=1}^{n} \left\{ \left(\sum_{k=1}^{n} \frac{|g_{ik}|}{max_j\, |g_{ij}|} - 1 \right) + \left(\sum_{k=1}^{n} \frac{|g_{ki}|}{max_j\, |g_{ji}|} - 1 \right) \right\} \tag{4.8}$$

Where g_{ij} is the (i, j) element of the global system matrix $G = WH$ (H is mixing matrix and W is demixing or separating matrix) and $max_j(g_{ij})$ represents the maximum value among the elements in the i^{th} row vector of G. Also, the term

$max_j(g_{ji})$ corresponds to the maximum value among the elements in the i^{th} column vector of G [50, 54], the most efficient NTF algorithm is the stable one having a minimum PI value. When the perfect separation is achieved, the PI is equal to zero. In practice, a PI value around 10^{-2} indicates quite a good performance [55, 56].

In our case study, the most efficient NTF algorithm is the stable one having a minimum PI value. For that reason, we classify the tested NMF/NTF algorithms according to their PI values. Indeed, we used the NTFLab Toolbox [53] which regroups 8 NMF/NTF algorithms. Among these algorithms, only SMART-NMF, NTF1 and NTF2 algorithms are the most robust and efficient NTF algorithms to analyze our mixed nuclear data.

Three common NTF algorithms used in our work are presented here. We focus here on explaining the optimization techniques.

4.3.1.1 The SMART-NMF algorithm

The SMART-NMF (Simultaneous Multiplicative Algebraic Reconstruction Technique) algorithms have been developed by A. Cichocki et al. [57]. They were specially designed for solving NMF related problems with supplementary constraints such as sparsity and/or smoothness. The SMART-NMF algorithms are characterized by improved efficiency and often very good convergence rate. They can be applied to analyze data in various scientific fields. The generalized form of SMART-NMF algorithms, as it has been reported by A. Cichocki et al. [50], is as follows:

Algorithm 1 Generalized SMART-NMF

Input: $Y \in \mathbf{R}_+^{I \times T}$: input data, J: rank of approximation
$\rho(y_{it}, q_{it}) = -\frac{\partial D(Y||Q)}{\partial q_{it}}$: error function
Output: $A \in \mathbf{R}_+^{I \times J}$ and $X \in \mathbf{R}_+^{J \times T}$ such that cost function $D(Y||AX)$ is minimized.
1: **begin**
initialization for A and X
2: **repeat**
$X \leftarrow X \circ exp(\eta_X \circ (A^T \rho(Y, AX)))$ /* update X */
$A \leftarrow A \circ exp(\eta_A \circ (\rho(Y, AX)X^T))$ /* update A */
foreach a_j of A **do** $a_j \leftarrow a_j / ||a_j||_p$ /* normalize to l_p unit length */
3: **until** a stopping criterion is met /* convergence condition */
4: **end**

4.3.1.2 The NTF1 algorithm

In 3D NTF1 model, which is an extension of the NTF model (Fig. 4.4), a given data tensor $\underline{Y} \in \mathbf{R}^{I \times T \times K}$ (Observed data) is decomposed to a set of matrices A, D and $\{X_1, X_2, ..., X_K\}$ with nonnegative entries.

$$Y_k = AD_kX_k + E_k, \quad (\text{k} = 1,2, \ldots , \text{K}) \tag{4.9}$$

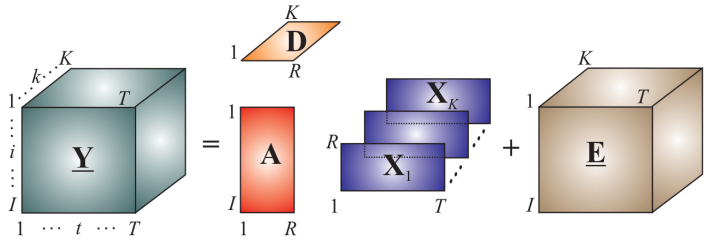

FIGURE 4.4: Illustration of NTF1 model.

Since the nonnegative diagonal matrices $D_k \in \mathbf{R}_+^{R\times R}$ are scaling matrices, they can usually be absorbed by the matrices $X_k \in \mathbf{R}_+^{R\times T}$ by introducing row-normalized matrices $X_k := D_k X_k \in \mathbf{R}_+^{R\times T}$, hence $Y_k = AX_k + E_k$ [53].

4.3.1.3 The NTF2 algorithm

In 3D NTF2 model, which is also an extension of the NTF model (Fig. 4.5), the observed data $\underline{Y} \in \mathbf{R}^{I\times T\times K}$ is decomposed to a set of matrices $\{A_1, A_2, ..., A_K\}$, D and X with nonnegative entries.

$$Y_k = A_k D_k X + E_k, \quad \text{(k = 1,2, ... , K)} \tag{4.10}$$

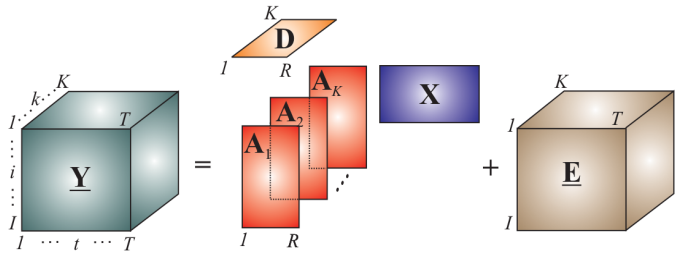

FIGURE 4.5: Illustration of NTF2 model.

The NTF2 model is similar to the NTF1 but in this case the nonnegative diagonal matrices $D_k \in \mathbf{R}_+^{R\times R}$ can usually be absorbed by the matrices $A_k \in \mathbf{R}_+^{I\times R}$ by introducing column-normalized matrices $A_k := A_k D_k \in \mathbf{R}_+^{I\times R}$, hence $Y_k = A_k X + E_k$ [53].

4.4 Conclusion

In this chapter, the Nonnegative Tensor Factorization problem was defined and three algorithms to compute this factorization were presented according to their PI which can be applied to obtain accurate estimates from reduced set of observations. In a forthcoming chapter, the three different effective algorithms will be applied to allow the processing of WL-7657 FC's output signals.

Part III

Results and discussion

Chapter 5

Neutron/gamma discrimination

5.1 Introduction

Gamma-rays are usually accompanying neutrons in neutron detection which reinforce the importance of neutron/gamma discrimination (NGD). Several methods have been developed to identify and reject the background events induced by gamma-ray in neutron counting measurements. Most of these methods use analog discrimination of neutrons and gamma-rays, such as rise time method (RT), zero crossing method (ZC) and charge comparison method (CC). Recently, systems based on digital signal processors (DSP) and field programmable gate arrays (FPGA) offer significant advantages over analog systems. In this chapter various analog and digital methods for NGD are discussed and compared.

5.2 Pulse Shape Discrimination methods (PSD)

Pulse shape discrimination (PSD) is basically used to distinguish between different type of radiations (i.e. alpha particles, beta particles, gamma-rays, and neutrons). It exploits the dependence of the signal on the characteristics of radiation type (charge, mass and energy). Difference in shape of the pulse is due to the difference in the time profile of the electric charge pulses produced at the neutron detector by different radiation. Sensing these differences in pulse shape i.e., time profile of the pulse serves a useful purpose when these method are applied to the output of a large number of different detector types.

Methods of PSD are totally dependent on whether detector output signal pulse is directly used for the analysis or the detector output pulse is processed in an attached preamplifier to produce the resulting output pulse that is subsequently analyzed. The PSD generally measure differences between the integrated charge in the entire pulse and the integrated charge over the rising or falling portion. The integrated charge over the entire pulse is a function of both the energy of the radiation and the type of radiation detected. The rising portion of the pulse is most representative of the energy of radiation detected while falling portion of the pulse is most representative of the type of radiation detected [58].

In digital PSD, the output of detector or preamplifier is digitized and sampled data are transferred to computer memory from an on board memory for future analysis. Digital PSD methods provide more flexibility than analog PSD methods in handling

individual pulses and performing pulse shape analysis. The main advantages of digital PSD methods over analog PSD methods are: reduction in the size of required electronics, multi parameter analysis feature, increased versatility, improved performance, increase in throughput rate, decreased jitter, fully computer-controlled operation, high reliability, flexibility etc.

5.2.1 Analog PSD methods

Three analog PSD methods implemented in time domain and traditionally used to perform the neutron/gamma discrimination are the following [59]:

- Rise Time method (RT);
- Zero Crossing method (ZC);
- Charge Comparison method (CC).

5.2.1.1 Rise Time method (RT)

The Rise Time method (RT) [59] does not work directly with the current pulse (i.e. of the anode pulse of the photomultiplier (PMT) (as in Fig. 5.1 (left)) but with its integral. The current output of a heavily ionizing particle, which in NGD is proton (neutron), has long tail; hence, the time at which this fraction is reached is normally longer than that of an electron (gamma-ray). When we normalize the integral of the neutron and gamma-ray pulses to 1, it is clear that the integral of a gamma-ray pulse will rise faster than that of a neutron pulse. An illustration of this method is in Fig. 5.1.

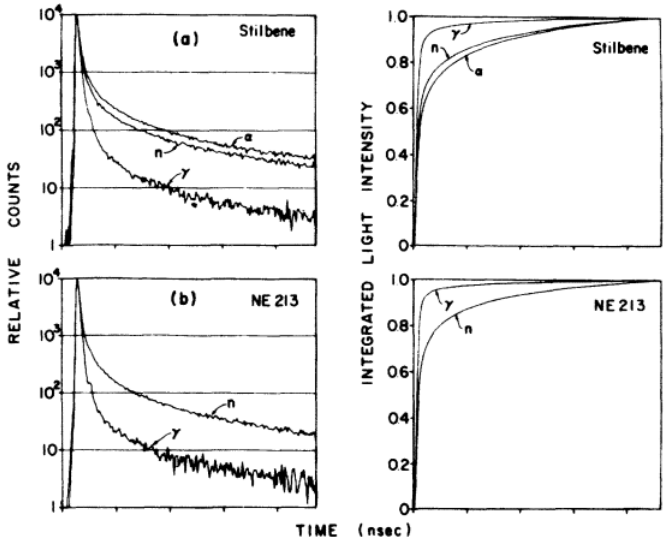

FIGURE 5.1: Current output (left) and integrated pulse (right) illustrating the NGD according to rise time method for organic scintillators stilbene and NE213 [59].

5.2.1.2 Zero Crossing method (ZC)

The Zero Crossing method (ZC) [60] is an indirect evaluation of the RT method. This method will shape the current pulse signal to bipolar form that crosses the threshold level (referred to as "zero") at different times depending on the detected particle. This shaping is made first by integrating the current pulse signal by a CR circuit, then differentiating the resulting pulse by a RC differentiator to eliminate the statistical fluctuations. It is based on the simple observation that the more slowly the pulse decays the "wider" it is; therefore, proton (neutron) pulses are generally wider than the electron (gamma-ray) ones. When the measuring device is configured in a certain way, the "width" of the pulse may be detected by means of zero-crossing as illustrated in Fig. 5.2.

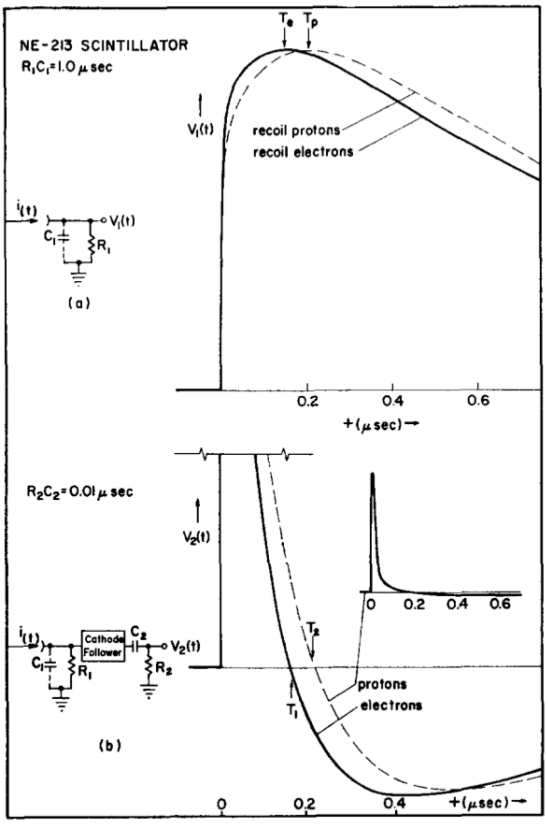

FIGURE 5.2: (a) The voltage pulse shapes integrated by CR circuit and (b) the voltage pulse shapes resulting from an RC differentiation within an NE-213 scintillator [60].

5.2.1.3 Charge Comparison method (CC)

The Charge Comparison method (CC), also known as charge integration method is based on a comparison of the integrals under a current pulse signal by using two charge-sensitive analog-to-digital converters (ADCs), one to integrate the entire charge of the pulse and the other to integrate the tail of it. The comparison of the two different integrals of the current pulse signal will reveal which particle created the pulse, proton (neutron) or electron (gamma-ray). The choice of the two timing intervals, at which the integration of the pulse should be measured, is based on a specific detector. Several researchers have been proposed or used CC method either by comparing the short and long, or total and

delayed, or total and tail components of the integral pulse [61–69]. For example, in [65], the integral ratio of two different pulse intervals, the first interval covers the tail of a pulse, while the second one covers the total pulse. These two intervals on a current pulse signal are shown in Fig. 5.3: T_{1start} is the starting point of the total integral (A_1) and T_{2start} is the starting point of the tail integral (A_2) and T_{end} is the ending point of both. The time intervals over which the total and tail integrals are calculated were optimized to increase the performance of the PSD method with the objective of minimizing the number of misclassified pulses. Since heavy particles produces pulses with a large fraction of light in the tail. This results in a shorter ratio of tail-to-total integrals for gamma-ray pulses when compared to neutron pulses. The ratio of tail-to-total integrals is calculated as:

$$E = \frac{\text{Tail integral}}{\text{Total integral}} = \frac{A_2}{A_1} \tag{5.1}$$

Neutron and gamma-ray pulses can be differentiated by plotting the ratio of tail-to-total integrals as shown in Fig. 5.4. The discrimination line indicated that the pulse above this line are classified as neutrons and pulse below this line as gamma-rays.

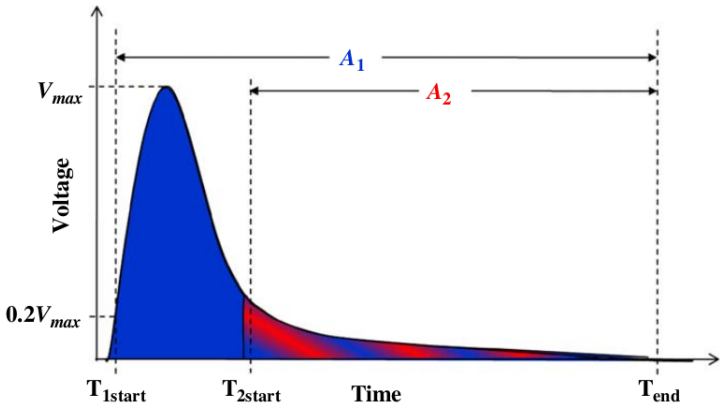

FIGURE 5.3: Illustration of the pulse shape obtained from the EJ-309 liquid scintillator. The total integral (A_1) and tail integral (A_2) are computed for each pulse and used for classification as a neutron or gamma-ray. Pulse timing was achieved by measuring the time at which the pulse reaches 20 % of the pulse amplitude [65].

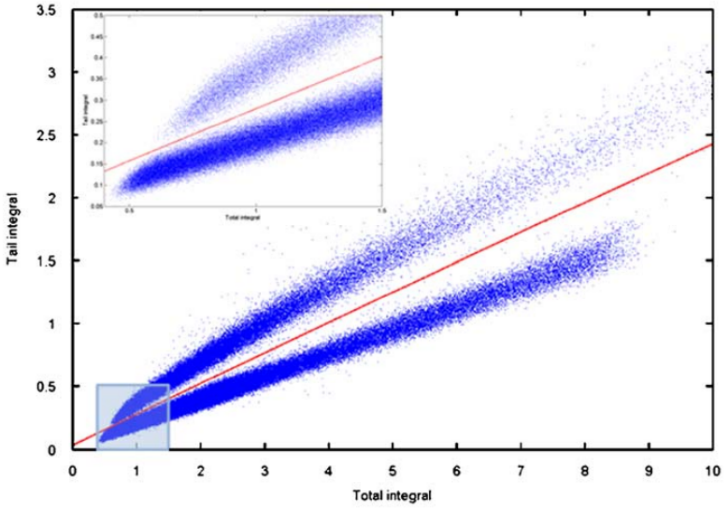

FIGURE 5.4: Tail and total pulse integrals for measured pulses from a 500-g, low-burnup PuO_2 sample [65].

5.2.2 Digital PSD methods

The development of fast analog-to-digital converters (ADCs) and the use of digital signal processors (DSP) allow the implementation of analog NGD methods with field programmable gate array (FPGA) technology and other electronic equipment (i.e. fast storage). The major difference between analog and digital PSD methods is that with the digital PSD method, the incoming pulse from the detector are immediately digitized and all operations of processing are carried out in software package.

Analog to digital PSD uses the three conventional methods that were developed for analog methods. Indeed, the conventional or analog methods have their digital counterparts:

- Rise Time method (RT) [70–74];
- Charge Comparison method (CC) [68, 71, 75];
- Zero-crossing method (ZC) [71, 72, 76].

The flexibility of digital processing allowed several digital PSD methods to be developed that were not feasible with analog PSD such as the curve fitting of a predefined response function to each pulse, pulse gradient analysis, frequency gradient analysis, simplified digital charge collection, neutron gamma model analysis, wavelet Transform and artificial neural network, which have been solely applied in the digital domain. However, due to the susceptibility of these methods to electronic noise or intensive computation time, the double integration method, which is a digital version of the conventional analogue charge comparison method, is mostly used [76].

5.2.2.1 Curve Fitting method (CF)

The radiation types are identified from the decay time of the pulse [77]. The decay time is assumed through the fitting of the tail part of the pulse with the following single curve given by the Eq. (5.2):

$$Y = e^{-\lambda t} \tag{5.2}$$

The decay constant λ is the shape parameter, and a scatter plot of λ versus peak-height gives the information of PSD. A typical fitting result is shown in the Fig. 5.5 and the result of the CF method is shown in the Fig. 5.6.

The result of this method shows better separation between neutron and gamma-ray than CC method, and is partly due to reduction of noise through the curve fitting procedure.

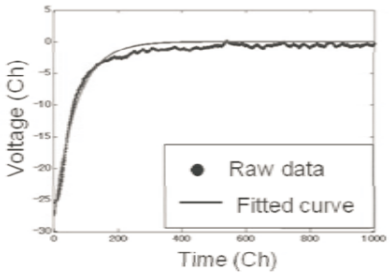

FIGURE 5.5: A typical results of fitting to the experimental data [77].

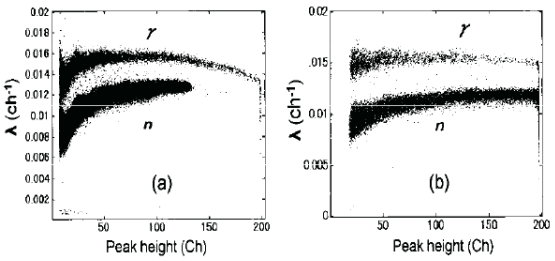

FIGURE 5.6: Scatter plots for λ ($channel^{-1}$) versus peak-height in the curve fitting method; (a) low gain, (b) high gain [77].

5.2.2.2 Pulse Gradient Analysis (PGA)

The Pulse Gradient Analysis (PGA) method, first presented by D'Mellow et al. [78] is a non-linear uses gradient analysis to discriminate radiation particles. PGA is based on the comparison of the relative heights of the samples in the trailing edge of the pulse. It is determined by calculating the ratio of pulse peak (P_p) and sample delayed by offset samples (S_p + delayed), found experimentally depending on detector type.

$$R = \frac{S_p + delayed}{P_p} \tag{5.3}$$

The value of R as given in Eq. (5.3) determines the type of particle. If the value of R is less than a specific threshold, the pulse is attributed to a gamma-ray; otherwise it is attributed to a neutron. Since it takes into account only two samples from the pulse data set, it is more sensitive to noise. To improve performance instead of considering second sample value its average over points N is considered. The PGA method plots the peak amplitude of the pulse on the ordinate and the discrimination amplitude of the pulse (the amplitude at a specified time after the peak amplitude) on the abscissa. An example scatter plot of this method is shown in Fig. 5.7. Two distinct clusters of pulse shapes are observed, which correspond to gamma-ray and neutron pulse shapes respectively.

This method has a great dependency on the de-noising algorithm. PGA method compared to digital implementation of CC method provides improvement in discrimination ability. Real-time implementation of PGA method takes less computation time than Artificial Neural Networks (ANN).

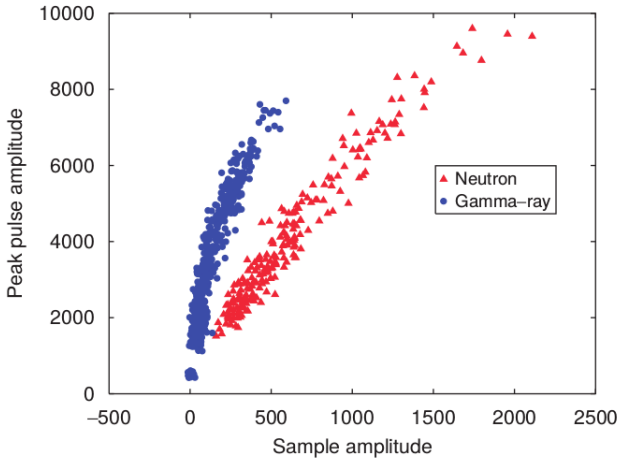

FIGURE 5.7: A scatter plot of the peak amplitude versus the discrimination amplitude, illustrating the NGD according to PGA [78].

5.2.2.3 Frequency Gradient Analysis (FGA)

The Frequency Gradient Analysis method (FGA) is a natural possible development of the PGA method [79] into the frequency domain. The method exploits the difference between the zero frequency components and the first frequency component of Fourier transform of the acquired signal. The discrimination parameter of this purpose is defined as:

$$K_f(f) = \frac{|X(0)| - |X(f)|}{f} \tag{5.4}$$

Where the |X(0)| is the average value of x(t) at the zero frequency, and the |X(f)| is the magnitude spectrum of x(t) at frequency f. Fig. 5.8 shows the dependence of |X(f)| with f for neutron and gamma-ray particles. From Fig. 5.8, we observe that the two waveforms intersect at 13.9 MHz, below this frequency the amplitude of each frequency component of the neutron pulse is greater than that of the gamma-ray pulse.

However, above this frequency the magnitude spectra of both pulses have nearly the same amplitude so it is impossible to discriminate.

FGA method exhibits a strong insensitivity to the variation in pulse response of the current pulse. It is shown that the FGA method results in an increased Figure Of Merit (FOM) which corresponds to a reduction in the area of overlap between neutron and gamma-ray pulses and can also be implemented real time as in case for the PGA method.

Performance of FGA is better than PGA since PGA is very sensitive to noise and variations of the light intensity from the detector. FGA is less sensitive to high-frequency components responsible for the variation in pulse shape giving a prominent improvement in FOM, but it is more computationally laborious than PGA.

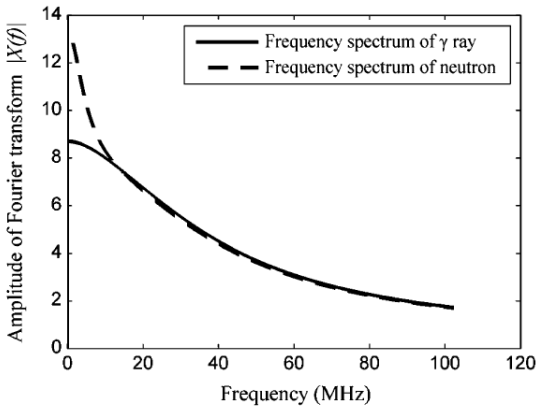

FIGURE 5.8: NGD according to FGA [79].

5.2.2.4 Simplified Digital Charge Collection (SDCC)

The Simplified Digital Charge Collection method (SDCC) [80] is based on the peak amplitude and a discrimination parameter (D), which is calculated with use of the short integral as in Eq. (5.5).

$$D = \log\left(\sum_{n=a}^{b} x_n^2\right) \tag{5.5}$$

Where x_n is the magnitude of the n^{th} sample of the pulse, and a and b are the samples associated with the start and the end number of the short integral, respectively. Generally, a and b correspond to the samples at three-sixteenths and one half of the pulse length, respectively. The discrimination parameter is plotted against the peak amplitude to get the pulse shape discrimination plot as shown in Fig. 5.9.

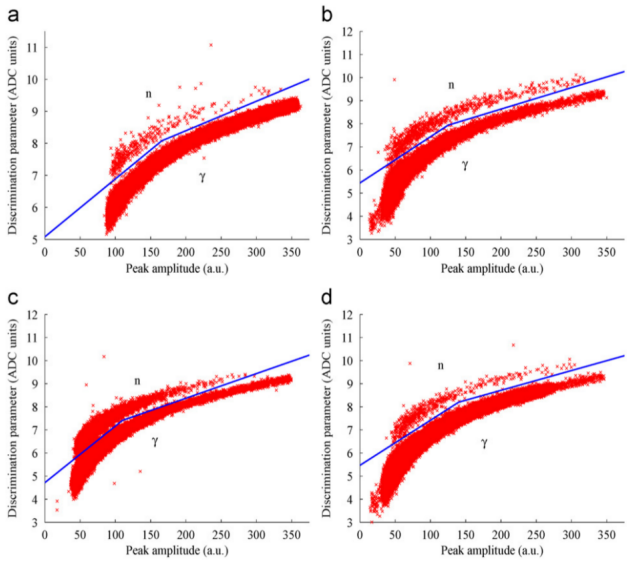

FIGURE 5.9: NGD according to SDCC [81] for (a) Am/Be, (b) Am/Li, (c) Cf, (d) Pu/Li.

5.2.2.5 Neutron Gamma Model Analysis (NGMA)

For the Neutron Gamma Model Analysis (NGMA) method as discussed in [81], neutron and gamma-ray pulse shapes are modelled and compared with the pulses obtained from the source. The modelling was performed using a set of known gamma-ray and neutron pulses. The neutron and gamma-ray pulses are distinguished by calculating the difference between the chi-squared χ^2 for the gamma-ray model (χ^2_γ) and neutron model (χ^2_n). If the chi-squared difference (χ^2_γ - χ^2_n) is negative, the unknown pulse is attributed to a gamma-ray model; otherwise it is attributed to a neutron model. The following equations are used in this modelling:

$$\chi^2_\gamma = \sum_{i=1}^{n} \frac{\left(\frac{Am_g}{Ap_u} p_u(i) - m_g(i)\right)^2}{m_g(i)} \tag{5.6}$$

$$\chi^2_n = \sum_{i=1}^{n} \frac{\left(\frac{Am_n}{Ap_u} p_u(i) - m_n(i)\right)^2}{m_n(i)} \tag{5.7}$$

$$\Delta\chi^2 = \chi^2_\gamma - \chi^2_n \tag{5.8}$$

Where p_u, m_g and m_n are unknown pulse, model gamma-ray pulse and model neutron pulse respectively, whilst Ap_u ,Am_g and Am_n are area of the unknown pulse, model gamma-ray pulse and model neutron pulse respectively, for i^{th} sample.

The Fig. 5.10 shows the NGD using NGMA. The lower branch corresponds to gamma-ray pulse shapes and the upper branch corresponds to neutron pulse shapes.

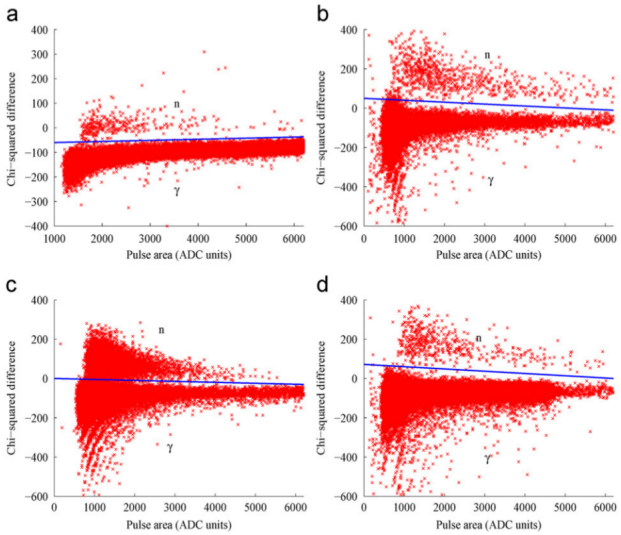

FIGURE 5.10: NGD according to NGMA [81] for (a) Am/Be, (b) Am/Li, (c) Cf, (d) Pu/Li.

5.2.2.6 Wavelet Transform based method (WT)

Wavelet Transform method [82] uses frequency domain features of neutron gamma-ray pulses for discrimination. It is efficient in NGD when compared to the time domain methods, particularly in the mixed radiation field with high noise frequency additive level. The wavelet transform of a function $f \in L^2(\mathbf{R})$ (the space of square integral functions over $\mathbf{R}$) at scale a and shift b, is defined as:

$$W_f(a,b) = \langle f, \Psi_{a,b} \rangle = \int_{-\infty}^{\infty} f(t) \frac{1}{\sqrt{a}} \psi^* \left(\frac{t-a}{b} \right) dt \tag{5.9}$$

Where $\psi \in L^2(\mathbf{R})$ is the wavelet function with zero average and unit L^2 norm $||\psi||^2 = 1$. It should be noted that before computing the wavelet transform, the input pulses must normalized to a unit peak-to-peak signal to remove the dependency of the wavelet transform on the amplitude of the pulse.

A new function P(a) called the "Scale Function" is computed using the equation below defined as the energy of the wavelet transform of the signal at a specific scale and with different shifts.

$$P(a) = \frac{1}{1+n_b} \sum_{j=0}^{n_b} \left| W_\psi^s(a, b_j) \right|^2 \tag{5.10}$$

Typical neutron and gamma-ray waveforms with their corresponding scale functions are plotted in Fig. 5.11. It can be observed that the scale function provides a good separation between neutron and gamma-ray pulses. The values of the scale function at two scales are selected as a discrimination parameter. These scales are chosen as power of 2, which is easily implemented in the discrete wavelet transform (DWT). The DWT can be easily implemented in digital processors and FPGAs [83]. The optimum features are selected using the following equations:

$$f_1 = P(a)|_{a=512} \tag{5.11}$$

And

$$f_2 = \frac{P(a)|_{a=1024}}{P(a)|_{a=512}} \tag{5.12}$$

This method provides an improved performance compared to the PGA and FGA methods. The NGD is obtained by defining simple boundaries, which make it easy when compared to PGA and FGA where the separation is defined by a non-linear discriminator line.

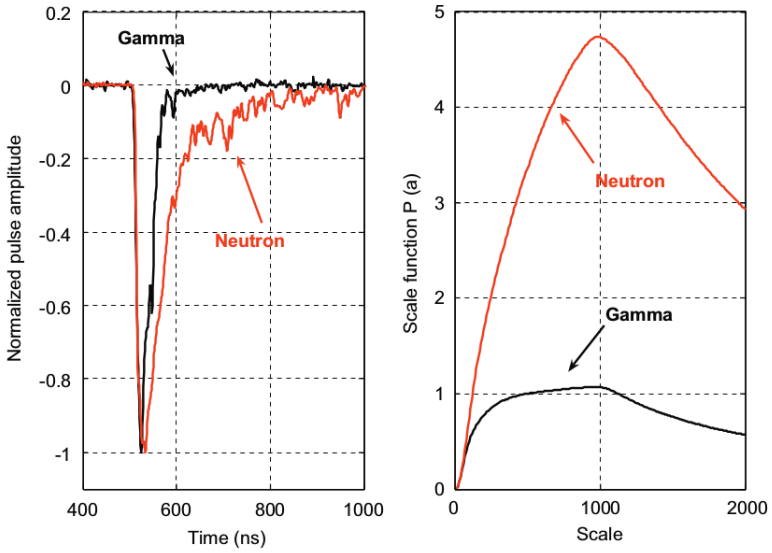

FIGURE 5.11: Typical neutron and gamma normalized pulse shapes with their corresponding scale functions.

5.2.2.7 Artificial Neural Networks (ANN)

Artificial neural networks (ANN) [84] are mathematical models similar to biological neurons in the human brain. They consist of several artificial neurons which are processing units and they are linked to each other via adaptive synaptic weights. By this synaptic links, the neurons in the different layers communicate with each other and the data is transmitted between them. The classical ANN consists of three layers: input layer, hidden layer(s) and output layer. The number of hidden layers and the number of units in each layer depends on the nature of the problem. The topological construction is shown in Fig. 5.12.

Several researchers have been proposed or used ANN algorithm to discriminate neutron and gamma-ray pulses [85–88]. For example, in the approach used in Ref. [85], perceptron and back-propagation (BP) neural networks that use pulse amplitude and pulse rise time information recorded by a single data acquisition system with a delay are used to neglect the energy dependence of the PSD bias. Results from this approach show that using neural network classifiers, one can obtain a separation of neutron and gamma-ray pulses with about 5 % error for neutrons with energies as low as 100 keV. In the technique used in Ref. [86], Esposito et al. suggested a method for nuclear

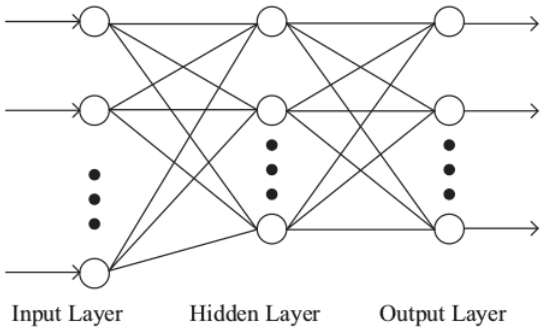

FIGURE 5.12: The architecture of the classical ANN.

fusion applications using ANN algorithm. The technique used in this work is based on two Multi-Layer Perceptrons (MLP). The first MLP allows to discriminate between neutrons, gamma-ray and fast pile-up pulses. If a pile-up is detected, the second MLP analysis the pulses and distinguishes the original pile-ups. In the Ref. [87] Ronchi et al. suggested other possibilities of ANN for classification of neutron and gamma-ray pulses and identification of pile-up pulses. In their work they tried several algorithms for ANN learning. They are Levenberg-Marquardt algorithm with Bayesian regularization, an algorithm of Resilient Back-propagation and an algorithm of Scaled Conjugated Gradients. They reached the best results with Levenberg-Marquardt algorithm, which is more suitable for approximation of functions rather than for classification. According to authors, the reason is the noise contained in the test data. In Ref. [88] the ANN discrimination system is consists of two units: a pile-up management unit and a discrimination unit based on ANN. First, in order to deconvolve pile-up pulses, a pile-up management unit based on a fitting method is designed. Next, each individual pulse is processed by a discrimination unit to recognize neutron and gamma-ray pulses.

5.2.3 Metrics to Compare PSD Methods

A few metrics are used to compare PSD methods. One of such gauge is the Figure Of Merit (FOM) used to quantify the performance of a PSD defined as:

$$FOM = \frac{S}{FWHM_n + FWHM_\gamma} \tag{5.13}$$

Where S is the separation between the peaks of neutron and gamma-ray pulses, the $FWHM_n$ and $FWHM_\gamma$ are the full width at half maximum (FWHM) of the spread of neutron and gamma-ray peaks, respectively (Fig. 5.13). Another is the R-factor, the ratio of number of gamma-ray counts to the number of neutron counts as defined in Eq. (5.13) which is often utilised to quantify the gamma-ray rejection efficiency in neutron detectors.

$$R = \frac{\sum_\gamma}{\sum_n} \tag{5.14}$$

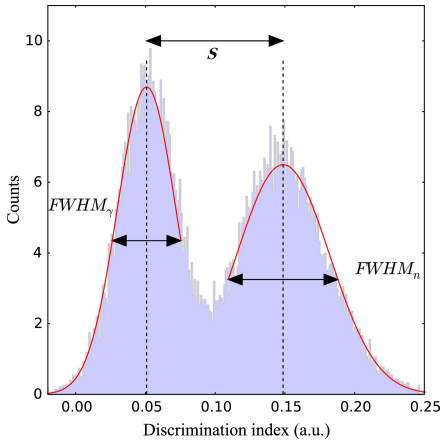

FIGURE 5.13: Illustration of FOM.

5.2.4 Comparison of PSD methods

Ref. [81] compares four different digital pulse shape discrimination, specifically the CC (referred in Ref. [81] to as CCM), PGA, NGMA and SDCC, for the data produced using an organic liquid scintillator detector (BC501) and radiation produced from sources such as ^{241}Am/Be, ^{241}Am/Li, ^{252}Cf, and ^{238}Pu/Li. The R-factor and FOM have been used to compare these four digital methods. Table 5.1 shows the results of the analysis. Ref. [81] concludes that SDCC is better when compared to the other three digital PSD methods (CC, PGA and NGMA) in terms of the FOM and therefore a better NGD.

TABLE 5.1: FOM and R-factor values for each the four different neutron/gamma discrimination algorithms

Source	Method	γ-rays	Neutrons	$FWHM_\gamma$	$FWHM_n$	FOM	R-factor
Am/Be	PGA	28851	358	2.69 ±0.01	3.98 ±0.01	0.831±0.002	81±4
	CCM	28856	353	109 ±1	170 ±1	0.753±0.005	82±4
	NGMA	28866	343	41 ±1	86 ±1	0.93±0.01	84±5
	SDCC	28852	357	0.39 ±0.01	0.60 ±0.01	0.97±0.02	81±4
Am/Li	PGA	49993	716	1.76 ±0.01	4.01 ±0.01	0.839±0.003	70±3
	CCM	49887	822	74 ±1	184 ±1	0.915±0.006	61±2
	NGMA	49839	870	63 ±1	201 ±1	0.806±0.006	57±2
	SDCC	49917	792	0.47 ±0.01	0.59 ±0.01	1.05±0.02	63±2
^{252}Cf	PGA	56377	9278	1.08 ±0.01	1.97 ±0.01	1.007±0.006	6.08±0.07
	CCM	56373	9282	45 ±1	66 ±1	1.04±0.02	6.07±0.07
	NGMA	56698	8957	51 ±1	98 ±1	1.05±0.01	6.33±0.07
	SDCC	56394	9261	0.36 ±0.01	0.45 ±0.01	1.19±0.02	6.08±0.07
Pu/Li	PGA	65291	513	2.67 ±0.01	2.98 ±0.01	0.889±0.03	127±6
	CCM	65265	539	87 ±1	197 ±1	0.870±0.006	121±5
	NGMA	65283	521	75 ±1	180 ±1	0.855±0.006	125±6
	SDCC	65278	526	0.35 ±0.01	0.64 ±0.01	1.14±0.02	124±5

5.3 Conclusion

As discussed in this chapter, due to the sensitivity of neutron detectors to gamma-rays, pulse shape discrimination methods are required to distinguish neutron and gamma-ray pulses. The two general categories of PSD methods are analog and digital methods which are researched and documented. The digital DSP methods offer significant advantages over the analog PSD methods in the areas of cost, accuracy, efficiency, and cost by eliminating necessitate for extra electronic modules.

It can be concluded that performance of frequency domain methods are less sensitive to noise effects and variations of the light intensity from detector. The relative performance of RT, ZC and CC methods varies for two different categories of PSD methods and depends on radiation detector (except CC Method) and also on signal-to-noise ratio (SNR). FGA method gives better NGD than PGA, but takes more computation time. Whilst Wavelet method gives improvement in FOM compared to the PGA and FGA methods and also takes more computational time and is well suited for embedded platforms. SDCC method appears to be an improvement over CC, PGA and NGMA methods in terms of its discrimination capabilities. The ANN method, as an effective non-parameter pattern recognition tool, has significant potential to discriminate neutron and gamma-ray pulses.

Chapter 6

Identification and characterization of sources

6.1 Introduction

Inside nuclear reactors, gamma-rays emitted from nuclei together with the neutrons introduce unwanted backgrounds in neutron spectra. For this reason, powerful extraction methods are needed to extract useful neutron signal from recorded mixture and thus to obtain clearer neutron flux spectrum. Actually, several methods have been developed to discriminate between neutrons and gamma-rays in a mixed radiation field; most of these methods are discussed in Chapter 5. As alternative to these methods, we aim in this chapter to verify the feasibility of using a Nonnegative Tensor Factorization (NTF) algorithms to blind extract neutron component from mixture signals recorded at the output of WL-7657 FC.

The computation of performance index of each Blind Source Separation (BSS) algorithm will allow us to select the most efficient NTF algorithm that allows to achieve the best neutron/gamma discrimination. Once the separation task is achieved, we evaluate the signal to noise or interference ratio (SNR/SIR) from individual columns of the mixing matrix; the values of this parameter allows us to detect easily the number of sources. In addition, the computation of the normalized correlation functions and the power spectral densities of the resulting independent components will provide a better characterization of these nuclear signals with very high precision.

In this study, a full simulation of a WL-7657 fission chamber detector based on the Geant4/Garfield++ interface has been developed and described in Chapter 3 and validated through comparison with the results of pyFC (python-based simulation of Fission Chambers).

6.2 Application of the Nonnegative Tensor Factorization in nuclear data processing

Due to the practical nature of Nonnegative Tensor Factorization (NTF) algorithms, they have been largely applied to problems in numerous application areas such as neurosciences, document identification and classification, telecommunications, multi-way data analysis, etc [50]. We introduce here the background of NTF in nuclear

data processing area, and discuss its applications within the context of the present work. Three common NTF algorithms used in our work were presented in Chapter 4 according to their corresponding performance indexes. The Fig. 6.1 below summarizes the steps which will be followed in this work.

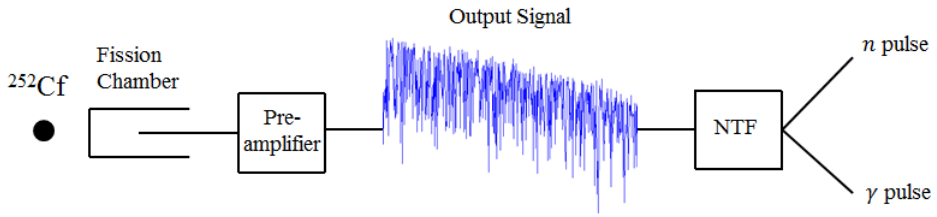

FIGURE 6.1: Block diagram of neutron/gamma discrimination based on NTF approach.

6.2.1 Application of SMART-NMF algorithm

To obtain the sampled data of mixed neutron and gamma-ray pulses, a full simulation of a WL-7657 FC detector based on the Geant4/Garfield++ interface has been developed using a thermal neutron source. In order to define the best NTF algorithm able to analyze simulated FC preamplifier's output signals, we performed various tests. Thus, we used the NTF toolbox which regroups several algorithms. We apply all NTF algorithms to 5 by 5 data matrix formed by signals issued from the preamplifier of Monte Carlo simulated FC. The best NTF algorithm is selected on the basis of its Performance Index of Separability (PI) [89].

According to A. Cichocki et al. [50], the most efficient NTF algorithm is the stable one having a minimum PI value. For that reason, we classify the tested NTF algorithms according to their PI values. Indeed, we used the NTFLab Toolbox developed by A. Cichocki et al., which is implemented under MATLAB® environment [53] and regroups 8 NTF algorithms. Among these algorithms, only 4 have a stable value of the PI as shown in Table 6.1 below. It appears from these results that the Simultaneous Multiplicative Algebraic Reconstruction Technique (SMART-NMF), based on Asymmetric Alpha Divergence criterion (described in Chapter 4), is the NTF method that allows to achieve the best extraction of all independent components of FC's output signals (PI = 0.5362).

TABLE 6.1: Performance Index (PI) of the four stable NTF algorithms

Algorithm	**Performance Index (PI)**
Fixed-Point NMF algorithms	0.6803
Second order NMF	0.6252
SMART-NMF	0.5362
NTF1	0.9307

In order to evaluate the effectiveness of the Asymmetric Alpha Divergence based SMART-NMF algorithm, we plot in the Fig. 6.2 the signal to interference ratio (SIR) of individual columns of the estimated mixing matrix. This plot shows that two independent sources are dominant since their SIR values are very high. These two sources may correspond to neutron and gamma-ray particles.

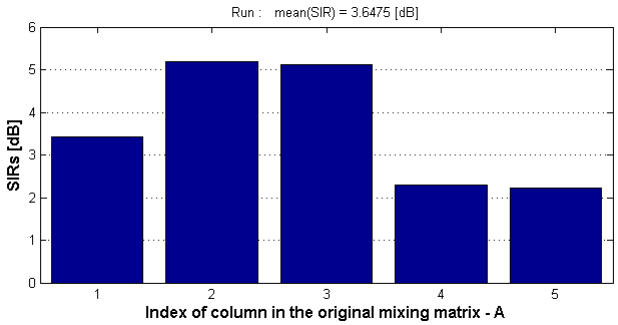

FIGURE 6.2: SIR evaluation according to the mixing matrix A.

In order to verify this assumption, we computed the normalized correlation between each extracted independent component and the recorded signals corresponding to neutron and gamma-ray pulses. Fig. 6.3 shows that the observation corresponding to the neutron signal is strongly correlated with the second extracted independent component. We exclude this component from the list of the estimated sources and we redo the same normalized correlation test. We compare the four remaining extracted sources to the gamma-ray signal. We found that the third estimated source is highly correlated with the gamma-ray signal as illustrated in Fig. 6.4.

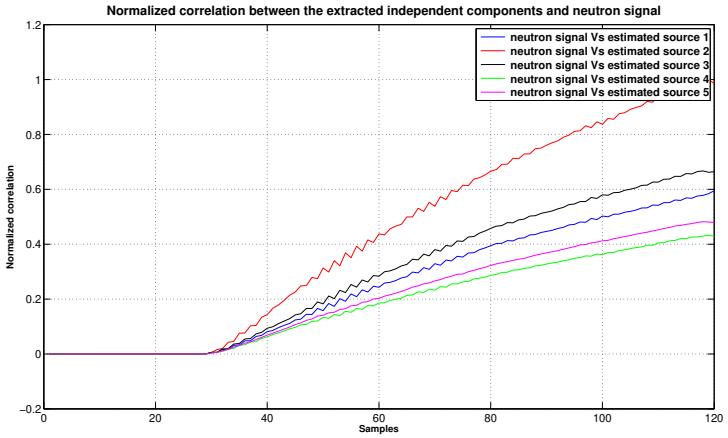

FIGURE 6.3: Normalized correlation between the extracted independent components and neutron signal.

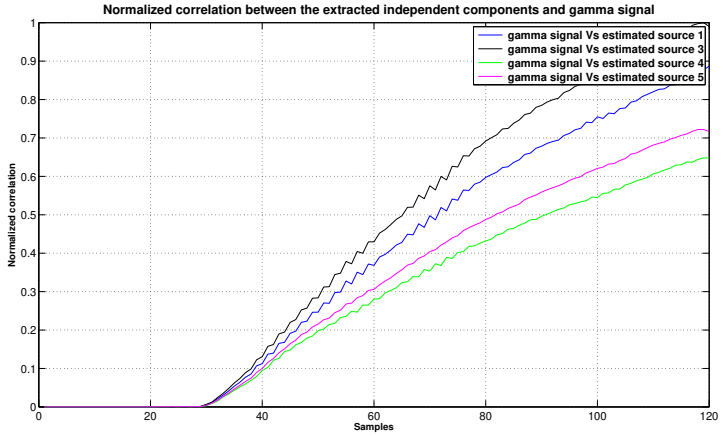

FIGURE 6.4: Normalized correlation between the extracted independent components and gamma-ray signal.

6.2.2 Application of NTF1 and NTF2 algorithms

The code used was updated to be capable of simulating the output signals with ^{252}Cf neutron source with an intensity of $2{\cdot}10^3$ n/s [90]. The aim of using a ^{252}Cf source was to check these methods and at the same time to investigate the differences in pulse shapes of neutron and gamma-ray radiations [91].

To demonstrate the effectiveness of NTF algorithms, tensor of size $5 \times 600 \times 5$ was created from the simulated FC preamplifier's output signals (Observations), as shown in the Fig. 6.5. The algorithms were evaluated according to the values of their performance index of separability (PI) (Table 6.2).

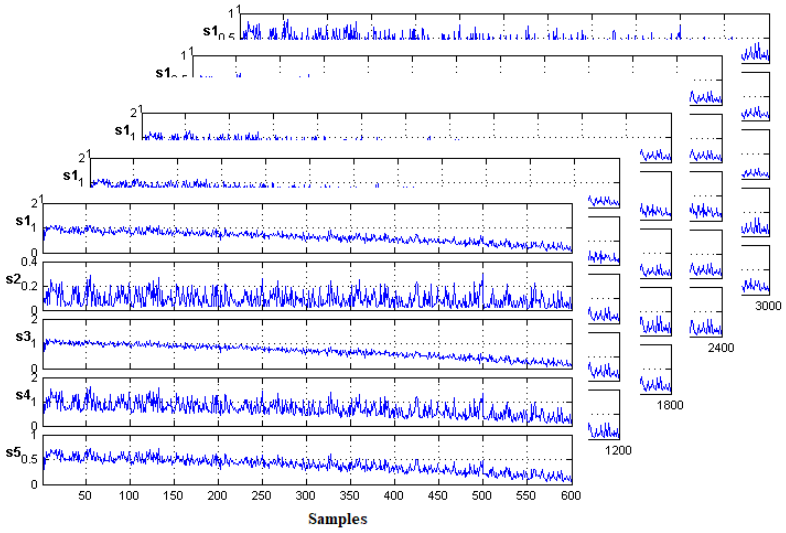

FIGURE 6.5: Slices of mixed signals.

TABLE 6.2: Performance Index (PI) of NTF1 and NTF2 algorithms

Algorithm	**Performance Index (PI)**
NTF1	0.3927
NTF2	0.3022

The Fig. 6.6 and 6.7 show the sources recovered by the application of NTF1 and NTF2 algorithms respectively. The simulations results have been performed for the WL-7657 FC output mixture signals in which the nonnegative depend 10 hidden components or sources are collected in 5 slices $X_k \in \mathbf{R}_+^{2\times 600}$ in case of NTF1 application and 2 hidden components or sources are collected in 1 slice $X \in \mathbf{R}_+^{2\times 600}$ in case of NTF2 application, each representing 2 different kind of radiations.

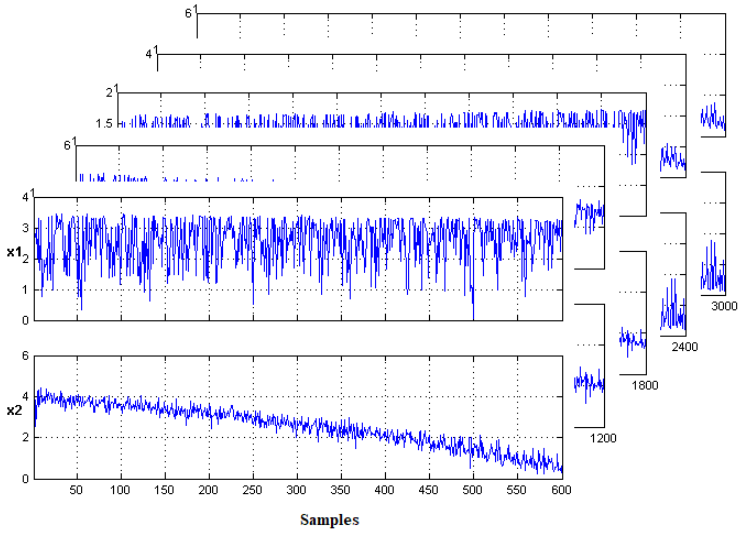

FIGURE 6.6: Spectra signals estimated with the NTF1.

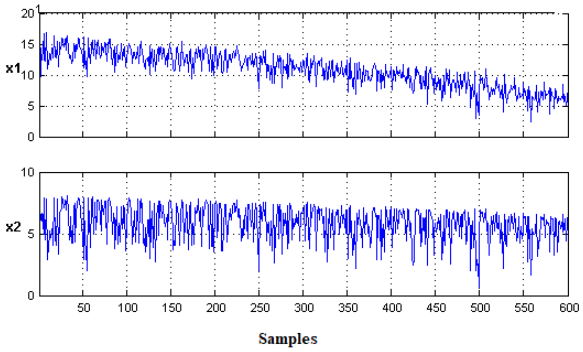

FIGURE 6.7: Spectra signals estimated with the NTF2.

It can be seen that the sources have been reasonably well separated. The computation of the signal to interference ratio (SIR) of individual columns of the mixing matrix A, permits us to confirm that the WL-7657 FC output mixture signals are formed by two main independent components which may be corrupted by noise (Fig. 6.8 and 6.9). One may therefore conclude that that the neutron/gamma discrimination task has been well achieved.

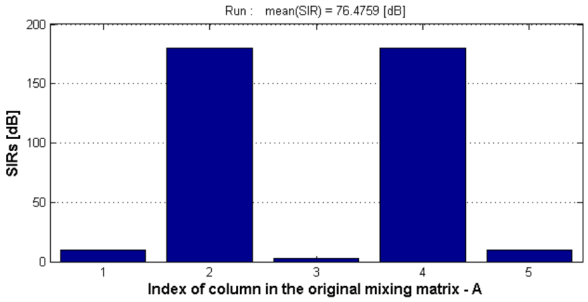

FIGURE 6.8: SIR evaluation according to the mixing matrix A with the NTF1.

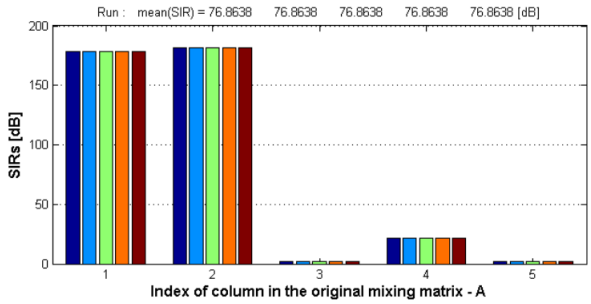

FIGURE 6.9: SIR evaluation according to the mixing matrix A with the NTF2.

6.2.3 Geant4/Garfield++ interface vs. pyFC suite

This work describes the performance of the application of the NTF2 algorithm to extract independent components from the Geant4/Garfield++ interface and from the pyFC simulations outputs respectively, and the verification of the results through comparison of the power spectral densities and normalized cross-correlation of these extracted independent components [92].

The pyFC (python-based simulation of Fission Chambers) illustrated in Fig. 6.10, is a code suite implemented in the Python language that was developed by Zs. Elter [43]. Although similar software tools already exist (such as described in [93–95]), the main goal of the pyFC is to provide a straight forward and fast computation route in order to facilitate the study of propagation of technological uncertainties of fission chamber signals. The pyFC makes use TRIM (Transport of Ions in Matter) in the transport code of the SRIM (Stopping power and Range of Ions in Matter) [41]. TRIM computes the heavy ion paths and the ionization process in the gas. The parameters of the charge collection (such as the electron mobility in the gas) between the electrodes are determined with the BOLSIG software [31]. The details of the implemented considerations behind the code system are described in [43].

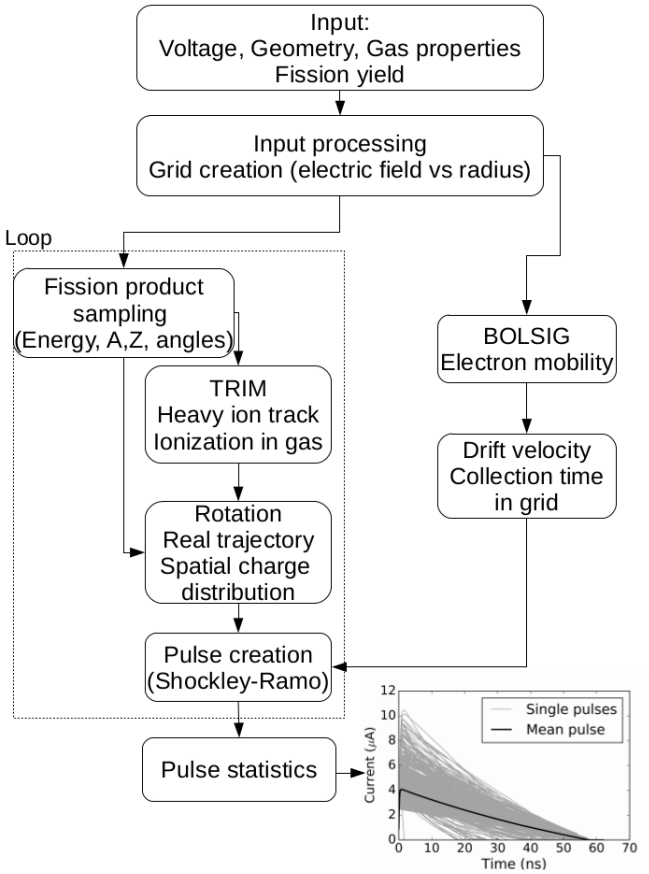

FIGURE 6.10: The structure of the pyFC suite code [43].

6.2.3.1 Application of NTF2 algorithm

In this section, we aim at applying NTF2 algorithm to analyze the WL-7657 FC's output signals simulated using Geant4/Garfield++ and pyFC. Indeed, the recorded signals are considered as time-series mixtures of several components (Observations) which we try to extract using NTF2 algorithm in order to reach the discrimination goal.

Current pulses spectra from Geant4/Garfield++ simulation of detector response to WL-7657 FC are shown in Fig. 6.11. Fig. 6.12 shows the sources recovered by the application of NTF2 algorithm (PI=0.3219). The simulation results have been performed for neutron and gamma-ray mixed radiation field in which the nonnegative dependent 5 hidden components or sources are collected in 1 slice $X \in \mathbf{R}_{+}^{5\times 600}$.

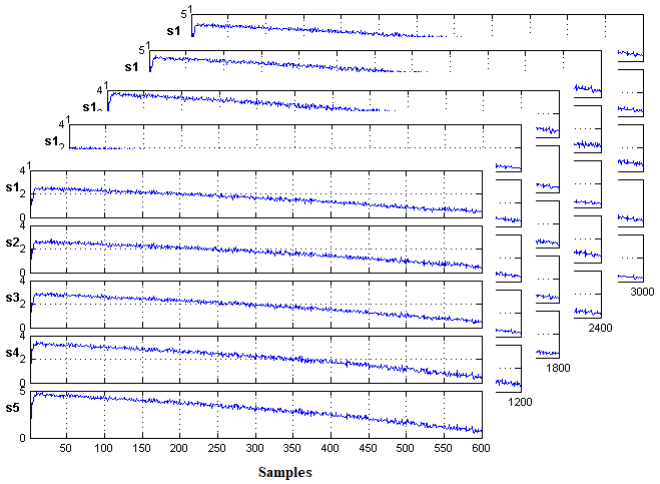

FIGURE 6.11: Slices of the mixed signals from Geant4/Garfield++.

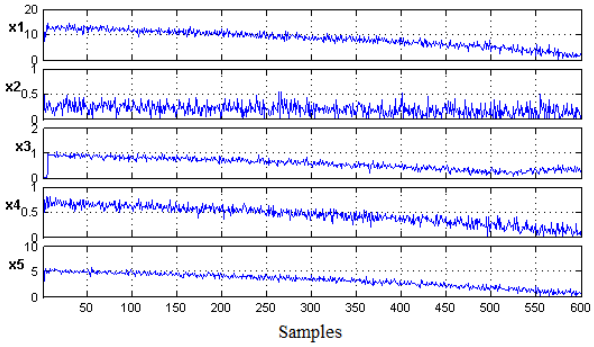

FIGURE 6.12: Spectra signals estimated with the NTF2 from Geant4/Garfield++.

The current pulses obtained from pyFC were loaded with additional Gaussian white noise at various slices (Fig. 6.13). Fig. 6.14 shows the sources recovered by the application of NTF2 algorithm (PI=0.1608). The simulation results have been performed for neutron and gamma-ray mixed radiation field in which the nonnegative dependent 5 hidden components or sources are collected in 1 slice $X \in \mathbf{R}_{+}^{5\times 600}$.

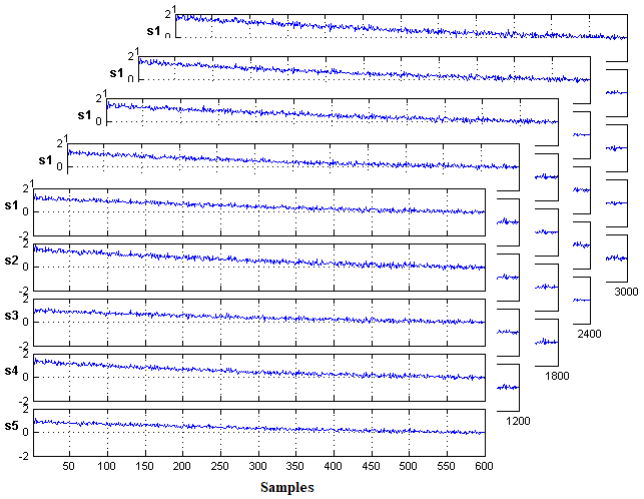

FIGURE 6.13: Slices of the mixed signals from pyFC.

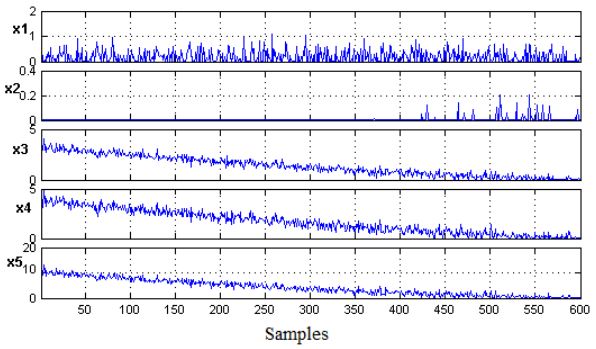

FIGURE 6.14: Spectra signals estimated with the NTF2 from pyFC.

The plot of the Signal to Interference Ratio (SIR) of individual columns of the mixing matrix A from both Geant4/Garfield++ and pyFC outputs (Fig. 6.15) shows that two independent components sources are dominating in both simulation cases since their SIR values are very high. These two sources may correspond to neutron and gamma-ray radiations which are completely buried in a background noise.

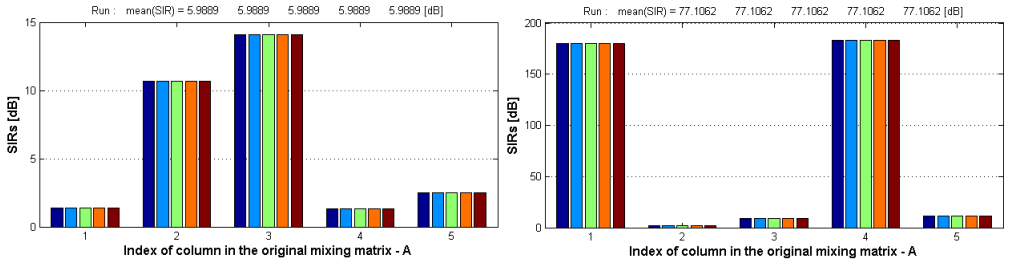

FIGURE 6.15: SIR evaluation according to the mixing matrix A from: (left) Geant4/Garfield++ (right) pyFC.

6.2.3.2 Verification and comparison

The sources being extracted by using NTF2 algorithm, in both Geant4/Garfield++ interface and pyFC simulation cases were analyzed through the computation of their power spectral densities and normalized cross-correlation functions which we compared in order to achieve neutron/gamma discrimination task. Indeed, the average of five of these extracted sources results from Geant4/Garfield++ strongly fit to the ones extracted from the pyFC output, as shown in Fig. 6.16.

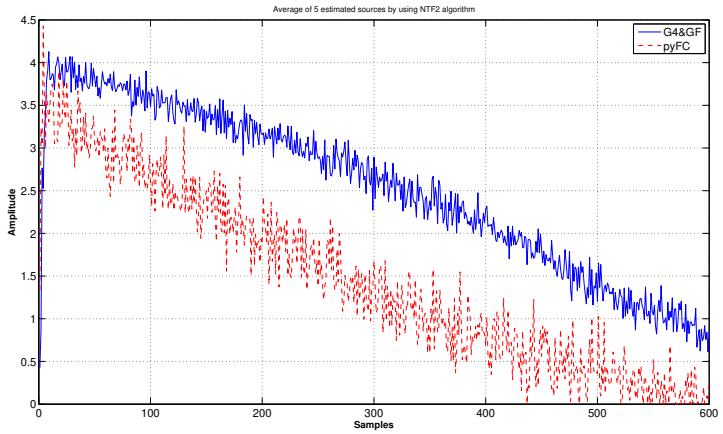

FIGURE 6.16: Average of 5 estimated sources from: Geant4/Garfield++ (blue) and pyFC (dashed red).

We compared the computed power spectral density functions of the extracted independent components calculated by using NTF2 algorithm from Geant4/Garfield++ to those computed from pyFC. Fig. 6.17 illustrates the results found in this study. Indeed, by comparing the power spectral density shape of plots, we notice that in the Geant4/Garfield++ case, the 2^{nd} estimated independent component is very close to the 1^{st} estimated independent component in the pyFC case. Furthermore, the spectrum of the 3^{rd} estimated independent component in the Geant4/Garfield++ case is very close to the 4^{th} estimated independent component in the pyFC case.

Our investigation aimed also to find if there is any relationship between the identified sources in both Geant4/Garfield++ and pyFC simulations. For this reason, we have calculated the normalized cross-correlation between 2^{nd} and 3^{rd} extracted independent components in the case of Geant4/Garfield++ and 1^{st} and 4^{th} extracted independent

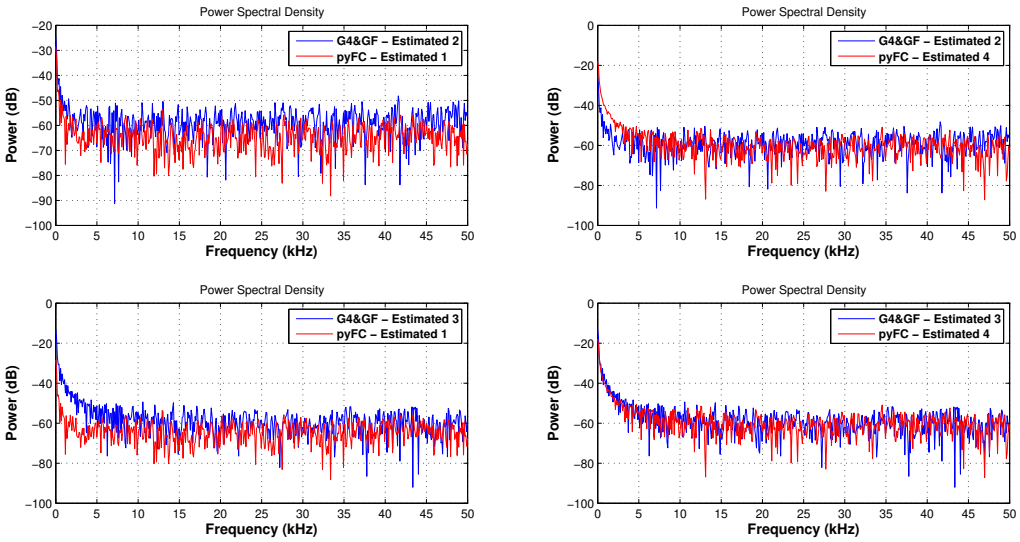

FIGURE 6.17: Power spectral density of estimated source from Geant4/Garfield++ simulation *vs*. Power spectral density of estimated source from the pyFC simulation.

components in the case of pyFC. Fig. 6.18 shows that a strong correlation exists between both the 2nd Geant4/Garfield++ and 1st pyFC estimated independent components sources and between the 3rd Geant4/Garfield++ and 4th pyFC estimated independent components sources. Consequently, the application of the NTF2 algorithm distinguishes neutron and gamma-rays with highly qualified discrimination and without any a priori information about the manner of their mixture inside the FC and under any neutron flux range.

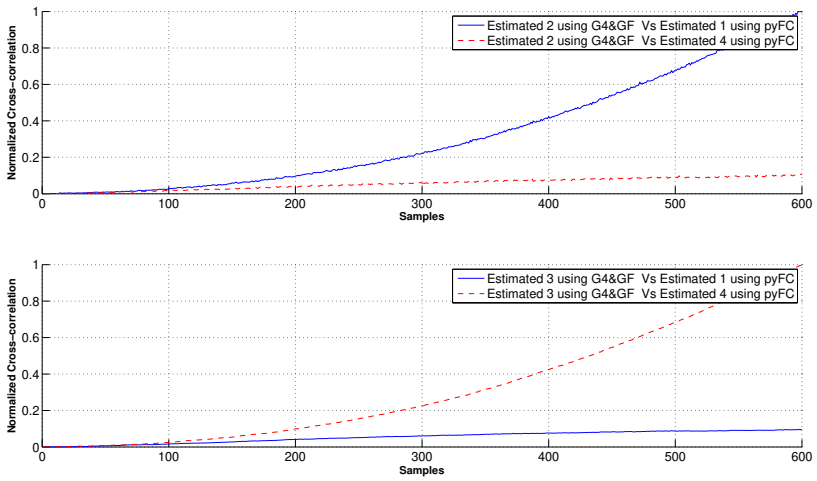

FIGURE 6.18: Normalized cross-correlation function between estimated sources in both the Geant4/Garfield++ and pyFC simulations.

6.3 Conclusion

The main objective and motivations of this study were to apply the Nonnegative Tensor Factorization (NTF) algorithms to achieve Blind Source Separation (BSS) task of preamplifier's outputs of a simulated fission chamber. The fission chamber was simulated through the Geant4 linked to Garfield++ using a neutron source, which emits both neutron and gamma-ray radiations.

In this study, three common NTF algorithms were used to discriminate the neutron and gamma-ray pulses captured in a mixed environment according to their corresponding performance indexes. These algorithms are the best blind source separation methods which can be applied to analyze such nuclear data. Indeed, the plot of the signal to noise interference ratio, computed along the columns of estimated mixing matrix, shows that only two independent components are dominants. In addition, the computation of the normalized correlation functions and the power spectral densities of the resulting independent components allows us to confirm that these two dominant sources corresponds to neutron and gamma-ray radiations respectively and at the same time we achieved the neutron/gamma discrimination. The verification of the implementation is made by comparing the Geant4/Garfield++ results to pyFC outputs which show a good agreement.

Conclusion

Neutron detectors are used in a wide range of applications starting from particle physics, going through nuclear medicine and biology research and ending in the defense industry. The main problem in neutron detection is the background noise. There are usually three sources of background noise in neutron detection: alpha, beta, and gamma-rays particles. Alpha and beta particles can easily be eliminated by various shielding materials (like lead, plastic, thermo-coal, and other mediums). However, gamma-rays pass through physical barriers and when mixed with neutrons in the detection environment, they behave almost the same as neutrons and make it uncertain whether neutrons are detected or gamma-rays. Fission chambers are widely used to measure either thermal or fast neutrons. ^{235}U is the preferred fissile deposit when the chamber is going to be used in a thermal neutron spectrum environment. However, when the chamber is intended to work in a fast neutron medium or to focus on the fast neutron component of a neutron spectrum, ^{235}U can be replaced by other isotopes, such as ^{238}U or ^{242}Pu.

In this thesis we have investigated the use of the Blind Source Separation (BSS) algorithms to extract independent components from the preamplifier's output signal of a simulated WL-7657 fission chamber installed inside the TRIGA Mark II reactor of the Nuclear Studies Centre of Maâmora (CNESTEN-Morocco). As the first step we simulated this fission chamber under Geant4 Monte Carlo toolkit linked to Garfield++. The code takes advantage of Monte Carlo methods to simulate the stochastic events taking place in these detectors and provides different simulation capabilities, such as fission fragments generated, pair production, field maps, drift lines of electrons and ions and finally the signal resulting from the passage of charged particle through the chamber and readout the signal. The code shows good agreement with the pyFC (python based simulation of Fission Chambers) results.

The output signal of the FC can be processed through pulse mode, Campbelling (also known as "fluctuation mode" or "mean square voltage mode") and current mode regarding the encountered neutron flux. The originality of our research work consists in the application of tensor-based BSS algorithms to extract independent components from signals recorded at the FC preamplifier's output at any neutron flux range. BSS algorithms now raise great interest and play an important role in many application areas. Their first application solved the "cocktail party" problem. More than that, no bibliographic reference has been found regarding the application of BSS algorithms or other digital signal processing techniques to process and analyze the output signals of FC.

The obtained output signals were processed using various NTF algorithms which were classified according to their corresponding performance indexes. For this reason, we used the NTFLab toolbox implemented under MATLAB® environment. The results show that NTF1 and NTF2 are the most effective and suitable algorithms to analyze our data among all stable NTF algorithms which have been tested, since it has the lowest performance index of separability. These algorithms allow us to separate between neutrons and gamma-rays. Indeed, the plot of the signal to noise or interference ratio (SNR/SIR), computed along the columns of estimated mixing matrix of each algorithms, showed that only two independent components are dominants. In

addition, the computation of the normalized correlation functions between the neutron and gamma-ray signals recorded and extracted independent components allowed us to confirm that these two dominant sources correspond to neutron and gamma-ray signals respectively and at the same time we achieved the neutron/gamma discrimination.

The simulation code has been validated by comparing its outputs with pyFC. It can be concluded that the simulation results are in good agreement with the results provided by the pyFC. In order to verify the feasibility of using a Nonnegative Tensor Factorization (NTF) to blind extract neutron component from mixture signals recorded at the output of fission chamber (WL-7657), we applied the NTF2 model as nonnegative tensor factorization algorithm to extract independent components from the Geant4/Garfield++ and from the pyFC and the validation of the results through comparison of the power spectral densities and normalized cross-correlation functions of these extracted independent components. The NTF2 algorithm was then incorporated into a nuclear signal separation algorithm which was shown to be capable of separation mixtures of neutron and gamma-ray radiations.

Nonnegative Tensor Factorization (NTF) showed that the computation of the SIR of individual columns of the mixing matrix in both Geant4/Garfield++ and pyFC cases allows us to confirm that the WL-7657 FC's output mixture signals are formed by two main independent components which may be corrupted by noise. Comparing the power spectral densities to estimated independent component sources and calculating the normalized cross-correlation functions confirms that these two dominant sources correspond to neutron and gamma-ray radiations.

The end of this dissertation is not the end of the research project because many new Functionality have been identified and/or requested, such as:

- Integrate the NTF algorithms to real time analyzing the fission chamber signals to better monitor neutron flux inside TRIGA Mark II reactor,
- Extending the implementation of the NTF/BSS with other types of neutron detectors, such as scintillator detectors,
- Implementing NTF/BSS on FPGA board,
- Development of a digital neutron measurement chain.

Bibliography

[1] S. N. Ahmed. *Physics and engineering of radiation detection*. Academic Press, 2007.

[2] *JANIS 4.0 - OECD Nuclear Energy Agency*. https://www.oecd-nea.org/janis/. Accessed January 24, 2019.

[3] A. Antolinez Garcia. "Fission chambers designer based on monte carlo techniques working in current mode and operated in saturation regime". PhD thesis. Universidad Politécnica de Madrid, 2016.

[4] A. Lyoussi. *Détection de rayonnements et instrumentation nucléaire*. EDP sciences, 2012.

[5] W. Mannhart. *Status of the Cf-252 fission neutron spectrum evaluation with regard to recent experiments*. Tech. rep. 1989.

[6] James E Martin. *Physics for radiation protection: a handbook*. John Wiley & Sons, 2006.

[7] G. F. Knoll. *Radiation detection and measurement*. John Wiley & Sons, 2010.

[8] R. J. Holmes. *Gamma ray and neutron sources*. Tech. rep. 1982.

[9] A. Wattenberg. *Photo-neutron sources*. Vol. 6. National Academies, 1949.

[10] H. Böck and M. Villa. *TRIGA reactor main systems*. Tech. rep. Atomic Institute of the Austrian Universities, 2007.

[11] A. Krása. "Spallation reaction physics". In: *Czech Republic: Czech Technical University Lecture* (2010).

[12] A. Kowalczyk. "Proton induced spallation reactions in the energy range 0.1-10 GeV". In: *arXiv preprint arXiv:0801.0700* (2008).

[13] A. Krása. "Neutron Production in Spallation Reactions of Relativistic Light Ions on Thick, Heavy Targets". PhD thesis. Czech Repub. Czech Tech. Univ. Lect., 2010.

[14] A. Lintereur and et al. "Boron-10 lined proportional counter model validation". In: *Nuclear Science Symposium and Medical Imaging Conference (NSS/MIC), 2012 IEEE*. IEEE. 2012, pp. 4290–4295.

[15] G. Grosshoeg. "Neutron ionization chambers". In: *Nuclear instruments and Methods* 162.1-3 (1979), pp. 125–160.

[16] S. Normand. "INSTRUMENTATION NUCLEAIRE POUR LES SYSTEMES INDUSTRIELS DE MESURE". PhD thesis. Université de Caen, 2010.

[17] M. Angelone et al. "Development of self-powered neutron detectors for neutron flux monitoring in HCLL and HCPB ITER-TBM". In: *Fusion Engineering and Design* 89.9-10 (2014), pp. 2194–2198.

[18] W. Lee et al. “A study on the sensitivity of self-powered neutron detector (SPND)”. In: *Nuclear Science Symposium, 1999. Conference Record. 1999 IEEE*. Vol. 2. IEEE. 1999, pp. 772–776.

[19] C. Duweke. “Neutron flux incore instrumentation of AREVA’s EPR”. In: *Advancements in Nuclear Instrumentation Measurement Methods and their Applications (ANIMMA), 2009 First International Conference on*. IEEE. 2009, pp. 1–6.

[20] O. Poujade and A. Lebrun. “Modeling of the saturation current of a fission chamber taking into account the distorsion of electric field due to space charge effects”. In: *Nuclear Instruments and Methods in Physics Research Section A: Accelerators, Spectrometers, Detectors and Associated Equipment* 433.3 (1999), pp. 673–682.

[21] P. Filliatre et al. “Reasons why Plutonium 242 is the best fission chamber deposit to monitor the fast component of a high neutron flux”. In: *Nuclear Instruments and Methods in Physics Research Section A: Accelerators, Spectrometers, Detectors and Associated Equipment* 593.3 (2008), pp. 510–518.

[22] P. Filliatre et al. “Estimating the γ-ray contribution to the signal of fission chambers with Monte Carlo simulations”. In: *Nuclear Instruments and Methods in Physics Research Section A: Accelerators, Spectrometers, Detectors and Associated Equipment* 648.1 (2011), pp. 228–237.

[23] I. B. Smirnov. “Modeling of ionization produced by fast charged particles in gases”. In: *Nuclear Instruments and Methods in Physics Research Section A: Accelerators, Spectrometers, Detectors and Associated Equipment* 554.1-3 (2005), pp. 474–493.

[24] L. Vermeeren et al. “Experimental verification of the fission chamber gamma signal suppression by the Campbelling mode”. In: *Advancements in Nuclear Instrumentation Measurement Methods and their Applications (ANIMMA), 2009 First International Conference on*. IEEE. 2009, pp. 1–8.

[25] P. Filliatre et al. “In vessel neutron instrumentation for sodium-cooled fast reactors: Type, lifetime and location”. In: *Annals of Nuclear Energy* 37.11 (2010), pp. 1435–1442.

[26] P. Filliatre et al. “Joint estimation of the fast and thermal components of a high neutron flux with a two on-line detector system”. In: *Nuclear Instruments and Methods in Physics Research Section A: Accelerators, Spectrometers, Detectors and Associated Equipment* 603.3 (2009), pp. 415–420.

[27] M. Reichenberger et al. “First-order numerical optimization of fission-chamber coatings using natural uranium and thorium”. In: *Nuclear Science Symposium and Medical Imaging Conference (NSS/MIC), 2014 IEEE*. IEEE. 2014, pp. 1–4.

[28] A. H. Snell and H. h. Bolotin. “Nuclear Instruments and their Uses”. In: *Physics Today* 16 (1963), p. 52.

[29] T. E. Bortner, G. S. Hurst, and W. G. Stone. “Drift velocities of electrons in some commonly used counting gases”. In: *Review of Scientific Instruments* 28.2 (1957), pp. 103–108.

[30] G. N. Haddad. “Drift Velocity of Electrons in Nitrogen? Argon Mixtures”. In: *Australian journal of physics* 36.3 (1983), pp. 297–304.

[31] G. J. M. Hagelaar and L. C. Pitchford. “Solving the Boltzmann equation to obtain electron transport coefficients and rate coefficients for fluid models”. In: *Plasma Sources Science and Technology* 14.4 (2005), p. 722.

[32] S. F. Biagi. "Monte Carlo simulation of electron drift and diffusion in counting gases under the influence of electric and magnetic fields". In: *Nuclear Instruments and Methods in Physics Research Section A: Accelerators, Spectrometers, Detectors and Associated Equipment* 421.1-2 (1999), pp. 234–240.

[33] N. R. Campbell and V. J. Francis. "A theory of valve and circuit noise". In: *Journal of the Institution of Electrical Engineers-Part III: Radio and Communication Engineering* 93.21 (1946), pp. 45–52.

[34] S. Agostinelli et al. "GEANT4 - a simulation toolkit". In: *Nuclear instruments and methods in physics research section A: Accelerators, Spectrometers, Detectors and Associated Equipment* 506.3 (2003), pp. 250–303.

[35] *Garfield++ - simulation of ionisation based tracking detectors*. https://garfieldpp.web.cern.ch/garfieldpp/. Accessed June 5, 2018.

[36] R. Brun and et al. *GEANT: Detector Description and Simulation Tool*. https://cds.cern.ch/record/1082634. Accessed June 26, 2018.

[37] *ROOT a Data analysis Framework*. https://root.cern.ch/. Accessed June 12, 2018.

[38] *Transport of electrons in gas mixtures*. http://consult.cern.ch/writeup/magboltz/. Accessed June 12, 2018.

[39] I. B. Smirnov. "Modeling of ionization produced by fast charged particles in gases". In: *Nuclear Instruments and Methods in Physics Research Section A: Accelerators, Spectrometers, Detectors and Associated Equipment* 554.1-3 (2005), pp. 474–493.

[40] *Geant4 interface*. https://garfieldpp.web.cern.ch/garfieldpp/examples/geant4-interface/. Accessed June 12, 2018.

[41] J. Ziegler. *SRIM & TRIM*. http://srim.org/. Accessed June 12, 2018.

[42] *Mirion Technologies: Nuclear Radiation Detection, Measurement & Safety*. www.mirion.com/. Accessed October 17, 2018.

[43] Zs. Elter. "pyFC: a TRIM-based fission chamber pulse shape simulator". In: *Chalmers University of Technology technical note* (2015).

[44] L. El Badri et al. "Development of wavelet based tools for improving the γ-ray spectrometry". In: *Advancements in Nuclear Instrumentation Measurement Methods and their Applications (ANIMMA), 2013 3rd International Conference on*. IEEE. 2013, pp. 1–5.

[45] T. Trigano et al. "Statistical pileup correction method for HPGe detectors". In: *IEEE Transactions on Signal Processing* 55.10 (2007), pp. 4871–4881.

[46] M. Amiri. "Neutron/gamma-ray measurement and discrimination". PhD thesis. Masarykova univerzita, Fakulta informatiky, 2014.

[47] A. Mekaoui, E-M. Hamzaoui, and R. Cherkaoui El Moursli. "Application of blind source separation algorithms to the preamplifier's output signals of an HPGe detector used in γ-ray spectrometry". In: *Advanced Studies in Theoretical Physics* 8.9 (2014), pp. 393–399.

[48] A. Mekaoui, E-M. Hamzaoui, and R. Cherkaoui El Moursli. "Blind source separation of HPGe output signals: a new pulse pile-up correction method". In: *Advanced Studies in Theoretical Physics* 8.16 (2014), pp. 681–688.

[49] A. Mekaoui et al. "Blind source extraction of hpge preamplifier's output signals using the thinica algorithm: detection and identification of gamma ray emitters". In: *Advanced Studies in Theoretical Physics* 8.26 (2014), pp. 1157–1164.

[50] A. Cichocki and S-I. Amari. *Adaptive blind signal and image processing: learning algorithms and applications*. Vol. 1. John Wiley & Sons, 2002.

[51] K. Matsuoka, M. Ohoya, and M. Kawamoto. "A neural net for blind separation of nonstationary signals". In: *Neural networks* 8.3 (1995), pp. 411–419.

[52] M. Flatz. "Algorithms for nonnegative tensor factorization". In: *University of Salzburg* (2013).

[53] *NTFLAB for Signal Processing*. http://www.bsp.brain.riken.jp/ICALAB/nmflab.html/. Accessed October 17, 2018.

[54] A. Cichocki et al. *Nonnegative matrix and tensor factorizations: applications to exploratory multi-way data analysis and blind source separation*. John Wiley & Sons, 2009.

[55] A. Cichocki and S-I. Amari. *Adaptive blind signal and image processing: learning algorithms and applications*. Vol. 1. John Wiley & Sons, 2002.

[56] E-M. Hamzaoui, F. Regragui, and M. M. Himmi. "Identification and characterization of the sources of the noise affecting the visual evoked potentials". In: *Contemporary Engineering Sciences* 4.1 (2011), pp. 25–35.

[57] A. Cichocki et al. "Extended SMART algorithms for non-negative matrix factorization". In: *International Conference on Artificial Intelligence and Soft Computing*. Springer. 2006, pp. 548–562.

[58] W. Bryan et al. "Fast neutron-gamma pulse shape discrimination of liquid scintillation signals for time correlated measurements". In: *Nuclear Science Symposium Conference Record, 2003 IEEE*. Vol. 2. IEEE. 2003, pp. 1192–1195.

[59] G. Ranucci. "An analytical approach to the evaluation of the pulse shape discrimination properties of scintillators". In: *Nuclear Instruments and Methods in Physics Research Section A: Accelerators, Spectrometers, Detectors and Associated Equipment* 354.2-3 (1995), pp. 389–399.

[60] M. L. Roush, M. A. Wilson, and W. F. Hornyak. "Pulse shape discrimination". In: *Nuclear Instruments and Methods* 31.1 (1964), pp. 112–124.

[61] F. D. Brooks. "A scintillation counter with neutron and gamma-ray discriminators". In: *Nuclear Instruments and Methods* 4.3 (1959), pp. 151–163.

[62] J. M. Adams and G. White. "A versatile pulse shape discriminator for charged particle separation and its application to fast neutron time-of-flight spectroscopy". In: *Nuclear Instruments and Methods* 156.3 (1978), pp. 459–476.

[63] A. Enqvist, M. Flaska, and S. Pozzi. "Measurement and simulation of neutron/gamma-ray cross-correlation functions from spontaneous fission". In: *Nuclear Instruments and Methods in Physics Research Section A: Accelerators, Spectrometers, Detectors and Associated Equipment* 595.2 (2008), pp. 426–430.

[64] C. Guerrero et al. "Analysis of the BC501A neutron detector signals using the true pulse shape". In: *Nuclear Instruments and Methods in Physics Research Section A: Accelerators, Spectrometers, Detectors and Associated Equipment* 597.2-3 (2008), pp. 212–218.

[65] S. D. Clarke et al. "Neutron and gamma-ray cross-correlation measurements of plutonium oxide powder". In: *Nuclear Instruments and Methods in Physics Research Section A: Accelerators, Spectrometers, Detectors and Associated Equipment* 604.3 (2009), pp. 618–623.

[66] M. Flaska and S. A. Pozzi. "Digital pulse shape analysis for the capture-gated liquid scintillator BC-523A". In: *Nuclear Instruments and Methods in Physics Research Section A: Accelerators, Spectrometers, Detectors and Associated Equipment* 599.2-3 (2009), pp. 221–225.

[67] M. Hamel et al. "A new fluorophore highly efficient for fast neutrons/gamma-rays discrimination in liquid media". In: *Nuclear Instruments and Methods in Physics Research Section A: Accelerators, Spectrometers, Detectors and Associated Equipment* 602.2 (2009), pp. 425–431.

[68] N. P. Hawkes, K. A. A. Gamage, and G. C. Taylor. "Digital approaches to field neutron spectrometry". In: *Radiation Measurements* 45.10 (2010), pp. 1305–1308.

[69] A. Lavagno, G. Gervino, and C. Marino. "High efficiency large volume multiparametric neutron detector". In: *Nuclear Instruments and Methods in Physics Research Section A: Accelerators, Spectrometers, Detectors and Associated Equipment* 617.1-3 (2010), pp. 492–494.

[70] S. D. Jastaniah and P. J. Sellin. "Digital pulse-shape algorithms for scintillation-based neutron detectors". In: *IEEE Transactions on Nuclear Science* 49.4 (2002), pp. 1824–1828.

[71] P. J. Sellin, G. Jaffar, and S. D. Jastaniah. "Performance of digital algorithms for n/γ pulse shape discrimination using a liquid scintillation detector". In: *Nuclear Science Symposium Conference Record, 2003 IEEE*. Vol. 2. IEEE. 2003, pp. 1057–1060.

[72] S. D. Jastaniah and P. J. Sellin. "Digital techniques for n/γ pulse shape discrimination and capture-gated neutron spectroscopy using liquid scintillators". In: *Nuclear Instruments and Methods in Physics Research Section A: Accelerators, Spectrometers, Detectors and Associated Equipment* 517.1-3 (2004), pp. 202–210.

[73] N. P. Hawkes. "Pulse shape discrimination in hydrogen-filled proportional counters by digital methods". In: *Nuclear Instruments and Methods in Physics Research Section A: Accelerators, Spectrometers, Detectors and Associated Equipment* 574.1 (2007), pp. 133–136.

[74] J. H. Kim, H. Park, and K. O. Choi. "Neutron spectrometer with a capture-gated liquid scintillator". In: *Journal of the Korean Physical Society* 56.1 (2010), pp. 34–41.

[75] D. Marocco et al. "A digital data acquisition system optimized for spectrometry with liquid scintillation detectors". In: *International Workshop on Fast Neutron Detectors and Applications*. Vol. 25. SISSA Medialab. 2007, p. 028.

[76] M. Nakhostin and P. M. Walker. "Application of digital zero-crossing technique for neutron–gamma discrimination in liquid organic scintillation detectors". In: *Nuclear Instruments and Methods in Physics Research Section A: Accelerators, Spectrometers, Detectors and Associated Equipment* 621.1-3 (2010), pp. 498–501.

[77] D. Takaku et al. "Development of neutron-gamma discrimination technique using pattern-recognition method with digital signal processing". In: *Progress in Nuclear Science and Technology* 1 (2011), pp. 210–213.

[78] B. D'Mellow et al. "Digital n-γ discrimination in liquid scintillators using pulse gradient analysis". In: *Nucl. Inst. and Meth. A* 578 (2007), pp. 191–197.

[79] G. Liu et al. "A Digital Method for the Discrimination of Neutrons and γ- Rays With Organic Scintillation Detectors Using Frequency Gradient Analysis". In: *IEEE Transactions on Nuclear Science* 57.3 (2010), pp. 1682–1691.

[80] D. I. Shippen, M. J. Joyce, and M. D. Aspinall. "A wavelet packet transform inspired method of neutron-gamma discrimination". In: *IEEE Transactions on Nuclear Science* 57.5 (2010), pp. 2617–2624.

[81] K. A. A. Gamage, M. J. Joyce, and N. P. Hawkes. "A comparison of four different digital algorithms for pulse-shape discrimination in fast scintillators". In: *Nuclear Instruments and Methods in Physics Research Section A: Accelerators, Spectrometers, Detectors and Associated Equipment* 642.1 (2011), pp. 78–83.

[82] S. Yousefi, L. Lucchese, and M. D. Aspinall. "Digital discrimination of neutrons and gamma-rays in liquid scintillators using wavelets". In: *Nuclear Instruments and Methods in Physics Research Section A: Accelerators, Spectrometers, Detectors and Associated Equipment* 598.2 (2009), pp. 551–555.

[83] J. B. Ballagh. "An FPGA-based run-time reconfigurable 2-D discrete wavelet transform core". PhD thesis. Virginia Tech, 2001.

[84] S. Haykin. *Neural networks: a comprehensive foundation*. Prentice Hall PTR, 1994.

[85] Z. Cao, L. F. Miller, and M. Buckner. "Implementation of dynamic bias for neutron–photon pulse shape discrimination by using neural network classifiers". In: *Nuclear Instruments and Methods in Physics Research Section A: Accelerators, Spectrometers, Detectors and Associated Equipment* 416.2-3 (1998), pp. 438–445.

[86] B. Esposito, L. Fortuna, and A. Rizzo. "Neural neutron/gamma discrimination in organic scintillators for fusion applications". In: *Neural Networks, 2004. Proceedings. 2004 IEEE International Joint Conference on*. Vol. 4. IEEE. 2004, pp. 2931–2936.

[87] E. Ronchi et al. "An artificial neural network based neutron–gamma discrimination and pile-up rejection framework for the BC-501 liquid scintillation detector". In: *Nuclear Instruments and Methods in Physics Research Section A: Accelerators, Spectrometers, Detectors and Associated Equipment* 610.2 (2009), pp. 534–539.

[88] G. Liu et al. "An investigation of the digital discrimination of neutrons and γ rays with organic scintillation detectors using an artificial neural network". In: *Nuclear Instruments and Methods in Physics Research Section A: Accelerators, Spectrometers, Detectors and Associated Equipment* 607.3 (2009), pp. 620–628.

[89] M. Laassiri, E-M. Hamzaoui, and R. Cherkaoui El Moursli. "Application of Nonnegative Tensor Factorization for neutron-gamma discrimination of Monte Carlo simulated fission chamber's output signals". In: *Results in physics* 7 (2017), pp. 1422–1426.

[90] *Fission Yield Graph*. https://wwwndc.jaea.go.jp/cgi-bin/FPYfig?iso=sCf252. Accessed June 18, 2018.

[91] M. Laassiri, E-M. Hamzaoui, and R. Cherkaoui El Moursli. "Nonnegative Tensor Factorization Approach Applied to Fission Chamber's Output Signals Blind Source Separation". In: *Journal of Physics: Conference Series*. Vol. 966. 1. IOP Publishing. 2018, p. 012063.

[92] M. Laassiri, E-M. Hamzaoui, and R. Cherkaoui El Moursli. "Validation of the Neutron and Gamma Fields in the Moroccan TRIGA Mark II Reactor Using Nonnegative Tensor Factorization Approach: Comparison of Performances of the Geant4/Garfield++ and pyFC Interfaces". In: *Acta Phys. Polon. Supp.* 11 (2018), p. 73.

[93] E. W. Pontes and A. Ferreira. "Using cumulants and spectra to model nuclear radiation detectors". In: *IEEE transactions on nuclear science* 53.3 (2006), pp. 1292–1298.

[94] P. Filliatre et al. "A Monte Carlo simulation of the fission chambers neutron-induced pulse shape using the GARFIELD suite". In: *Nuclear Instruments and Methods in Physics Research Section A: Accelerators, Spectrometers, Detectors and Associated Equipment* 678 (2012), pp. 139–147.

[95] P. Loiseau, B. Geslot, and J. André. "On the fission chamber pulse charge acquisition and interpretation at MINERVE". In: *Nuclear Instruments and Methods in Physics Research Section A: Accelerators, Spectrometers, Detectors and Associated Equipment* 707 (2013), pp. 58–63.

Résumé

L'un des aspects de la sûreté et de la sécurité des réacteurs nucléaires consiste à cerner la distribution du flux neutronique à l'intérieur du réacteur avec la meilleure précision possible. A cet effet, les détecteurs chambres à fission sont largement utilisées pour mesurer le champ neutronique et ainsi permettre le contrôle du flux neutronique au sein des réacteurs. Toutefois, avec les neutrons, les rayonnements gamma sont également émis par les noyaux et détectés par les chambres à fission. Par conséquent des processus physiques sont utilisés pour ressortir le spectre neutronique désiré.

Dans cette thèse, nous proposons une nouvelle approche pour résoudre le problème de la discrimination neutron/gamma à la sortie du préamplificateur d'une chambre à fission. Il s'agit de l'application des méthodes de séparation aveugle des sources basée sur la décomposition des signaux en élément de tenseurs pour extraire les composantes indépendantes constituant les signaux délivrés par une chambre à fission.

Pour des raisons de sûreté nucléaire, nous avons procédé à la simulation du flux de neutrons à l'intérieur du réacteur TRIGA Mark II du CNESTEN à l'aide des méthodes de Monte Carlo sous Geant4 lié à Garfield++. En effet, Geant4 nous a permis la modélisation de la chambre à fission tandis que Garfield++ nous a permis de simuler les paramètres de dérive à partir de l'ionisation du gaz de remplissage. Nous avons comparé ces modèles avec ceux obtenus en utilisant interface pyFC (python-based simulation of Fission Chambers).

Mots-clefs (5): Discrimination neutron/gamma, Chambre à fission, Geant4/Garfield++, Séparation aveugle des sources, Factorisation en tenseurs nonnégatifs.

Abstract

One aspect of the safety and security of nuclear reactors is to identify the distribution of neutron flux within the reactor with the highest possible accuracy. For this purpose, fission chamber detectors are widely used to measure the neutron field and thus allow control of the neutron flux within the reactors. However, with neutrons, gamma-rays are also emitted by nuclei and detected by fission chambers. As a result, physical processes are used to bring out the desired neutron spectrum.

In this thesis, we propose a new approach to solve the problem of neutron/gamma discrimination at the output of the preamplifier of a fission chamber. It is the application of blind source separation methods based on the decomposition of tensor element signals to extract the independent components constituting the signals delivered by a fission chamber.

For nuclear safety reasons, we simulated the neutron flux inside CNESTEN's TRIGA Mark II reactor using Garfield++ bound Geant4 Monte Carlo methods. Indeed, Geant4 allowed us to model the fission chamber whereas Garfield++ allowed us to simulate the drift parameters from the ionization of the filling gas. We compared these models with those obtained using pyFC (python-based simulation of Fission Chambers).

Key Words (5): Neutron/gamma discrimination, Fission chamber, Geant4/Garfield++ interface, Blind source separation, Nonnegative tensor factorization.